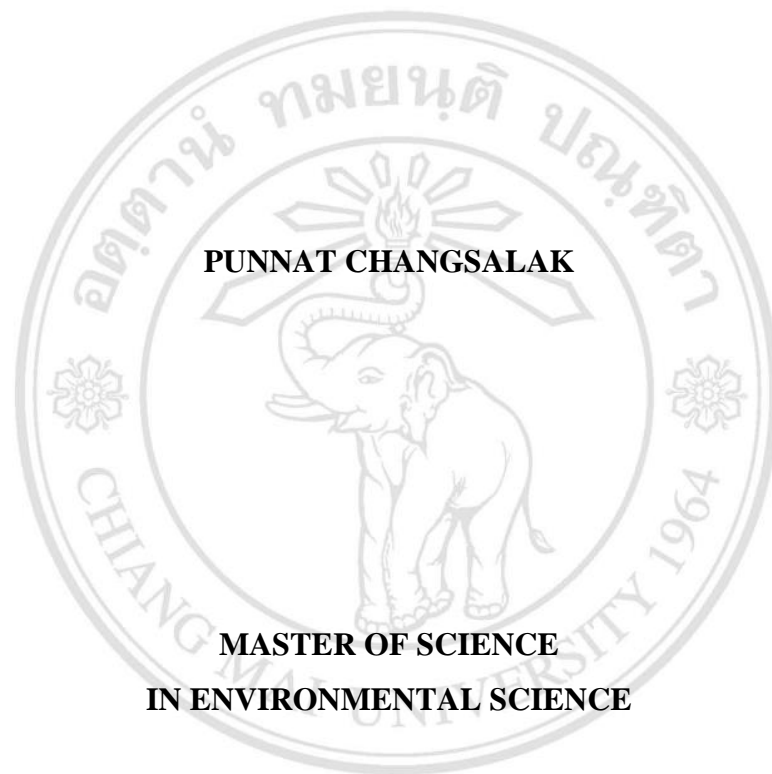


**USE OF UNMANNED AERIAL VEHICLE (UAV) IMAGERY TO
MONITOR PROGRESS OF EARLY FOREST ECOSYSTEM
RESTORATION IN AN OPENCAST MINE**



PUNNAT CHANGSALAK

**MASTER OF SCIENCE
IN ENVIRONMENTAL SCIENCE**

ลิขสิทธิ์มหาวิทยาลัยเชียงใหม่
Copyright© by Chiang Mai University
All rights reserved

**GRADUATE SCHOOL
CHIANG MAI UNIVERSITY
SEPTEMBER 2022**

**USE OF UNMANNED AERIAL VEHICLE (UAV) IMAGERY TO
MONITOR PROGRESS OF EARLY FOREST ECOSYSTEM
RESTORATION IN AN OPENCAST MINE**

PUNNAT CHANGSALAK

**A THESIS SUBMITTED TO CHIANG MAI UNIVERSITY IN PARTIAL
FULFILLMENT OF THE REQUIREMENTS FOR THE DEGREE OF
MASTER OF SCIENCE**

IN ENVIRONMENTAL SCIENCE

ลิขสิทธิ์มหาวิทยาลัยเชียงใหม่
Copyright© by Chiang Mai University
All rights reserved

**GRADUATE SCHOOL, CHIANG MAI UNIVERSITY
SEPTEMBER 2022**

**USE OF UNMANNED AERIAL VEHICLE (UAV) IMAGERY TO
MONITOR PROGRESS OF EARLY FOREST ECOSYSTEM
RESTORATION IN AN OPENCAST MINE**

PUNNAT CHANGSALAK

THIS THESIS HAS BEEN APPROVED TO BE A PARTIAL FULFILLMENT OF
THE REQUIREMENTS FOR THE DEGREE OF
MASTER OF SCIENCE
IN ENVIRONMENTAL SCIENCE

Examination Committee:

Sasaker Nophea
..... Chairperson

(Prof. Dr. Nophea Sasaki)

Pimonrat Tiansawat
..... Member

(Asst. Prof. Dr. Pimonrat Tiansawat)

S. Elliott
..... Member

(Assoc. Prof. Dr. Stephen Elliott)

Advisory Committee:

Pimonrat Tiansawat
..... Advisor

(Asst. Prof. Dr. Pimonrat Tiansawat)

S. Elliott
..... Co-advisor

(Assoc. Prof. Dr. Stephen Elliott)

7 September 2022

Copyright © by Chiang Mai University

ACKNOWLEDGEMENTS

This research could not have been finished without contributions from many people, all of whom I thank for my success in this step.

First, I thank my advisor, Asst. Prof. Dr. Pimonrat Tiansawat and co-advisor, Assoc. Prof. Dr. Stephen Elliott, for their invaluable help on this research, especially in writing period.

Second, I am also grateful to all FORRU-CMU's staff involved, who played an important role in the ground survey and data collection. Similarly, thanks also due to SCG's staffs that supported our team every single time we had been to their place.

Thanks, due to The Development and Promotion of Science and Technology Talented Project (DSTP), for financial support during studying in a master's degree at Chiang Mai University. In addition, FORRU-CMU covered various unforeseen costs of field work supported via a grant from SCG.

Finally, I greatly thank Bhanuwat Foojakham indeed, who was always by my side and encouraged me to finish this thesis. I appreciate his support for the whole study duration, otherwise, I might be done with my work since the first year of my degree.

Punnat Changsalak

ลิขสิทธิ์มหาวิทยาลัยเชียงใหม่
Copyright© by Chiang Mai University
All rights reserved

หัวข้อวิทยานิพนธ์	การใช้ภาพถ่ายจากอากาศยานไร้คนขับเพื่อติดตามความก้าวหน้าของการฟื้นฟูระบบนิเวศป่าระยะเริ่มต้นในพื้นที่เหมืองเปิด	
ผู้เขียน	นายปณณัตต์ ช่างสลัก	
ปริญญา	วิทยาศาสตรมหาบัณฑิต (วิทยาศาสตรสิ่งแวดล้อม)	
คณะกรรมการที่ปรึกษา	ผศ.ดร. พิมลรัตน์ เทียนสวัสดิ์	อาจารย์ที่ปรึกษาหลัก
	รศ.ดร. สตีเฟน เอลเลียต	อาจารย์ที่ปรึกษาร่วม

บทคัดย่อ

การติดตามตรวจสอบการฟื้นฟูป่าเป็นสิ่งจำเป็นเพื่อความก้าวหน้าของเทคนิคการฟื้นฟู แต่ด้วยค่าใช้จ่ายในการดำเนินการที่สูง โดยเฉพาะอย่างยิ่งในแง่ของค่าจ้างแรงงาน ภาพถ่ายทางอากาศจากอากาศยานไร้คนขับ (UAV) มีความเป็นไปได้ที่จะเข้ามาทดแทนในส่วนของแรงงานสำหรับการติดตามตรวจสอบการฟื้นฟูนี้ อย่างไรก็ตาม การตรวจสอบกล้าไม้ที่ปลูกใหม่ด้วยภาพถ่ายทางอากาศยังคงเป็นเรื่องที่มีความท้าทาย เนื่องจากกล้าไม้มีขนาดเล็ก งานวิจัยที่นำเสนอนี้มีจุดประสงค์ที่จะพัฒนาและทดสอบเทคนิคการใช้ภาพถ่ายทางอากาศ เพื่อติดตามการรอดและการเจริญเติบโตของกล้าไม้ที่ปลูกเพื่อฟื้นฟูพื้นที่เหมืองแบบเปิด โดยใช้อากาศยานไร้คนขับประเภท 4 ใบพัดที่มาพร้อมกล้อง RGB ความละเอียด 20 เมกะพิกเซล สำหรับถ่ายภาพพื้นที่ปลูกจากความสูง 10 เมตรเหนือพื้นดิน เป็นระยะเวลาทุก ๆ 3 เดือนในช่วงปีแรกหลังจากการปลูก ตัวแปรที่ได้จากการรังวัดด้วยภาพถ่าย (รูปภาพ ออร์โธโมซายคและโครงสร้างพอยต์คลาวด์ 3 มิติ) ถูกเปรียบเทียบกับตัวแปรเดียวกันที่ได้จากการวัดภาคพื้นด้วยวิธีการทั่วไป ซึ่งผลจากการเปรียบเทียบเครื่องมือในซอฟต์แวร์รังวัดด้วยภาพถ่ายจากอากาศยานไร้คนขับในเบื้องต้น ทำให้ทราบว่า DroneDeploy มีประสิทธิภาพเหนือกว่าซอฟต์แวร์ทดลองอีก 2 ซอฟต์แวร์ในแง่ของการสร้างโครงสร้างพอยต์คลาวด์ 3 มิติและการวัดความสูงของกล้าไม้แบบแมนนวล ดังนั้นจึงถูกนำไปใช้กับการศึกษาส่วนที่เหลือ ผลในส่วนถัดมาพบว่าอัตราการรอดจับกล้าไม้ในภาพออร์โธโมซายคและโครงสร้างพอยต์คลาวด์ 3 มิติ อยู่ที่ 85% และ 64 % ตามลำดับ การวัดความสูงของกล้าไม้จากภาพถ่ายมีความสัมพันธ์กับการวัดแบบภาคพื้นดินเป็นอย่างมาก โดยมีความสัมพันธ์กันในระดับปานกลาง ($R^2 = 0.57, P < 0.001$) ในขณะที่การวัดพื้นที่ทรงพุ่ม (ทั้ง 2 รูปแบบการวัด) มีความสัมพันธ์กับการวัดแบบภาคพื้นดินเช่นกัน โดยมีความสัมพันธ์กันในระดับปานกลาง ($R^2 = 0.62$ และ $0.68, P < 0.001$) หลังจากที่ถูกกล้าไม้เติบโตครบ 1 ปี ความสัมพันธ์ของเส้นผ่านศูนย์กลางคอรากของกล้าไม้ที่ได้จากการประมาณค่าความสูงมีความสัมพันธ์กันในระดับต่ำ

($R^2 = 0.36$, $P < 0.001$) หลังจากที่ถูกกล้าไม้เติบโต 9 เดือนหลังปลูก ความน่าเชื่อถือในการตรวจนับและวัดขนาดกล้าไม้เพิ่มขึ้นในช่วงฤดูฝนที่สองหลังปลูก ซึ่งกล้าไม้ส่วนใหญ่โตได้สูงกว่า 0.8 เมตร ปัจจุบันการติดตามความคืบหน้าของกล้าไม้ที่ปลูกใหม่ด้วยวิธีการภาคพื้นนั้นแม่นยำกว่าการวิธีการติดตามโดยใช้โดรน อย่างไรก็ตาม ผลการศึกษาแสดงให้เห็นความสัมพันธ์ที่เพิ่มขึ้นของการติดตามโดยใช้โดรนภายหลังการเติบโต 1 ปี การศึกษาแสดงให้เห็นว่าฤดูกาล ลักษณะในแต่ละชนิดของกล้าไม้ อายุ และขนาดที่เหมาะสมของต้นกล้าเป้าหมาย ทั้งหมดต้องได้รับการ พิจารณาเพื่อพัฒนาเทคนิคทางอากาศที่เหมาะสม เพื่อติดตามความคืบหน้าของพื้นที่ฟื้นฟูระบบนิเวศป่าไม้ที่มีความซับซ้อนมากขึ้น ทั้งนี้เทคนิคที่ใช้ให้ผลที่มีความแตกต่างอย่างมากระหว่างข้อมูลที่ได้จากโดรนและภาคพื้นดินใน ส่วนของการจัดอันดับตามดัชนีประสิทธิภาพสัมพัทธ์ (relative performance index) เพื่อใช้ในการเลือกชนิดพันธุ์ จำเป็นต้องมีการปรับปรุงอย่างมากในการรวบรวมและวิเคราะห์ข้อมูลที่ได้จากภาพ ก่อนที่การเลือกชนิดพันธุ์โดยอิงจากข้อมูลทางอากาศนี้จะสามารถใช้ประกอบการตัดสินใจได้อย่าง น่าเชื่อถือ โดยเฉพาะอย่างยิ่งการประยุกต์ใช้เทคโนโลยี AI เพื่อทดแทนการวัดด้วยตนเอง ด้วยเหตุนี้ เมื่อการพัฒนาดังกล่าวบรรลุผลสำเร็จ เป็นไปได้ว่าเทคนิคการใช้ภาพถ่ายเพื่อติดตามกล้าไม้ใน ระยะแรกของการฟื้นฟูป่าจะกลายเป็นทางเลือกที่ปฏิบัติได้จริงแทนการสำรวจภาคพื้นดิน

ลิขสิทธิ์มหาวิทยาลัยเชียงใหม่
Copyright© by Chiang Mai University
All rights reserved

Thesis Title	Use of Unmanned Aerial Vehicle (UAV) Imagery to Monitor Progress of Early Forest Ecosystem Restoration in an Opencast Mine	
Author	Mr. Punnat Changsalak	
Degree	Master of Science (Environmental Science)	
Advisory Committee	Asst. Prof. Dr. Pimonrat Tiansawat	Advisor
	Assoc. Prof. Dr. Stephen Elliott	Co-advisor

ABSTRACT

Monitoring forest restoration is essential for improving and advancing restoration techniques, but human-based monitoring is costly as it requires intensive labour in the field. Although aerial images from unmanned aerial vehicles (UAVs) could potentially replace labour, aerial monitoring of newly planted trees is challenging because of small tree sizes, especially during the planting and initial growing stage. This research developed and tested an aerial technique to monitor survival and growth of young trees, which were planted to restore an open-cast mine. A quadcopter with 20-megapixel RGB camera was used to capture tree growth in the planted sites from 10 m above ground, every 3 months over the first year after planting. Tree variables, derived from photogrammetry (orthomosaic images and 3D point cloud software) were compared with conventional ground-survey measurements. Three photogrammetric software tools for this purpose were compared, DroneDeploy outperformed trial versions of 2 other software in terms of producing 3D point clouds and preliminary manual sapling height measurements. It therefore was used to perform the study. Orthomosaic images and 3D point clouds were able to detect rates of survival saplings up to 85% and 64 %, respectively. Tree-height measurements from imagery correlated well with ground-survey measurements ($R^2 = 0.57$, $P < 0.001$) with a moderate correlation, while crown area measurements (both methods) correlated with image-based measurement ($R^2 = 0.62$ and 0.68 , $P < 0.001$), after the trees had been growing 1 year. Correlation of tree root-collar diameter predictions from image-based height was low ($R^2 = 0.36$, $P < 0.001$), after the trees had been growing 9 months. Reliability of tree detection and measurements

increased during the second rainy season after planting, when most of the trees had grown taller than 0.8 meters. At present, monitoring progress of newly planted trees is more accurate by ground than by drone surveys. However, the study showed increased correlation of drone surveys after 1 year's growth. The study shows that seasonality, species traits, appropriate age and size of the target saplings all need to be considered during development of appropriate aerial-based techniques, to monitor the progress of forest ecosystem restoration sites of greater complexity. Differences between drone-acquired and ground data, when ranking species by relative performance index were large. Improvements in the collection and analysis of image-derived data will be needed, before aerial base species-selection decision making becomes reliable, particularly application of AI technologies to replace manual measurements. However, once such developments are achieved, it is likely that image-based methods to monitor saplings in the early stages of forest restoration will become a viable alternative to ground surveys.



ลิขสิทธิ์มหาวิทยาลัยเชียงใหม่
Copyright© by Chiang Mai University
All rights reserved

CONTENTS

ACKNOWLEDGEMENTS	iii
CONTENTS	viii
LIST OF TABLES	xi
LIST OF FIGURES	xiii
LIST OF ABBREVIATIONS	xvii
CHAPTER 1 Introduction and Literature Review	1
1.1 Background and Rational	1
1.2 Monitoring of Implemented Forest Restoration	2
1.3 Potential of Unmanned Aerial Vehicles to Monitor Forests	4
1.4 Using UAVs to Monitor Young Planted Trees	8
1.5 Using UAVs to Monitor Restoration Project in Mine Area	9
1.6 Research Objectives:	12
1.7 Scope and Limitations:	12
CHAPTER 2 Study Site and General Methods	13
2.1 Study Site	13
2.1.1 Site Preparation	14
2.1.2 Planted Saplings	15
2.1.3 Planting Method	15
2.2 Data Acquisition	17
2.2.1 Ground-based Survey	17
2.2.2 Aerial-based Survey	18
2.3 Image Processing and Image-based Data Measurement	20
2.3.1 Image Processing (Orthomosaic and 3D Point Clouds Generation)	20
2.3.2 Measuring variables from Orthomosaic Image	21
2.3.3 Measuring variables from 3D point clouds	23
CHAPTER 3 Comparison of Sapling Detection and Height Measurement Using 3D Point Cloud Models from Three Software Tools: Applications in Forest Restoration	25
Abstract	25
3.1 Introduction	26
3.2 Materials and Methods	27

3.2.1	Study Site	27
3.2.2	Data Acquisition	27
3.2.3	Software packages	27
3.2.4	Point Cloud Generation and Height Measuring Procedures	28
3.2.5	Output Comparison and Correlation Assessment	29
3.3	Results	29
3.3.1	Software Outputs and Ease of Use of Each Software	29
3.3.2	Sapling Detection Percentage	30
3.3.3	Correlation of Height Measurements	31
3.4	Discussion	32
CHAPTER 4	The Use of Imagery for Monitoring Sapling Survival and Growth over Time and Correlations with Non-Visible Sapling Variables	34
4.1	Introduction	34
4.2	Materials and Methods	35
4.2.1	Study Site	35
4.2.2	Data Acquisition	35
4.2.3	Image Processing and Image-based Data Measurement	35
4.2.4	Data Analysis	36
4.2.5	Relative Performance Index	37
4.3	Results	39
4.3.1	Sapling Survivorship and Detection	39
4.3.2	Aerial Measurements - Efficiency Over Time	42
4.3.3	The Relative Growth (RGR-H) and Performance Index	51
4.4	Discussion	55
4.4.1	Sapling Survivorship and Detection	55
4.4.2	The Correlation of Image-based Measurements	57
4.4.3	RGR and Relative Performance Index	61
4.4.4	Limitation of Image-based Techniques and Further Suggestion	63
4.4.5	Pros and Cons of Manual Image-based Measurements (compared with AI analyses)	67
CHAPTER 5	Conclusions	68
REFERENCES		70

APPENDICES	79
APPENDIX A (Additional) Ground-based Data	80
APPENDIX B (Additional) Image-based Data	84
CURRICULUM VITAE	98

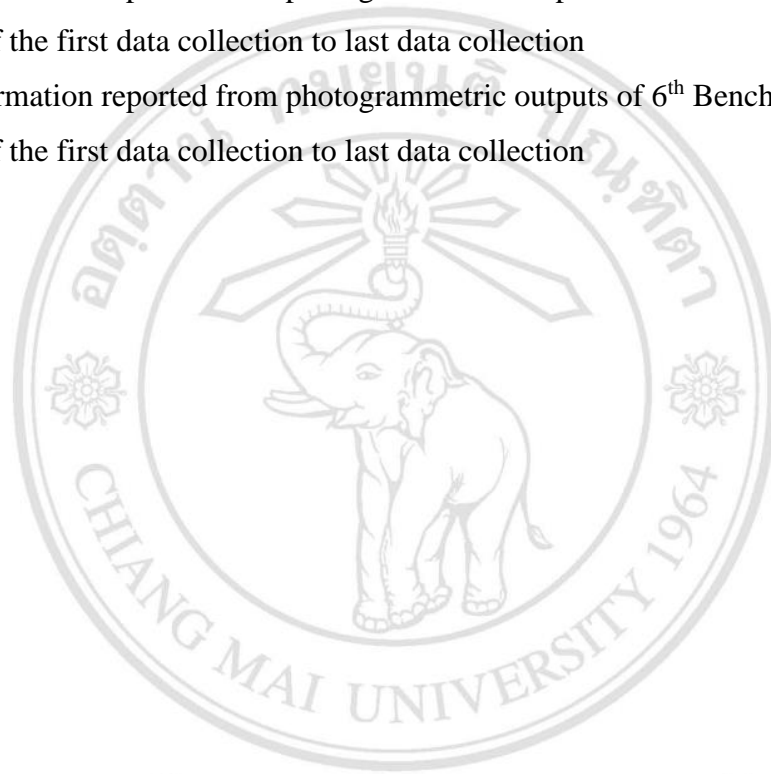


ลิขสิทธิ์มหาวิทยาลัยเชียงใหม่
Copyright© by Chiang Mai University
All rights reserved

LIST OF TABLES

Table 1 Average width and total length of the benches within the study site	14
Table 2 Native species of planted saplings in restoration plot year 2020 as the total number 1,298 saplings	16
Table 3 UAV flight mission settings	20
Table 4 Characteristic report of the 3D point clouds from each software. Check marks (✓) indicate “reported” while blank cells indicate “not reported” from the software	30
Table 5 The criteria indicating the ease of use of the three selected software	30
Table 6 Percentage of saplings detected by each software	31
Table 7 Comparison of mean height from ground-based data, image-based data, and percentage of under/over-estimation	42
Table 8 Comparison of mean crown area (CA-LW) value from ground-based data, image-based data, and percentage of under/over-estimation	44
Table 9 Comparison of mean crown area (direct-CA) value from ground-based data, image-based data, and percentage of under/over-estimation	46
Table 10 Slope (m), intercept (c), and coefficient of determination (R^2) from ground-survey data: height vs RCD, and CA vs root collar diameter	49
Table 11 Comparison of mean RCD value from ground-based data, image-based data, and percentage of under/over-estimation	50
Table 12 Comparison of mean root collar diameter and height from ground-based data between alive saplings and alive-not-found (ANF) saplings	56
Table 13 Slope (m), intercept (c), and coefficient of determination (R^2) from relationship between height vs RCD for individuals of the 17 cohort species	60
Table 14 Number of live saplings detected in ground surveys by time and species	80
Table 15 Numbers of sample saplings for which ground-based data acquired during each time of data collection by bench and time	81
Table 16 Simple regression coefficient predicting root collar diameter (N=428)	81
Table 17 Simple regression coefficient predicting root collar diameter of individual sapling cohort species (N>20)	81
Table 18 Information reported from photogrammetric outputs of 1 st Bench; in the order of the first data collection to last data collection	84

Table 19 Information reported from photogrammetric outputs of 2 nd Bench; in the order of the first data collection to last data collection	84
Table 20 Information reported from photogrammetric outputs of 3 rd Bench; in the order of the first data collection to last data collection	84
Table 21 Information reported from photogrammetric outputs of 4 th Bench; in the order of the first data collection to last data collection	85
Table 22 Information reported from photogrammetric outputs of 5 th Bench; in the order of the first data collection to last data collection	85
Table 23 Information reported from photogrammetric outputs of 6 th Bench; in the order of the first data collection to last data collection	85



ลิขสิทธิ์มหาวิทยาลัยเชียงใหม่
 Copyright© by Chiang Mai University
 All rights reserved

LIST OF FIGURES

Figure 1 Monitoring by hand: measuring tree height and root collar diameter	4
Figure 2 Technology for data collection; ground-based methods (left), and aerial-based method (right) (Heliguy, 2022)	5
Figure 3 Comparison of costs for the same site (US\$ thousands) between ground-based methods (gray bar), and aerial-based method (color bar) (DroneDeploy, 2022)	6
Figure 4 Additional UAV-mounted sensors; Multispectral camera, Thermal camera, and Dual camera and Lidar (from left to right)	6
Figure 5 Examples of generated orthomosaic images, DSM, DTM and CHM from the UAV imagery for tree-damage detection (Klein Hentz & Strager, 2018)	7
Figure 6 Examples of sapling monitoring (<i>Lupinus angustifolia</i> , red polygons indicate the outline of target sapling), captured from the RGB images (top row) and multispectral (bottom row)	9
Figure 7 The limestone quarry locates in The Siam Cement Public Company Limited mine site (Satellite map acquired from Google Earth)	13
Figure 8 The forest restoration area plot year 2019 (left-handed side with 1 year planted saplings) and year 2020 (right-handed side without any sapling before planting date)	14
Figure 9 Phantom 4 Pro V2.0 UAV (left), landing after finishing mission by manual catching (right), due to unstable ground surface	19
Figure 10 UAV waypoint mission in Litchi flight planner, for 1 st bench; indicating the above ground height of each way point; 4 route lines with different camera angles	20
Figure 11 Orthomosaic image (a), elevation model (b), and 3D point cloud model (c), example of 1 st bench result from last data collection	21
Figure 12 Distance measuring tool in DroneDeploy website interface; the perpendicular line indicates the length and width of sapling crown	22
Figure 13 Area measuring tool in DroneDeploy website interface; the covered light red-color area indicates the selected crown of the sapling	23
Figure 14 Point Picking tool in CloudCompare software; the vertical line indicates the sapling height (quantity information shown in tiny red box)	24

Figure 15 Linear regressions between the measured height from 3D models and ground truth data (for detected saplings): (a) Pix4D mapper (n = 51), (b) DroneDeploy (n = 75) (b) and (c) WebODM (n = 29)	31
Figure 16 Linear regression between the measured height from 3D model and ground truth data: overlapping detected saplings among three software (n = 15) from Pix4D mapper (a), DroneDeploy (b), WebODM (c)	32
Figure 17 Ground-based variables relationship utilization	36
Figure 18 Comparison of sapling number between ground-based data (yellow bar) and image-based data (blue bar in 3 gradient color) from five collection date. The number at the top of the bar represents saplings percent detected from each measurement image-based method	39
Figure 19 Percentage survival from ground and aerial surveys on the last data collection (16/9/2021). The number at the end of each bar is the per cent aerial detection rate of each species (drone-based survival as a percent of ground-based survival)	40
Figure 20 Scatter plot between species-level mean sapling height (cm) and percentage species-level detectability (17 species with n > 20) at September 2021	41
Figure 21 Scatter plot between species-level mean sapling crown area (cm ²) and percentage species-level detectability from CA-LW (yellow dot, R ² = 0.0959) and direct-CA (red dot, R ² = 0.0487) method. at September 2021	41
Figure 22 Regression analysis against height of ground-based and image-based data from each data collection; (a) 29/9/2020 10/12/2020 (b), 11/3/2021 (c), 13/6/2021 (d), and 16/9/2021 (e) (a-e; P < 0.05). Histogram of residuals indicates normality distribution between the fitted line and each data collection	44
Figure 23 Regression analysis against CA-LW of ground-based and image-based data from each data collection; 29/9/2020 (a), 10/12/2020 (b), 11/3/2021 (c), 13/6/2021 (d), and 16/9/2021 (e) (a-e; P < 0.05). Histogram of residuals indicates normality distribution between the fitted line and each data collection	46
Figure 24 Regression analysis against direct-CA of ground-based and image-based data from each data collection; 29/9/2020 (a), 10/12/2020 (b), 11/3/2021 (c), 13/6/2021 (d), and 16/9/2021 (e) (a-e; P < 0.05). Histogram of residuals indicates normality distribution between the fitted line and each data collection	48

Figure 25 Regression analyses between RCD of ground-based and image-based data from each data collection; 29/9/2020 (a), 10/12/2020 (b), 11/3/2021 (c), 13/6/2021 (d), and 16/9/2021 (e) (a-c; $P > 0.05$, d-e; $P < 0.05$). Histogram of residuals indicates normality distribution between the fitted line and each data collection	51
Figure 26 Relative growth rate calculated based on measured height of 17 cohort sapling species	53
Figure 27 Relative Performance Index calculated from % survival and RGR of 17 cohort sapling species	54
Figure 28 Comparison between <i>Fernandoa adenophylla</i> (left) and <i>Phyllanthus emblica</i> (right) leaf characteristic; upper row – orthomosaic image, lower row – raw RGB image	57
Figure 29 Scatter plot between species-level mean relative growth rate (% per year) and percentage species-level detectability (17 species with $n > 20$)	62
Figure 30 <i>Cajanus cajan</i> (Pigeon Pea) caused difficulty in tree distinction and variables measurement; A part of orthomosaic image on 16/9/2021 (1-year old tree) (a), one of the raw RGB images used in this processed image (b)	65
Figure 31 Difficulty of height measurement on the youngest age of planted sapling (0 month); original RGB-perspective (a), edited color related to attitude failed to detect sapling pixels (b)	66
Figure 32 The orthomosaic images of 1 st Bench. In the order of the first data collection to last data collection (left to right); a-e, respectively. The letter “N” to represent North	86
Figure 33 The 3D point clouds images of 1 st Bench. In the order of the first data collection to last data collection (left to right); a-e, respectively. The letter “N” to represent North	87
Figure 34 The orthomosaic images of 2 nd Bench. In the order of the first data collection to last data collection (left to right); a-e, respectively. The letter “N” to represent North	88
Figure 35 The 3D point clouds of 2 nd Bench. In the order of the first data collection to last data collection (left to right); a-e, respectively. The letter “N” to represent North	89

Figure 36 The orthomosaic images of 3 rd Bench. In the order of the first data collection to last data collection (left to right); a-e, respectively. The letter “N” to represent North	90
Figure 37 The 3D point clouds of 3 rd Bench. In the order of the first data collection to last data collection (left to right); a-e, respectively. The letter “N” to represent North	91
Figure 38 The orthomosaic images of 4 th Bench. In the order of the first data collection to last data collection (left to right); a-e, respectively. The letter “N” to represent North	92
Figure 39 The 3D point clouds of 4 th Bench. In the order of the first data collection to last data collection (left to right); a-e, respectively. The letter “N” to represent North	93
Figure 40 The orthomosaic images of 5 th Bench. In the order of the first data collection to last data collection (left to right); a-e, respectively. The letter “N” to represent North	94
Figure 41 The 3D point clouds of 5 th Bench. In the order of the first data collection to last data collection (left to right); a-e, respectively. The letter “N” to represent North	95
Figure 42 The orthomosaic images of 6 th Bench. In the order of the first data collection to last data collection (left to right); a-e, respectively. The letter “N” to represent North	96
Figure 43 The 3D point clouds of 6 th Bench. In the order of the first data collection to last data collection (left to right); a-e, respectively. The letter “N” to represent North	97

LIST OF ABBREVIATIONS

m	meter
m ²	square meter
cm	centimeter
cm ²	square centimeter
mm	millimeter
in	inch
RCD	root collar diameter
CA	crown area
CA-LW	crown area from length and width
Direct-CA	direct crown area
RPI	Relative Performance Index
RGR	Relative Growth Rates
RGR-H	Relative Growth Rates from height
px	pixel
r	coefficient of correlation
r ²	coefficient of determination
RMSE	root mean square error

ลิขสิทธิ์มหาวิทยาลัยเชียงใหม่
Copyright© by Chiang Mai University
All rights reserved

CHAPTER 1

Introduction and Literature Review

1.1 Background and Rational

Deforestation is a damaging form of long-term land-use change (FAO, 2020) resulting in resource depletion at the landscape level, diminished ecological functioning (Picchio et al., 2020; Kyere-Boateng & Marek, 2021), biodiversity loss and contributing towards global climate change (Yaduv et al., 2018; Kyere-Boateng & Marek, 2021). From 2015 to 2020, the rate of natural forest declined was estimated at 10 million hectares per year (FAO, 2020), with remaining forest unequally distributed around the globe (FAO and UNEP, 2020). Deforestation has resulted in fluctuations in rainfall and increased dry-season length and drought frequency (Boulton et al., 2022). Over 3 billion people and 30% of Earth's arable land are affected by the critical problem of land degradation. Consequently, nationally determined forest restoration measures are needed (<https://www.bonnchallenge.org/>).

Over the past decade, awareness of such environmental problems has grown, as the impact of development on nature and human life becomes more apparent (Gann et al., 2019). Forest restoration is one method to counteract continued forest ecosystem destruction and degradation (Picchio et al., 2020; Brudvig, 2011). At the global level, the Bonn Challenge aims to restore 150 million hectares of damaged and deforested landscapes by 2020 and 350 million hectares by 2030 (<https://www.bonnchallenge.org/>). Currently, 74 pledges from 61 countries amount to an intention to restore 210.12 million hectares of degraded and deforested lands (<https://www.bonnchallenge.org/progress>).

Tree planting is advocated to address a range of degrees of degradation (Sasaki et al., 2011), because it accelerates biomass accumulation and provides wildlife habitat (Omeja et al., 2016). After tree planting, two important questions are how many

of the planted trees survive and how fast do they grow? Therefore, monitoring the survival and growth of both planted and natural trees is essential, to evaluate the success of restoration projects (Dash et al., 2017). However, planted tree saplings are small at the initial stage of restoration and skilled labor is required to monitor them by hand—a time consuming process. Therefore, techniques advanced techniques to reduce time and laboru requirements of restoration monitoring are needed (Fujimoto et al., 2019).

Drone can fly close to monitored objects and capture high-resolution images (Yue et al., 2015). The application of such technologies is feasible to rapidly monitor individual saplings. Therefore, drones may become an efficient alternative to ground-based monitoring (Yao et al., 2019). However, research is needed to develop the potential of drones and to identify limitations associated with their use.

1.2 Monitoring of Implemented Forest Restoration

Forest restoration is likely to be the only long-term option to meet the growing demand for ecosystem services offered by forests, particularly the many provisioning services from forests, as many people strongly rely on forests for livelihoods and products. As a result, restoration is an important approach that can help promote biodiversity in human-affected ecosystems whilst also mitigating the effects of climate change (Aerts & Honnay, 2011). After forest restoration projects have been implemented, adequate monitoring is essential but is also often overlooked. It is necessary not only to collect data on tree survival and growth, but also to learn from past successes and failures to modify future practices. However, at the start of restoration, planted tree saplings (and most of the naturally regenerating ones) are small and extremely vulnerable to competition with herbaceous weeds and pests etc. Degraded areas are harsh environments, leading to high mortality of planted trees, if they are not given proper care and protection during the first two years after planting. This results in wasted effort. The time and supplies needed to guarantee that newly planted trees thrive are frequently underestimated (Elliott et al., 2020). Monitoring is essential, but it is also challenging (Buters et al., 2019a).

Monitoring methods must be adaptable to site conditions, such as substrate, vegetation, topography, and geology (Moreno-de las Heras et al., 2008) and may vary with restoration objectives. Consequently, the specific objectives of monitoring must be clearly defined from the start; baseline data collected, and subsequent data collection scheduled at appropriate intervals (significant time) thereafter, and compared with control plots (Buters et al., 2019b). A crucial requirement is sufficient labor needed to collect data on the progress of planted trees performance (Dash et al., 2017). In conventional monitoring, the variables of interest include basic counts of live and dead trees, as well as measurements of sapling growth such as tree height, girth at breast height (GBH), and/or root collar diameter (RCD), and crown width. Recording the state of planted trees (assigning a health score or making notes about any unique health problems found) would be beneficial for a more thorough assessment of tree growth (Elliott et al., 2020). All variables are measured by hand during ground surveys (Figure 1), in sample plots (usually circular plots 10 m in diameter), with results extrapolated to provide an estimate (usually with large error limits) across the entire site (Anderson & Gaston, 2013).

Workers work in pairs, with one taking measurements and the other entering data; one pair can gather data on up to 400 trees each day. In Northern Thailand, two people are required to monitor approximately 500 saplings per day (~an area of 40 x 40m) (Elliott et al., 2020). Measurements are made 1–2 weeks after planting, to provide a baseline for growth calculations and to check for immediate post-planting mortality, due to transplantation shock or rough handling during planting. After that, monitoring is performed annually at the end of each rainy season. The most critical monitoring event occurs at the conclusion of the second rainy season after planting (or after 18 months), when field performance data may be utilized to measure each tree species' suitability for the existing site conditions (Elliott et al., 2020). Nevertheless, the availability of skilled labor can be limiting, for identifying saplings individually and monitoring saplings frequently. The work is time-consuming and can be extremely difficult in dense vegetation communities and on exposed harsh conditions or rough terrain such as that of open cast mines. This has led to an urgent need for the application of reliable technologies to provide restoration researchers with rapid and scalable plant-based monitoring

solutions (Buters et al., 2019a). Data acquisition via technologies is therefore an attractive alternative (Yao et al., 2019).



Figure 1 Monitoring by hand: measuring tree height and root collar diameter.

1.3 Potential of Unmanned Aerial Vehicles to Monitor Forests

The choice of remote-sensing platforms and sensors is dependent on the specific spatial and temporal scales of the research (Reis et al., 2019; Torresan et al., 2017) and the researchers should select a platform that is not only capable of attaining project objectives but is also labor- and cost-efficient (Miranda et al., 2020; Tahar, 2015). Many studies employ remote sensing to analyze a process, an object, or a phenomenon without having to be physically present, thus having a negligible impact upon ecologically sensitive areas or species of interest. Researchers can use remote sensing to evaluate and survey areas that are otherwise inaccessible or where trespassing is prohibited. Remote sensing measures reflected and emitted radiation at a distance—frequency, and wavelength. Among the numerous technologies used for remote sensing, unmanned aerial vehicles (UAVs); one type of remote sensing technology besides aircraft and satellites; can fly without the need for a human pilot. UAVs can traverse large areas rapidly and are

unaffected by the difficulty of the terrain. Forest monitoring at the landscape level has progressed greatly since the introduction of UAVs. They can collect large numbers of high-resolution images even during short flights, allowing researchers to conduct virtual site surveys over large areas (Johansen et al., 2019). Since they can fly close to surveyed objects, UAVs provide the most flexible data-acquisition platform and the highest imaging resolution (Yue et al., 2015). Consequently, data from UAVs allow for the characterization and quantification of the different phases of forest degradation in unprecedented detail. UAVs are efficient for monitoring small objects or even distinguishing trees from complex backgrounds (Berni et al., 2009; Buters et al., 2019a).



Figure 2 Technology for data collection; ground-based methods (left), and aerial-based method (right) (Heliguy, 2022).

The cost and availability of UAVs have been significant barriers to their use in research initiatives in the past. However, costs are coming down and UAVs are relatively inexpensive, when compared to manned aircraft or satellites (Ogden, 2013). Most UAVs are equipped with common optical sensors, factory-standard digital Red-Green-Blue (RGB) cameras carried by most commercial UAVs, sensors also include multispectral and hyperspectral cameras, thermal imaging, and light detection and ranging (Lidar) units. RGB cameras are viable options for obtaining several kinds of forest information such as vegetation maps, canopy maps, height maps, biomass estimation, invasive weed mapping, forest structural and property measurement, etc. In addition, the use of RGB images is cheaper than the lidar itself (Grenzdörffer et al., 2008). Other sensors such as multispectral and hyperspectral produce imagery with even more detail for land-use classification, disease detection, and identification, water status

estimation, forest fire detection, and monitoring or even wildlife detection and identification (Frame & Garzon-Lopez, 2020; Fromm et al., 2019; Pádua et al., 2017; Gatziolis et al., 2015; Shimizu et al., 2014), but they are also more expensive than RGB cameras and interpretation of their data requires advanced software, with steep learning curves. Consequently, their use in native species' ecological recovery monitoring has been limited.



Figure 3 Comparison of costs for the same site (US\$ thousands) between ground-based methods (gray bar), and aerial-based method (color bar) (DroneDeploy, 2022)



Figure 4 Additional UAV-mounted sensors; Multispectral camera, Thermal camera, and Dual camera and Lidar (from left to right).

A particularly attractive feature of UAV imagery is the potential to stitch adjacent images together to produce 3D forest models, using structure-from-motion (SfM) photogrammetry (Lindberg and Holmgren, 2017). Soft-copy triangulation and image-based terrain extraction techniques have greatly improved the quality of terrain data that can be extracted from overlapping images. UAV imagery can provide several kinds of output, including orthomosaic images, 3D point cloud models, elevation models,

digital terrain models (DTM), digital surface models (DSM), and canopy height models (CHM) (Zhang et al., 2015). Some of these outputs can be integrated, to increase classification correlation and perform accurate and precise object interpretation and classification, scene analysis, and change detection (Yao et al., 2019).

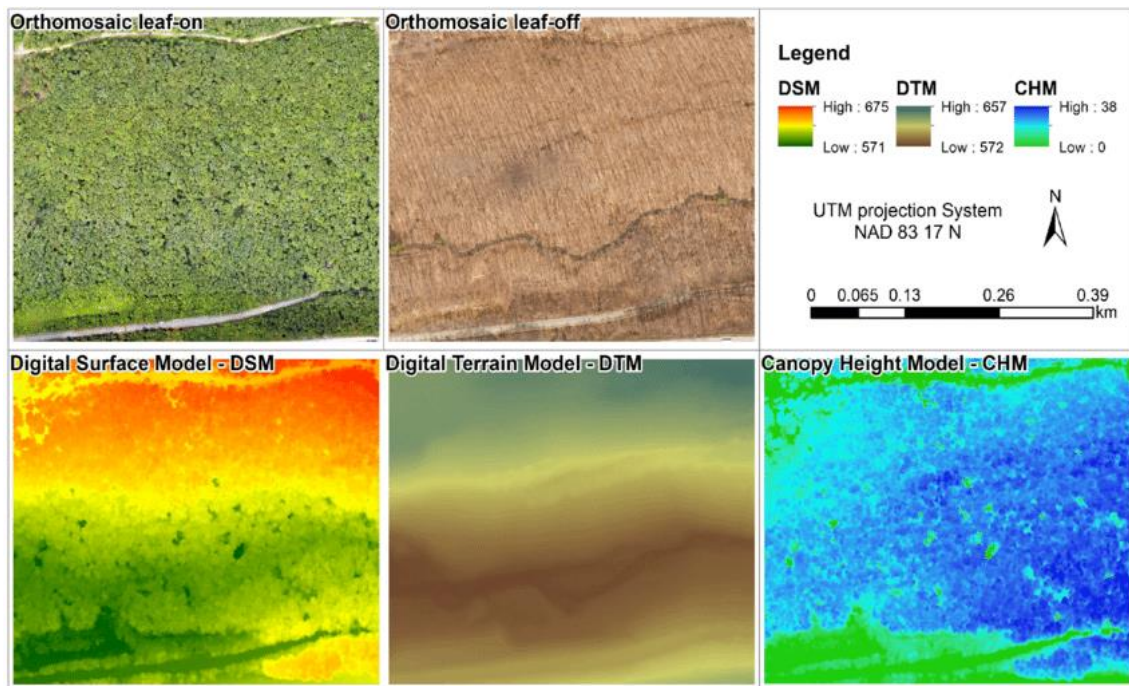


Figure 5 Examples of generated orthomosaic images, DSM, DTM and CHM from the UAV imagery for tree-damage detection (Klein Hentz & Strager, 2018).

Therefore, the use of UAVs has improved the efficiency of forest monitoring and has been widely used to monitor not only vegetation but also ecological change (Aerts & Honnay, 2011). Relatively cheap operating costs and fewer infrastructure needs (compared with conventional aircraft or satellites) result in accessible and cost-effective data collection with significantly greater spatial resolution. It is also useful for long-term dynamic vegetation monitoring when compared to traditional forest monitoring. Potential limits on the feasibility of UAVs in ecological restoration monitoring must be studied, and ways to reduce them must be investigated in order to maximize the quality, reliability, and comparability of data provided (Itkin et al., 2016; Buters et al., 2019b).

1.4 Using UAVs to Monitor Young Planted Trees

Nonetheless, using UAV technology, to monitor the early stages of forest restoration, is particularly difficult, because the saplings are small, weeds may appear similar to the saplings or obscure them with a high reflectance, and the fact that they may be hidden beneath a canopy of herbaceous weeds. Another difficulty is due to small changes in leaf reflectance during the day, which can affect image recognition (Mahlein et al., 2013). Furthermore, Nebiker et al. (2008) suggest that lack of near-infrared detection by RGB cameras may limit their use for identifying or monitoring small trees.

Processing technologies such as object-based image analysis (OBIA), can detect distinct spectral signatures to accurately differentiate between target and non-target vegetation. The ability of UAV-based monitoring to undertake performance monitoring of individual plants at extremely fine spatial scales has been shown by accurately tracking individual target objects across time using OBIA classification from acquired imagery. Individual treetops can also be described using segmentation imaging techniques, which combine spectral information and digital surface models. Accurate OBIA requires use of multi-spectral cameras to detect distinct spectral signatures. In fact, using multispectral images with classification algorithms significantly improves individual target-plant recognition. However, even multi-spectral sensors could not provide enough information to fully understand every component of observed plant performance. Therefore, more advanced sensors, such as thermal and hyperspectral sensors, are likely to improve this capacity, although they are currently three to twelve times more expensive than multi-spectral cameras (Buters et al., 2019c). Chisholm and Swinfield (2020) added that using UAV images to assess regeneration is tough; only lidar can be used to directly measure understory features. When small saplings growth beneath the forest understory, UAV-mounted lidar technology allows for below-canopy measurements to be taken while flying above the canopy or between the trees within the forest, although such technologies are costly than RGB cameras.

When monitoring goals necessitate the identification of small characteristics of interest, a high spatial resolution, additional sensors other than the custom camera are required (Buters et al., 2019c). At the same time, monitoring of several characteristics of

these young regenerants, greater volumes of data will be collected, making imagery classification a more difficult task (Buters et al., 2019b)

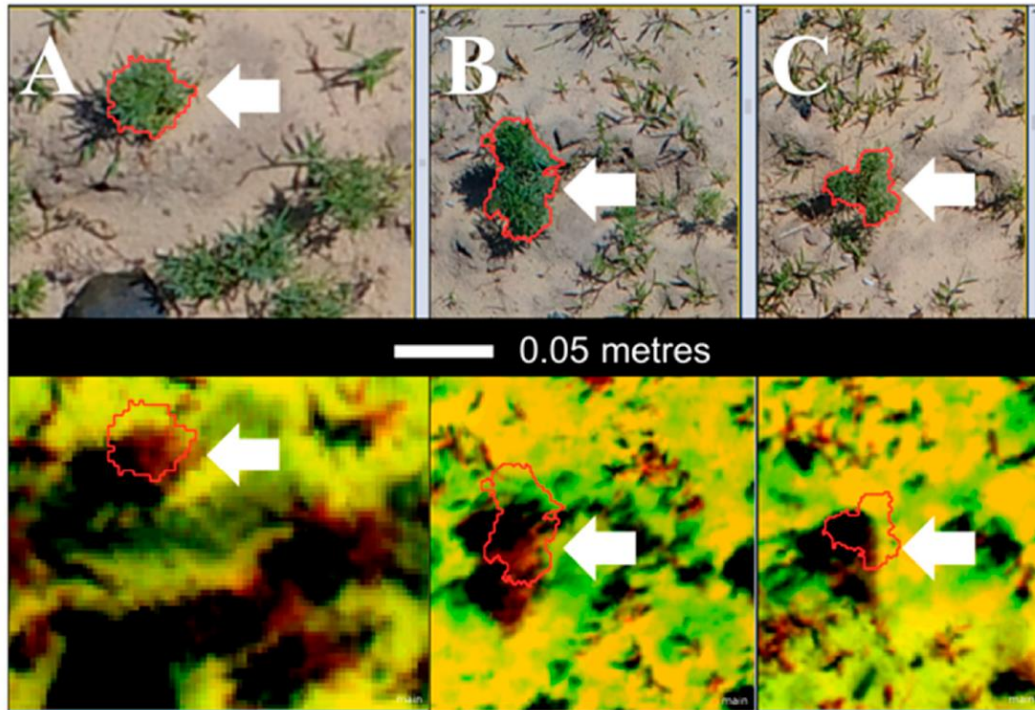


Figure 6 Examples of sapling monitoring (*Lupinus angustifolia*, red polygons indicate the outline of target sapling), captured from the RGB images (top row) and multispectral (bottom row).

1.5 Using UAVs to Monitor Restoration Project in Mine Area

Most governments recognize the necessity for post-mining restoration and have enacted legislation requiring mining corporations to meet certain requirements for restored landforms, topsoil, flora and water quality (McKenna et al., 2020). Ecological monitoring is the most typical technique for mining corporations to show restoration achievement and give assurance for mine closure. Restoration starts with landscapes made up of isolated vegetation patches at various phases of development, with underlying soil quality and terrain topography varying substantially over short distances, compared with unmined land. Furthermore, restoration managers frequently change inputs like seed mixes, topsoil depth and site preparation processes, resulting in significant levels of spectral variation within and between patches on post-mining landscapes. Several studies

demonstrate that multi-temporal assessment of mine restoration sites is required, to determine their eligibility for relinquishment. (Erskine & Fletcher, 2013)

The International Society for Ecological Restoration (SER) has created a “ecological recovery wheel” monitoring tool, to assist restoration initiatives and quantify recovery paths in comparison with native ecosystems. By focusing on the important indicators of restoration: structural diversity, species composition, physical conditions, external exchanges, ecosystem functioning and the absence of threats, this tool assists in defining the qualities and sub-attributes that are required to identify successful ecosystem recovery (Gann et al., 2019). Monitoring ecological recovery programs, such as ecological restoration, is critical to ensure that predetermined targets are accomplished and to inform adaptive management where trajectories are unsatisfactory. It is a complicated process, which involves extensive planning, precise and focused on-the-ground efforts, and precise subsequent monitoring and adaptive management over lengthy time periods. With increasing spatial and temporal scales of ecological recovery projects, the demand for more rapid and accurate techniques of predicting restoration trajectory is growing. With many mining operations being in remote areas, post-mine landforms are frequently steep, unstable, or dangerous to walk across (e.g., waste rock landforms and tailings storage facilities). When viewed from above, modern mines are recognized by open cut pits, waste rock dumps, tailings dams, water storage ponds, access roads, milling and processing facilities, infrastructure (e.g., worker housing). Such characteristics are difficult to monitor on the ground, but their environmental impacts can be seen clearly in aerial images (Buters et al., 2019c).

Over the last decade, the amount of ecologically focused remote sensing studies on mine site restoration has gradually expanded (Buters et al., 2019b; Park & Choi, 2020). UAV-based sensors have enabled researchers to gain better knowledge of vegetation development during post-mining restoration. UAVs offer an effective monitoring solution for these landforms, on which restoration or ecological restoration are frequently regulatory requirements because UAVs can access areas not accessible by foot. Furthermore, the use of UAVs avoids trampling of regenerating plant communities. It also avoids human exposure to hazardous conditions. UAV technology has made it

possible to visualize, map, and monitor mining impacts and landscape recovery for the mining sector all over the world. UAV data can be used to map restoration success and generate evidence of meeting restoration site requirements at various scales. (Johansen et al., 2019). UAVs can be used to infer useful ecological information over recovering landscapes with specific spectral, temporal, and spatial patterns. For example, progressive restoration creates patchworks of distinct age-classes, which can be examined with a single image, to create change trajectories of ecological metrics like vegetation cover, woody density, and species richness. A field-based understanding of establishment age, site preparation techniques, seeding mixtures, and reflectance values is also necessary for the application of UAVs to monitor the restoration site. However, using UAVs may ignore the significance of preferred plant species, the absence of weeds, and the structural elements of developing ecosystems, all of which are required to accomplish the desired landscape recovery traits (McKenna et al., 2020). The focus of studies on spatial mosaics demonstrates the need for better knowledge of UAVs' capacity to monitor restoration performance. Therefore, further investigations of the capacity of UAV to assist with restoration projects are necessary (Chen et al., 2018).

Due to high levels of disturbance, post-mining restoration differs from non-mining restoration operations. The use of UAVs to monitor restoration in mine areas also differs from non-mining areas. Moreover, interpreting analysis outputs and extracting relevant results from UAV assessments of mine site restoration requires a high level of knowledge and experience. Automated mapping can be used in a variety of mine restoration scenarios, as they are not site-specific and can thus be extended to different locations and situations. However, it is crucial that UAV images of maximum quality are acquired to maximize the quality of structure-from-motion derived DSMs, allowing accurate tree, shrub, and grass discrimination, based on height information (Johansen et al., 2019).

New approaches to the use of UAVs for restoration are needed to make use of recent technical breakthroughs and improvements in our understanding of restoration. Moving beyond traditional land cover evaluations and adopting standardized methodologies, to measure a variety of ecological variables, as defined by SER

International standards, has tremendous potential. These opportunities could occur as a result of the creation of tools to assist restoration practitioners and regulators, such as methods to quantify long-term success, such as resistance to climate change and stochastic events, or methods to measure short-term achievement of success criteria.

Therefore, the study reported in this thesis investigated the potential and limitations of an UAV-based protocol, to monitor the early stage of forest restoration on and open-pit mine.

1.6 Research Objectives:

1. To develop a rapid aerial-based technique to monitor young saplings, planted for open-cast mine restoration, which minimizes labor input whilst meeting required industry standards.
2. To determine what sapling variables can be quantified directly from low-altitude UAV imagery.
3. To compare ground-based and aerial-image-based measurements of survival, growth and crown expansion of young trees planted for restoration of an open-cast mine.

1.7 Scope and Limitations:

1. This was a proof-of-concept study, to determine what can be achieved in terms of monitoring survival and growth of recently planted saplings, under ideal visibility conditions, using currently available technologies.
2. Its scope was restricted to clearly quantifiable variables (height, crown size etc.), rather than subjective variable (e.g., health score).
3. Its scope was restricted to a mine site, where saplings (from recently planted to 1 year old) were easily visible against the plain background of mine substate.
4. Its scope of the study was restricted to manual measurements on orthophotos and 3D models, using tools within photogrammetric software (by single operator), compared with the same field measurements (i.e., use of AI to perform measurements within images was excluded).

CHAPTER 2

Study Site and General Methods

2.1 Study Site

The Siam Cement Public Company Limited (SCG) limestone quarry, with a total concession area of 12.144 km² (7,590 rai) Chae Hom district, Lampang province (18°32'41.7"N 99°34'11.4"E; elevation 423 m) (Figure 7). It is the first Semi-Open Cut Mine in northern Thailand and the company's fifth limestone quarry. Open-cut mining effectively removes mountain peaks, whereas mines on flat areas (open-pit mining) create deep depressions in the landscape. Semi open cut mining (the innovative technique of the SCG, Thailand) combines these 2 techniques. SCG has been open for operation since 1996, with a production capacity of 2.4 million tons per year. The study was conducted in a forest restoration area (initiated post-mining in the year 2020) covering a total area of 5 rai, in the 1st phase pit during as it was being decommissioned.

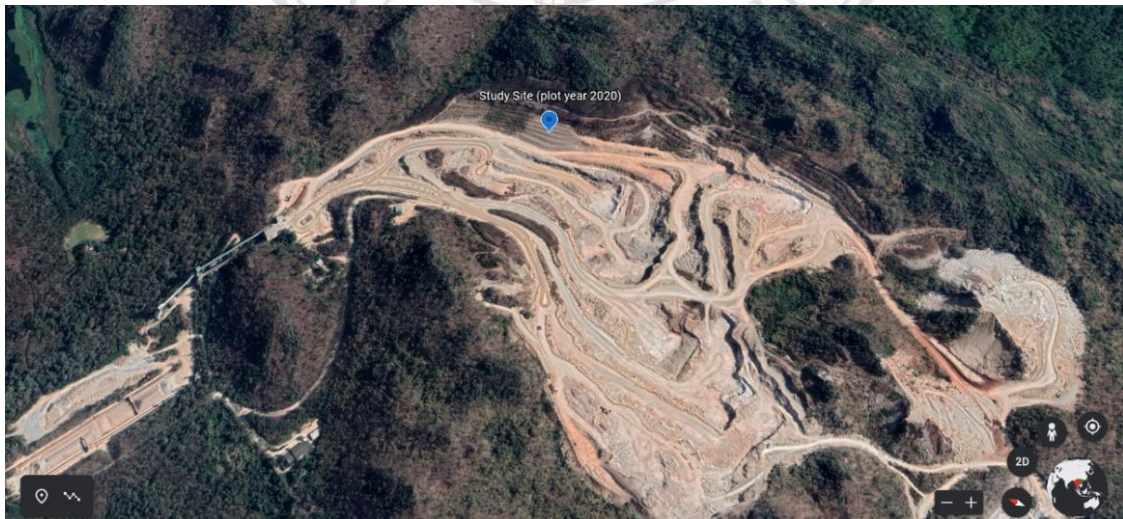


Figure 7 The limestone quarry is located in The Siam Cement Public Company Limited mine site (Satellite map acquired from Google Earth).

2.1.1 Site Preparation

Before planting saplings to restore the area, additional soil was spread across the site and bulldozed into terraces, resulting in 6 flat benches (of various lengths/widths) (Table 1) separated by 45°-angle walls, to minimize soil erosion (Figure 8). Along the benches, 30×30-centimeter square holes were dug randomly (i.e., not in straight lines, spacing range approximately 1-3 m. apart; averaging 1.9 m apart). The polymer was placed at the bottom of each hole (to increase the substrate's water-holding capacity) along with manure.

Table 1 Average width and total length of the benches within the study site

Bench Order	Average Width (m)	Length(m)
1 st	8.01	123.38
2 nd	5.67	120.89
3 rd	5.79	114.51
4 th	5.04	102.57
5 th	6.78	100.14
6 th	5.23	96.67



Figure 8 The forest restoration area plot year 2019 (left-handed side with 1 year planted saplings) and year 2020 (right-handed side without any sapling before planting date).

2.1.2 Planted Saplings

A total of 1,303 saplings of 30 species of native trees, representative of the reference forest ecosystem (bamboo deciduous forest *sensu* Maxwell and Elliott, 2001), were included in the study. SCG staff collected the fruits of each species in the appropriate season and germinated them in the on-site tree nursery. Saplings were grown in the nursery for 8-18 months (depending on species) until they had well-developed root systems. They varied in height (depending on species) from 10 to 40 cm. Saplings were hardened off, with reduced watering and increased exposure to direct sunlight, for at least 4 weeks before planting. Seven days before the planting date, the nursery staff cut off half of the sapling leaves to reduce transplantation shock. Individual saplings were then labeled for monitoring, using soft aluminum strips (of the type used to bind electrical cables). Code numbers were species codes followed by consecutive numbers for each species: e.g., S01_01, S24_01, etc. (Table 2).

2.1.3 Planting Method

Saplings were randomly assigned to planting holes) and planted on August 20th, 2020, by SCG and the Forest Restoration Research Unit (FORRU) staff. The rows followed a zigzag pattern (not straight) to create a more natural looking forest. The number of rows differed among the benches due to variability on bench width. Average distance between adjacent saplings was slightly more than that recommended by FORRU (>1.8 meters apart). SCG staff will continue to monitor this plot for the first 3 years (first 2 rainy season following procedure of FORRU method). In addition, mine officers were appointed to prevent and watch out for forest fires and landslides.

Table 2 Native species of planted saplings in restoration plot year 2020 as the total number 1,298 saplings.

Label number	Sapling number	Thai Name	Species	Deciduous Habit
S01	1-50	ซ้อ	<i>Gmelina arborea</i> Roxb.	✓
S24	1-50	มะกอกป่า	<i>Spondias pinnata</i> (L.f.) Kurz	✓
S06	1-50	มะขามป้อม	<i>Phyllanthus emblica</i> L.	✓
S07	1-50	มะค่าโมง	<i>Azelia xylocarpa</i> (Kurz) Craib	✓
S08	1-50	สมอพิเภก	<i>Terminalia bellirica</i> (Gaertn.) Roxb.	✓
S09	1-30	สัก	<i>Tectona grandis</i> L.f.	✓
S11	1-50	เสี้ยวดอกแดง, ชงโค	<i>Bauhinia purpurea</i> L.	✓
S26	1-63	พญาสัตต (ฝักตุล)	<i>Albizia lebeck</i> (L.) Benth.	✓
S30	1-63	มะแฟน	<i>Protium serratum</i> (Wall. ex Colebr.) Engl.	Briefly*
S34	1-50	มะกอกเกลี้ยง	<i>Canarium subulatum</i> Guillaumin	✓
S36	1-50	ประดู่	<i>Pterocarpus macrocarpus</i> Kurz	✓
S39	1-50	แดง	<i>Xylia xylocarpa</i> (Roxb.) Taub.	✓
S40	1-10	กระโดน, หูกวาง	<i>Careya arborea</i> Roxb.	✓
S43	1-50	ตะคร้อ	<i>Garuga pinnata</i> Roxb.	✓
S45	1-50	ขมหิน	<i>Acrocarpus fraxinifolius</i> Arn.	✓
S46	1-10	ทองหลาง, ทองเดือนห้า	<i>Erythrina stricta</i> Roxb.	✓
S49	1-50	ปอขาว	<i>Sterculia pexa</i> Pierre.	✓
S50	1-30	รัง	<i>Shorea siamensis</i> Miq.	✓
S60	1-50	ชะจาว	<i>Holoptelea grandis</i> (Hutch.) Mildbr.	✓
S65	1-50	ตะคร้อ, มะจ๊ก	<i>Schleichera oleosa</i> (Lour.) Merr.	✓
S66	1-50	เพกา	<i>Oroxylum indicum</i> (L.) Kurz	Semi*
S67	1-50	ขางเหียง	<i>Dipterocarpus obtusifolius</i> Teijsm. ex Miq.	✓
S69	1-50	เสี้ยวขาว	<i>Bauhinia variegata</i> L.	✓
S70	1-30	แกหางค่าง (แคบีด)	<i>Fernandoa adenophylla</i> (Wall. ex G.Don) Steenis	✓
S71	1-40	มะหาด	<i>Artocarpus lacucha</i> Buch. -Ham.	✓
S72	1-50	มะตูม, มะปิ่น	<i>Aegle marmelos</i> (L.) Corrêa	✓
S79	1-10	กระท่อมเนิน	<i>Mitragyna rotundifolia</i> (Roxb.) Kuntze	Semi*
S80	1-50	จิว, จิวแดง	<i>Bombax ceiba</i> L.	✓
S81	1-30	ผ้าสีขน	<i>Vitex canescens</i> Kurz	✓
S82	1-30	กระท่อม, ตุ่มหลวง	<i>Breonia chinensis</i> (Lam.) Capuron	✓

Note: “semi” and “briefly” in the category deciduous habit means that species may lose their foliage for a short period of time before it spring flushing (Elliott et al., 2006).

2.2 Data Acquisition

2.2.1 Ground-based Survey

1) Required Variables

Variables of interest were individual sapling height (measured from the root collar to the uppermost meristem), crown dimensions (longest dimension (length) and width perpendicular to length direction), and root collar diameter (where the stem joined the root). The height of the stem of each sapling was measured from the soil surface to the shoot meristem (Wangpakapattanawong & Elliott, 2008). Such measurements were used as ground-truth data to compare variable correlations among software programs (in Chapter 3) and image-based measurement via highest performance software (in Chapter 4). In addition, the health score and weed cover score were recorded, for later individual sapling verification (both on a variable scale ranging from 0 to 3). These variables were measured for all sampled saplings within the restoration plot and recorded against each sapling's label code. In addition, the position of all saplings was mapped, to help with the detection of missed or dead saplings, and to clarify whether unclear bushy crowns were saplings or weeds. Survival was defined as the number of live saplings, detected during each data-collection event, expressed as a percentage of the number planted (*equation 1*). To identify whether saplings were dead or alive, all unhealthy saplings were checked by scratching their stem to check for green tissue. If the saplings still have green tissue, they are assigned a low health score. The scoring systems were as follows: for health: score 0 —sapling appeared dead; score 1 — sapling in poor condition (few, discolored leaves, insect damage, and so on.); score 2 — saplings slightly damaged but still had mostly intact healthy foliage and score 3 — saplings in perfect health. For weeds score, a circle around target sapling 1 meter diameter was visualized: score 0— absence of any herbaceous plants; score 1— a few weeds growing around; score 2— approximately ½ area covered by weeds and score 3 score — most of the ground covered densely in weeds.

All measurement techniques were based on Forest Restoration Research Unit (2008).

$$\% \text{ survival} = \frac{\text{no. detected live sapling}}{\text{no. planted sapling}} \times 100 \quad (\text{Equation 1})$$

2) Equipment

The tools used for ground-based survey included a) 1.5 tape measures mounted on plastic poles for sapling height and crown dimension measurements. b) Digital calipers for root collar diameter measurements c) 40-meter tape measures for width and length of benches measurements.

2.2.2 Aerial-based Survey

1) Required Outputs

Red-Green-Blue (RGB) color spectrum images (5,472 x 3,078 pixels) were downloaded from the UAV memory card after flights. The number of raw RGB images depended on the length of each bench and the flight routes.

2) Equipment

The UAV used was a Phantom 4 Pro V2.0, drone-DJI (quadcopter drone type), a smart consumer “drone” which can shoot 4K video at 60 frames per second and capture still images at a resolution of 20 megapixels. It can intelligently avoid obstacles during flying, due to obstacle avoidance sensors in 5 directions (the exception is immediately above). (For full technical details see the link: dl.djicdn.com/downloads/phantom_4_pro/Phantom+4+Pro+Pro+Plus+User+Manual+v1.0.pdf).



Figure 9 Phantom 4 Pro V2.0 UAV (left), landing after finishing mission by manual catching (right), due to unstable ground surface.

3) Flight planning

The waypoint mission function of Litchi flight planner, v. 4.18.0-g (flight planning application) was used to fly the UAV autonomously in a grid pattern 10 m above the ground, along each bench with a velocity of 2 km/h, acquiring images every 3 seconds, resulting in > 80% overlap/side-lap. According to the different length of the plots and limited battery duration (maximum 20 minutes per flight time, with 3-5 minutes for taking off and landing), individual flight missions had to be planned for each specific bench (so totally 6 missions, Table 6). Thus, the UAV was flown, 1 flight mission per bench (Figure 12) and repeated every 3 months. In addition, some minor edits of missions were made after checking previously acquired images that covered excessive areas outside of the study areas.

Table 3 UAV flight mission settings

Mission for Bench Order	Flight Take Time	No. of Aerial Images	Overlap of Image	No. of Flight Route	Average Distance Between Flight Routes	UAV Speed
1 st	21 mins	325	83 %	4 lines	2.67 m	2 km/hr
2 nd	21 mins	311	88 %	4 lines	1.89 m	2 km/hr
3 rd	20 mins	382	88 %	4 lines	1.93 m	2 km/hr
4 th	18 mins	271	90 %	4 lines	1.68 m	2 km/hr
5 th	18 mins	272	86 %	4 lines	2.26 m	2 km/hr
6 th	14 mins	167	89 %	3 lines*	1.74 m	2 km/hr

*NOTE: The edge of highest bench (6th bench) is close to nearby tree canopy (trees outside of our study area), therefore, one of the flight routes was cut to avoid UAV crash.



Figure 10 UAV waypoint mission in Litchi flight planner, for 1st bench; indicating the above ground height of each waypoint; 4 route lines with different camera angles.

2.3 Image Processing and Image-based Data Measurement

2.3.1 Image Processing (Orthomosaic and 3D Point Clouds Generation)

Raw RGB images from each UAV flights mission were stitched together using the photogrammetric software, which performs photogrammetry, based on structure-from-motion (SfM) algorithms (Özyeşil et al., 2017), capable of producing orthomosaic images, elevation models, 3D point cloud models (Figure 13) and digital terrain models (DTMs). After determining the best of 3 software packages in Chapter 3, DroneDeploy was subsequently selected for all image processing requirements. Although DroneDeploy generates all data types

from one raw-image set, only the 3D point-cloud model was downloaded for further data extraction (for height measurement). DroneDeploy web-based software comes with a measurement tool, used with orthomosaic images (corresponding with elevation model), Therefore, export of outputs for analysis in other software packages was not needed except for sapling heights). Each orthomosaic image had a final resolution of 0.3 inches per pixel for flights undertaken 10 m above ground.

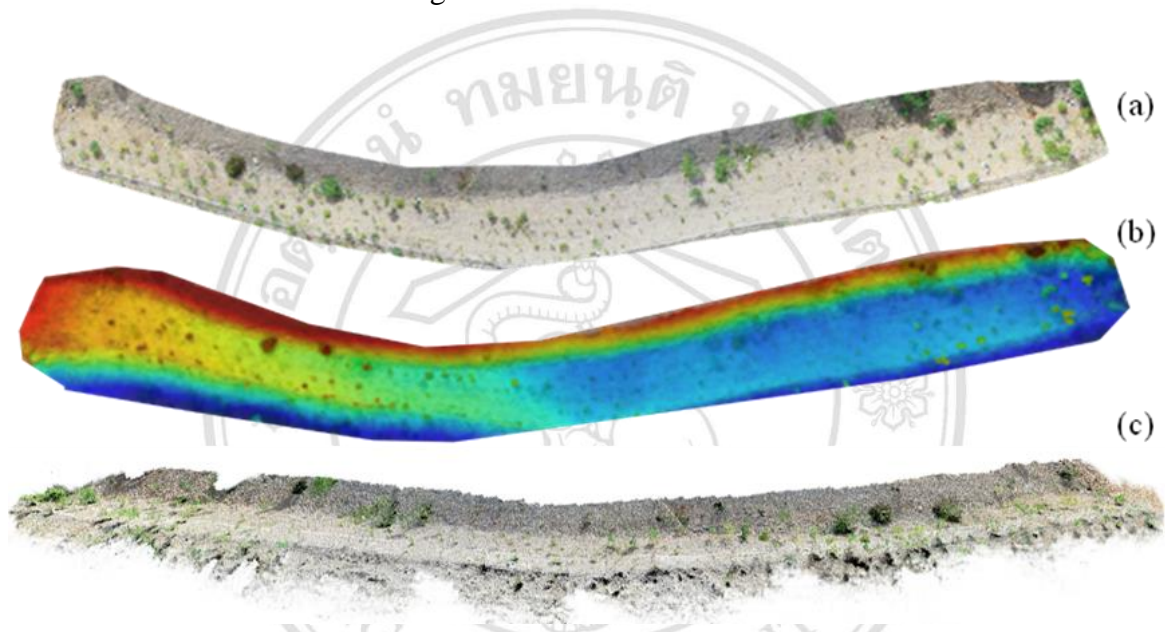


Figure 11 Orthomosaic image (a), elevation model (b), and 3D point cloud model (c), example of 1st bench result from last data collection.

2.3.2 Measuring variables from Orthomosaic Image

1) Crown Dimensions

Sapling-crown dimensions were measured manually in the orthomosaic images, utilizing the overlaid elevation model to identify sapling crowns by 2 methods. The first method was perpendicular dimensional measurement, which included the longest crown measurement (deemed crown length), with the measurement perpendicular to it, deemed crown width, using the distance tool of DroneDeploy. The measured cross lines and other properties were displayed in the left-hand panel on of the DroneDeploy

website interface (Figure 14) and the crown area was calculated as a sapling assuming the crown shape was an ellipse; as *equation 2*). Since delineating crown length/width was difficult (due to the small size of sapling crowns, limited zoom capability, and differences in elevation between the ground and sapling crowns), the crown area was measured directly; as a second method, by placing multiple points around the visible circumference of the crown, also using the area tool of DroneDeploy. (Figure 15). Moreover, direct-CA is feasible to be measured in most of the available saplings rather than CA-LW. The measuring process was conducted by the same operator each time, to reduce the observer bias.

$$\text{Crown Area} = \pi \times \left(\frac{\text{crown length}}{2}\right) \times \left(\frac{\text{crown width}}{2}\right) \quad (\text{Equation 2})$$

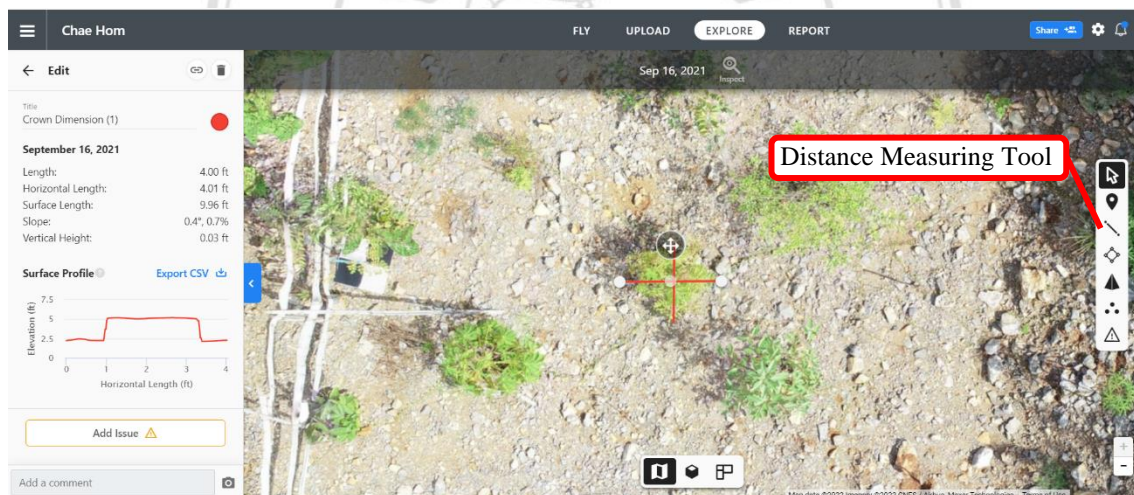


Figure 12 Distance measuring tool in DroneDeploy website interface; the perpendicular line indicates the length and width of sapling crown.

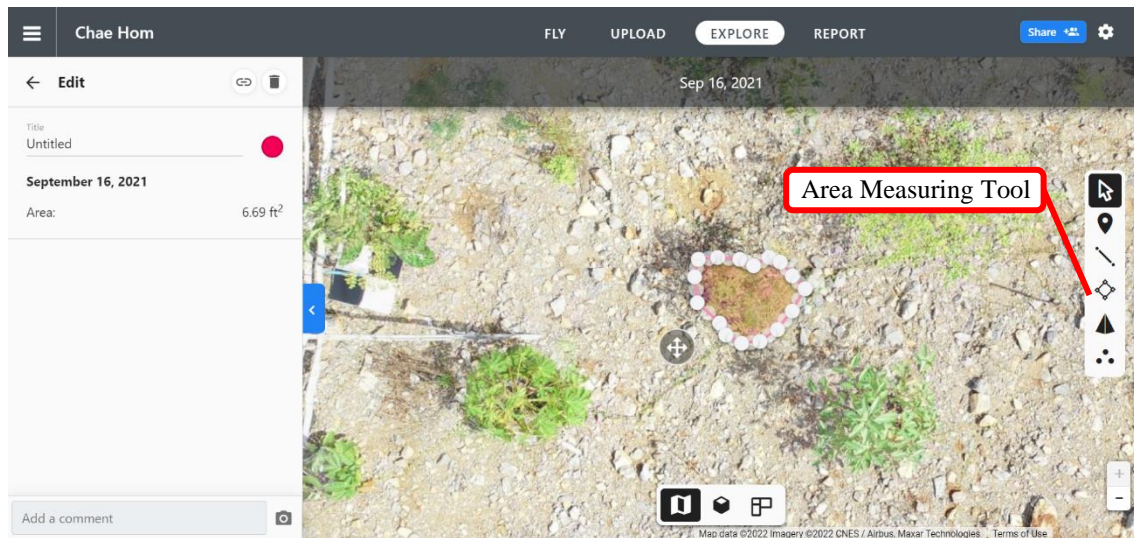


Figure 13 Area measuring tool in DroneDeploy website interface; the covered light red-color area indicates the selected crown of the sapling

2) Number of Detected Saplings from Crown Dimensions

Detected saplings were defined as those for which crown area measurements could be made in the orthomosaic images by CA-LW and direct-CA. The total number of detected saplings on all 6 benches in orthomosaic image was expressed as a percentage of those detected on the ground (separately for CA-LW and direct-CA methods). The method which detected the highest percentage was selected as indicative of the capability of the orthomosaic images to detect planted saplings.

2.3.3 Measuring variables from 3D point clouds

1) Height

Sapling-height data were extracted from the 3D point cloud models, exported from DroneDeploy website, via CloudCompare (latest stable release: 2.11.3), open-source software for point cloud processing. Isolated trees, clearly visible in the point cloud (not overlapping with weeds etc.) were selected for manual height measurements, since the user could easily determine where the highest point was. CloudCompare's point-picking

tool, which displays the distance between 2 selected points in 3D point cloud models. (Figure 16). The measuring process was conducted by the same operator each time to reduce the observer bias.

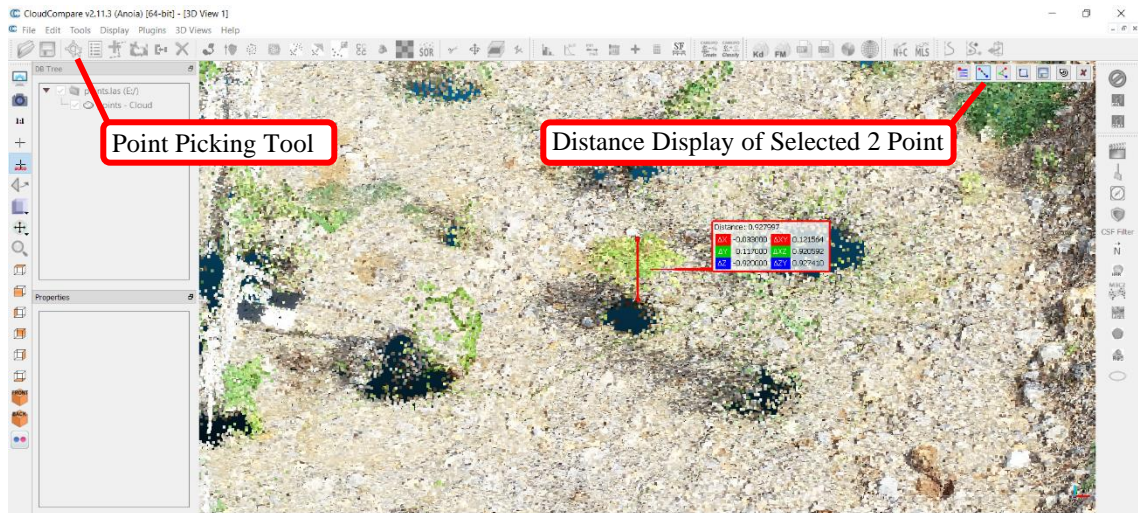


Figure 14 Point Picking tool in CloudCompare software; the vertical line indicates the sapling height (quantity information shown in tiny red box).

2) Number of Detected Saplings from Height

All saplings, for which height measurement was possible, were counted as a third estimate of detection percent.

CHAPTER 3

Comparison of Sapling Detection and Height Measurement Using 3D Point Cloud Models from Three Software Tools: Applications in Forest Restoration¹

Abstract

A challenge for forest restoration is the monitoring of its success, particularly of sapling survivorship. Three D-point-cloud models, generated from aerial images taken from unmanned aerial vehicles (UAVs), are useful for monitoring vegetation recovery. However, the use of aerial images is challenging, due to the small sapling size. Many photogrammetry software tools are available for creating 3D models, but they differ in their performance. This research compared the ease of use, sapling detectability, and correlation of sapling-height measurements, using 3D-point-cloud models from the free versions of three tools: Pix4Dmapper, DroneDeploy, and WebODM. The study site was at a forest restoration plot on an open cast limestone quarry of the Siam Cement Group (SCG) Public Company Limited, Lampang, Thailand. The heights of 178 planted saplings were measured manually, to provide ground-truth data. On the same day, a UAV was used to autonomously capture RGB images, subsequently processed to produce 3D models, using three software tools with default settings. The percentage detection and the correlation of height measurements were compared. DroneDeploy correctly detected 42% of the saplings, followed by Pix4Dmapper (29%) and WebODM (16%). There were a few errors of commission: 3% detection of saplings that were not there, with DroneDeploy and Pix4Dmapper and 1% with WebODM. Differences in sapling detection may be due to differences in the algorithms and the default settings among the 3 software

¹ Changsalak P. and Tiansawat P. (2021) Comparison of Sapling Detection and Height Measurement Using 3D Point Cloud Models from Three Software Tools: Applications in Forest Restoration. *EnvironmentAsia Journal* 2022, 15 (special issue), 100-105.

packages. The correlation of sapling-height measurements was assessed using linear regression against ground-truth data. All 3 software tools performed well (R-squared > 85%). The pros and cons of each software tool and its future applications are discussed.

Keywords: UAV; Photogrammetric software; Sapling monitoring; linear regression
Sapling height

3.1 Introduction

A point-cloud is a three-dimensional dataset, generated from many geo-referenced points, produced by photogrammetry software (Lindberg and Holmgren, 2017). The raw data, used to generate 3D point clouds, can include remote sensing imagery, such as aerial images taken from unmanned aerial vehicles (UAVs) (Yang et al., 2017). A collection of two-dimensional (2D) images, is converted into 3D models combining camera motion data, with positional shifts in coincident points between overlapping images. Overlapping aerial image sequences are analyzed using photogrammetric techniques (Lindberg and Holmgren, 2017), such as structure-from-motion (SfM) algorithms, to produce a 3D point cloud (Özyeşil et al., 2017). Various photogrammetric software tools on various platforms can perform such analyses (Talib et al., 2021), including open-source and non-open-source software with limited trial periods. However, 3D point-cloud model outputs can vary (Westoby et al., 2012) among the software packages. Therefore, software selection is a crucial step towards using UAVs to monitor forest ecosystem restoration.

Remote sensing has been applied for ecological restoration monitoring in various situations (Buters et al., 2019a). For forest restoration, monitoring the performance of planted saplings has been a crucial step in determining progress (Dash et al., 2017). Traditionally, monitoring sapling performance is done by hand by ground surveys. The use of 3D point cloud models, generated from UAV aerial images, has the potential to replace traditional ground surveys. Three-dimensional point cloud models can speed up monitoring and lower implementation costs (Itkin et al., 2016). Several photogrammetric software tools have been used to measure trees in 3D point cloud models (e.g., 3DSurvey, Agisoft Photoscan, Pix4Dmapper Pro, SURE, and Autodesk

123D, etc.) (Lindberg and Holmgren, 2017). Monitoring sapling performance with a 3D point cloud model is challenging though, due to its small size (Buters et al., 2019a). The question remains as to whether software tools, recommended for tree measurements can be used for small saplings. Since cost is a crucial factor, we tested freeware versions of the photogrammetric software. Therefore, this study compared ease of use, sapling detection, and the correlation of sapling height measurement using 3D point cloud models from free versions of three currently available photogrammetric software programs: Pix4D mapper, DroneDeploy, and WebODM.

3.2 Materials and Methods

3.2.1 Study Site

Study site preparation and tree planting methods were as described above (sections 2.1.1 - 2.1.3).

3.2.2 Data Acquisition

Data acquisition was as described in sections 2.2.1 - 2.2.2, except that only the variable “height” was focused on for this chapter, from data collected on 13/6/2021 (when trees are 9 months old), from only the 1st bench (out of 6 in the total study).

3.2.3 Software packages

Images were processed by the following 3 software packages to generate 3D models via photogrammetry.

- 1) Pix4D mapper

The non-commercial version of Pix4D mapper version 4.4.12, was applied (https://assets.ctfassets.net/go54bjdzbrgi/1Gm0UGAZ9WQMSOewk6Kya4/816a0735dd93eafb3d912520939bebfe/Pix4Dmapper_feature_list_v4.6_English.pdf)

2) DroneDeploy

The 14-day trial version of DroneDeploy (online version, 2021), was used. It is cloud-based software that allows users to control the UAV and take images at the required altitude. The DroneDeploy website, accessed by a personal laptop, allows the user to upload images and automatically generate all data types from those acquired images. The free version was limited to 10 processing tasks or within a 14-day trial period (help.dronedeploy.com/hc/en-us/articles/1500004861881-How-To-Process-Datasets-Into-Maps-and-Models).

3) WebODM

The free open-source WebODM software version 2.6.2 was applied. It is a user-friendly web interface to OpenDroneMap (ODM), with community support and instructions for free installation (docs.webodm.org/#introduction)

3.2.4 Point Cloud Generation and Height Measuring Procedures

The same set of 333 aerial images were used to generate the point cloud models “only once” with the three photogrammetric software tools. For each software, default settings were used, and steps taken from tutorials provided by the software publishers:

1. Open Pix4D mapper software → click *New Project* → type *Project Name* → click *Add Images* → *Image Properties* as default → *Auto Detected: WGS 84/UTM zone 47N* as default → select *3D Models* in the *Standard of the Processing Options Template* → wait for processing,
2. Open DroneDeploy software browser → click *+Project* → click *Upload* → type *Map Name* and click *Select Photos* → click *Upload Images* → wait for processing

3. Open WebODM software manager → open software browser → log in account → click *Add Project* → type *Project Name* → click *Select Images and GCP* → *Additional Options* as default → click *Review and Start Processing* → wait for processing

The 3D point cloud outputs from each software were used to detect individual saplings manually and measure their height. For sapling height, the outputs from WebODM and DroneDeploy were exported, and the height was measured in CloudCompare, open-source software for point cloud processing (as mentioned in 2.3.3). For the Pix4D Mapper, height measurement was done by calculating the distance between each sapling's apex and the ground point immediately beneath, directly from the software interface.

3.2.5 Output Comparison and Correlation Assessment

The properties of the 3D point cloud model outputs were recorded. In addition, their ease of use was evaluated, based on installation, pre-processing procedures, processing time and time spent on height measurement after obtaining the 3D point clouds. In terms of sapling detection, the total number of correctly detected saplings (out of 178 saplings on the ground) from each software was counted and the percentage of correctly identified saplings was calculated. The percentage of saplings that were not detected was reported as an omission error (%). The percentage of objects mistakenly identified as saplings was also calculated as commission error (%). The relationship between the height measurements, derived from the ground-truth data (x-axis) and derived from point-cloud models (y-axis) was tested by linear regression.

3.3 Results

3.3.1 Software Outputs and Ease of Use of Each Software

A comparison of the information relating to 3D point cloud model properties produced for each of the three software programs is presented in Table 3. Ease of use, based on four criteria, is compared in Table 4.

Table 4 Characteristic report of the 3D point clouds from each software. Check marks (✓) indicate “reported” while blank cells indicate “not reported” from the software

Reported information	Pix4D-mapper	DroneDeploy	WebODM
Average ground sampling distance (GSP)	✓	✓	✓
Area coverage		✓	✓
Image quality	✓	✓	
Matching quality	✓		
Tie points quality	✓		
Georeferencing quality	✓	✓	✓
Camera position and orientation uncertainties	✓	✓	✓
RMS error	✓	✓	✓
Rolling shutter statistics	✓	✓	✓
Point cloud densification details	✓	✓	✓
Result preview	✓	✓	✓
Reporting unit within output	meter	feet	meter

Table 5 The criteria indicate the ease of use of the three selected software.

Comparison criteria	Pix4D-mapper	DroneDeploy	WebODM
Complexity of software installation	simple	none (online browser)	complicated*
Complexity of steps before processing	moderate	simple	moderate
Processing time	1 hr 33 mins	32 mins	47 mins
Time spent on height measurement	1 hr 9 mins	1 hr 3 mins	19 mins

*complicated = requires installing docker, to run the software (without docker it would not be possible to run WebODM, but it also used up internal storage).

3.3.2 Sapling Detection Percentage

Table 6 compares sapling-detection percentage, as well as errors of omission and commission among the three software packages. DroneDeploy performed the highest correctly detected (42%), and the lowest omission error (58%). However, the commission error of Dronedeploy is as high as Pix4D-mapper.

Table 6 Percentage of saplings detected by each software.

Percentage of detection	Pix4D-mapper	DroneDeploy	WebODM
Correctly identified	29	42	16
Omission error	71	58	84
Commission error	3	3	1

3.3.3 Correlation of Height Measurements

Height measurements from the point cloud models correlated closely with ground-truth data (Figure 9) for all three software packages, with DroneDeploy performing the best. Due to the difference of the number of saplings detected by each model, the number of data points in each regression analysis was different: Pix4D-mapper $n = 51$; DroneDeploy $n = 75$; WebODM $n = 29$.

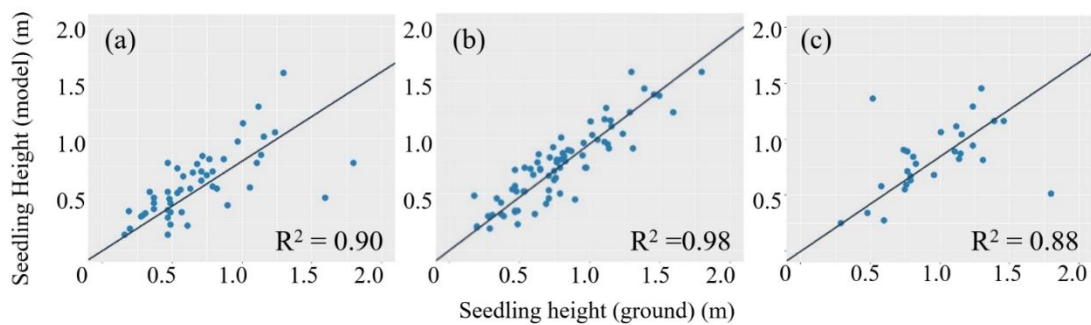


Figure 15 Linear regressions between the measured height from 3D models and ground truth data (for detected saplings): (a) Pix4D mapper ($n = 51$), (b) DroneDeploy ($n = 75$) (b) and (c) WebODM ($n = 29$).

In addition, we tested the linear relationship between the height data from the point cloud models and the ground truth data for those saplings that were correctly detected by all three software tools ($n = 15$) (Figure 10). Again, DroneDeploy performed the best.

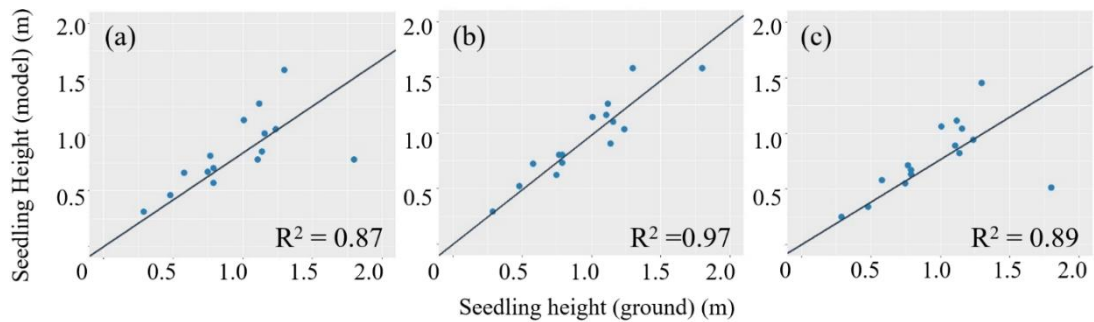


Figure 16 Linear regression between the measured height from 3D model and ground truth data: overlapping detected saplings among three software (n = 15) from Pix4D mapper (a), DroneDeploy (b), WebODM (c).

3.4 Discussion

For the software outputs, DroneDeploy and WebODM allow users to export PDF reports summarizing software performance and outputs, however Pix4D-mapper does not allow exporting and only provides the reports on a pop-up window. Although Pix4D-mapper provided useful information in its reports, the convenience of being able to export the reports from DroneDeploy and WebODM is significant. For ease of use, DroneDeploy was ranked highest, followed by Pix4D-mapper, and then WebODM. In addition, DroneDeploy took the least time and computer storage during the installation and processing.

Sapling detection percentage showed that DroneDeploy correctly detected the greatest number of saplings with the smallest omission error, in comparison to Pix4D-mapper, and WebODM (Table 6). The omission errors (failures to detect saplings when they are present) may arise from the size and health of the saplings e.g., crown not fully projected or where deciduous saplings have lost their leaves (Dash et al., 2017).

The regressions were statistically significant and the linear relationships between the height measurements from the ground survey and from the point cloud models from all three software were strong (Pix4D-mapper $R^2 = 0.90$, $p < .001$; DroneDeploy $R^2 = 0.98$, $p < .001$; WebODM $R^2 = 0.88$, $p < .001$). The relationship between height measurements from the point-cloud models and the ground-truth data for the 15 sapling individuals that were detected by all three software tools (n =15) was also

statistically significant (Pix4D-mapper $R^2 = 0.87$, $p < .001$; DroneDeploy $R^2 = 0.97$, $p < .001$; WebODM $R^2 = 0.89$, $p < .001$;))

All software tools generated point cloud models that allowed height measurements that were strongly related to the ground truth data. However, there were still some errors in height measurements from the point cloud models. The free versions of the software tools have limited features which may affect the correlation of the height measurement. We are aware that there are commercial versions of these software tools which provide more features. Users should investigate what features are available in each software product to choose the appropriate software for a given task.

Differences in ease of use also set the software apart. In our study, DroneDeploy worked well in detecting saplings using aerial images and was relatively simple to use.

For monitoring saplings in forest restoration studies, our study shows that the use of UAV aerial images has the potential to replace ground surveys, provided errors of omission can be reduced. Further work that reduces such errors is clearly needed. Better sapling detection may come from the combination of using UAVs with more powerful cameras, developing different flight plans for different stages of restoration, investigating further into image preprocessing steps before generating point cloud models, and applying other advanced remote sensing equipment e.g., lidar, etc.

CHAPTER 4

The Use of Imagery for Monitoring Sapling Survival and Growth over Time and Correlations with Non-Visible Sapling Variables

4.1 Introduction

To monitor the progress of restoration projects, sapling survival and growth are measured on the ground. Such monitoring is labor-intensive and, therefore, costly (McKenna et al., 2020; Buters et al., 2019a). Although protocols for monitoring older sites with larger trees have been widely published (Shimizu et al., 2014; Rokhmana, 2015; Gatziolis et al., 2015; Lindberg & Holmgren, 2017; Dash et al., 2017; Piermattei et al., 2019; Fromm et al., 2019; Talib et al., 2021), they are often not applicable for monitoring changes in newly planted sites, especially in the open-pit mine restoration. The previous chapter established the relatively high performance of DroneDeploy for detecting surviving saplings and to generate height data from 3D point clouds. Therefore, in this Chapter, DroneDeploy was used to i) track the survival and growth of tree saplings every 3 months over the first year after planting and ii) examine relationships between drone and ground data for a greater range of sapling variables in orthomosaic images. To meet established standards of sapling monitoring (Amorós & Ledesma, 2020), values of sapling variables that cannot be directly quantified from low-altitude UAV imagery were estimated from other acquired data via correlation. This chapter also examines whether image-based data from an UAV can be used to generate the same species-suitability ranking order as ground data as an aid to species selection decision making. The potential and limitations of an aerial-based monitoring protocol, to monitor early forest restoration on open-pit mine, is discussed.

4.2 Materials and Methods

4.2.1 Study Site

Details of site preparation and planting methods were described in sections **2.1.1 - 2.1.3**.

4.2.2 Data Acquisition

Data acquisition was performed using methods described in sections **2.2.1-2.2.2**.

Moreover, ground survival data included “not-found” trees if they could reasonably be assumed to be alive. For example, trees that were missed or recorded as dead in one survey but recorded as alive in a subsequent survey had their “alive” status backdated to previous survey records. This was especially true of deciduous species, which were leafless in the dry season and easily missed. Some were missed, whilst others were erroneously recorded as dead. Staff also mistook trees in poor health for dead ones, because many such trees had no additional data recorded for them during ground surveys (especially on 11/3/2021, when sapling 6 months old), but staff recorded as alive and in good health in subsequent surveys. The status of such trees was reclassified as “alive not found” in the dry season and the count of alive trees at that time corrected accordingly.

4.2.3 Image Processing and Image-based Data Measurement

DroneDeploy was employed for image processing and image-based variable measurement (crown dimensions) as described above in sections **2.3.1 - 2.3.3**.

4.2.4 Data Analysis

1) Ground-based Variable Relationship Analysis and Utilization

Since root collar diameter (RCD) is far too small to be measured in orthomosaic images and 3D point cloud models, it was derived via correlation with measurable variables. Ground-based data, including sapling height, crown area (multiplication of crown length and width of the ground measurement; ground-CA) and root collar diameter, were subjected to linear regression analysis (Vetter TR & Schober P., 2018) via R 4.0.3 (statistical software). The strongest relationship between variables was chosen, based on correlation coefficient (r) and coefficient of determination (R^2), and an equation generated from simple linear regression. Moreover, the train-test split technique was used with the data set that had the strongest relationship, for evaluating the performance of equations from root-mean-square-error (RMSE). Then the generated equation was used to predict changes in the dependent variable (RCD) for each change in the independent variable (sapling height or CA) using image-based data.

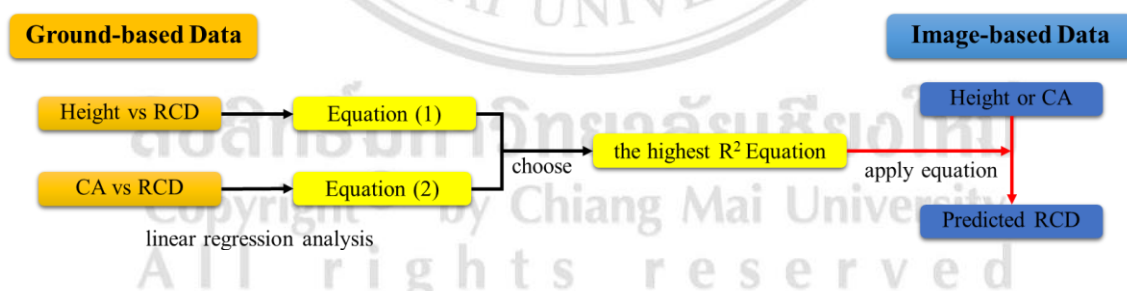


Figure 17 Ground-based variables relationship utilization

2) Sapling Detection

The number of surviving saplings from ground-based surveys was compared with the sapling number acquired from the orthomosaic image and 3D point cloud model (assuming all saplings detected by each of the 3 methods were alive: height, CA-LW, and direct-CA measurement). The

percentage detection rate was the number of saplings detected in the orthomosaic image and 3D point-cloud model as a percentage of the number found during ground counts.

3) Correlation and Mean Percent Difference Analysis for Correlation of Measurement Evaluation

Ground based and UAV-based variables (sapling height, crown area, and root collar diameter) were correlated to derive R^2 , RMSE and mean percent difference also via R 4.0.3. Since sapling variables data were normally distributed, Pearson's correlation coefficient was used to determine the strength and direction of pairwise associations between variable pairs (values range from 0 to 1), with 0.1 indicating weak association to >0.9 indicating strong association (Schober & Schwarte, 2018). Also, simple regression models were constructed to quantify the closeness of correlations by R^2 and RMSE. Mean percent differences (\pm SD) between ground-based data and image-based data were calculated by *equation 3* (for detected surviving saplings). R^2 , RMSE and mean percent difference were used to measure how much the predictions from UAV images deviate from ground-based measurements.

$$\text{Percentage Difference} = \frac{\Delta V}{V_1} \times 100 \quad (\text{Equation 3})$$

$$\text{Percentage Difference} = \frac{(\text{Image-based Data}) - (\text{Ground-based Data})}{\text{Ground-based Data}} \times 100$$

4.2.5 Relative Performance Index

The Relative Performance Index (RPI; no units) was calculated to compare performance among tree species planted (Elliott et al., 2000; Forest Restoration Research Unit, 2005). RPI is used to rank species in descending order of performance based on a combination of survival and growth. Multiplication of the standardized % survival and Relative growth rates (RGR) provided a raw performance index (*equation 4*). The final index was expressed

as a percentage of that of the top-performing species (with a maximum value of 100). Each species was then ranked in descending order of RPI, calculated both from aerial and ground data. Such bar charts are standard practice when reporting early results of forest restoration trials.

RGR were calculated via *equation 5* for each surviving labeled sapling from height data (Figure 27) – from 29/9/2020 to 16/9/2021. RGR indicates an annual percentage increase in size (relative to the mean size of the plant over the data-collection period). It controls for differences in original sapling size (since large plants grow faster than smaller ones). An RGR of 100% therefore indicates an annual doubling in plant size. A negative value indicates the plant is shrinking (due to disease or being cut). A value of -100% indicates the plant will mostly likely die within a year.

$$RPI \text{ (no unit)} = \% \text{ survival} \times RGR \quad (\text{Equation 4})$$

$$RGR \text{ (\%/year)} = \frac{(\ln Height_2 - \ln Height_1)}{(T_2 - T_1)} \times 100 \times 365 \quad (\text{Equation 5})$$

where $\ln Height$ (cm) is natural logarithm of tree height and T (days) is number of days between 2 data collection date which less than 1 year.

ลิขสิทธิ์มหาวิทยาลัยเชียงใหม่
Copyright© by Chiang Mai University
All rights reserved

4.3 Results

4.3.1 Sapling Survivorship and Detection

A total of 1,303 saplings were planted, of which 255 were omitted from the study, because they were outside bench boundaries (and therefore excluded from ground surveys) or because they were located on the edges of raw aerial images (half visible). So, the study was based on a starting cohort of 1,048 saplings. Figure 18 shows survivorship over 1 year using ground-based data (yellow bar).

Sapling detection rates in of up to 85% were achieved in drone derived imagery. Using orthomosaic images, the direct CA method was better than the CA-LW method for detecting and counting saplings. Use of 3D point clouds produced poorer results (Figure 18). All image-based techniques detected more saplings as they grew larger, exceeding 50% by nine months. The lowest detection occurred in March when most saplings were leafless and less visible.

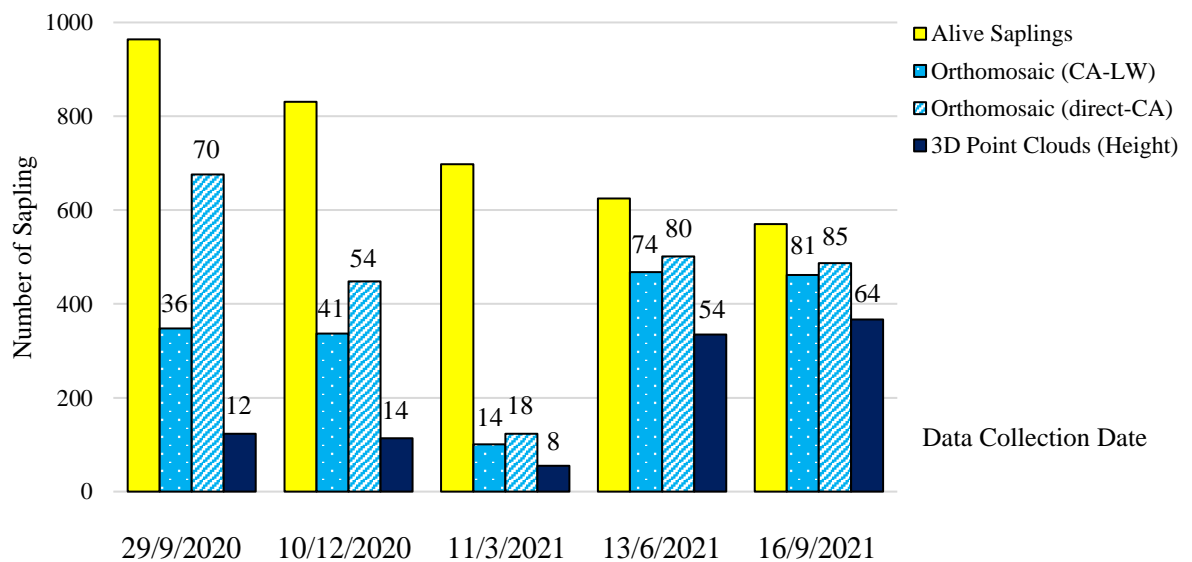


Figure 18 Comparison of sapling number between ground-based data (yellow bar) and image-based data (blue bar in 3 gradient colors) from five collection dates. The number at the top of the bar represents the percentage of saplings detected from each measurement image-based method.

Using ground-based data and image-based collected on 16/9/2021, we examined differential survival and % detection (by the 3D point cloud; height measurement), among 17 species with 20 or more surviving individuals. The percentage of image-based detection of those 17 cohort species on the date of last data collection (16/9/2021) was calculated (Figure 19).

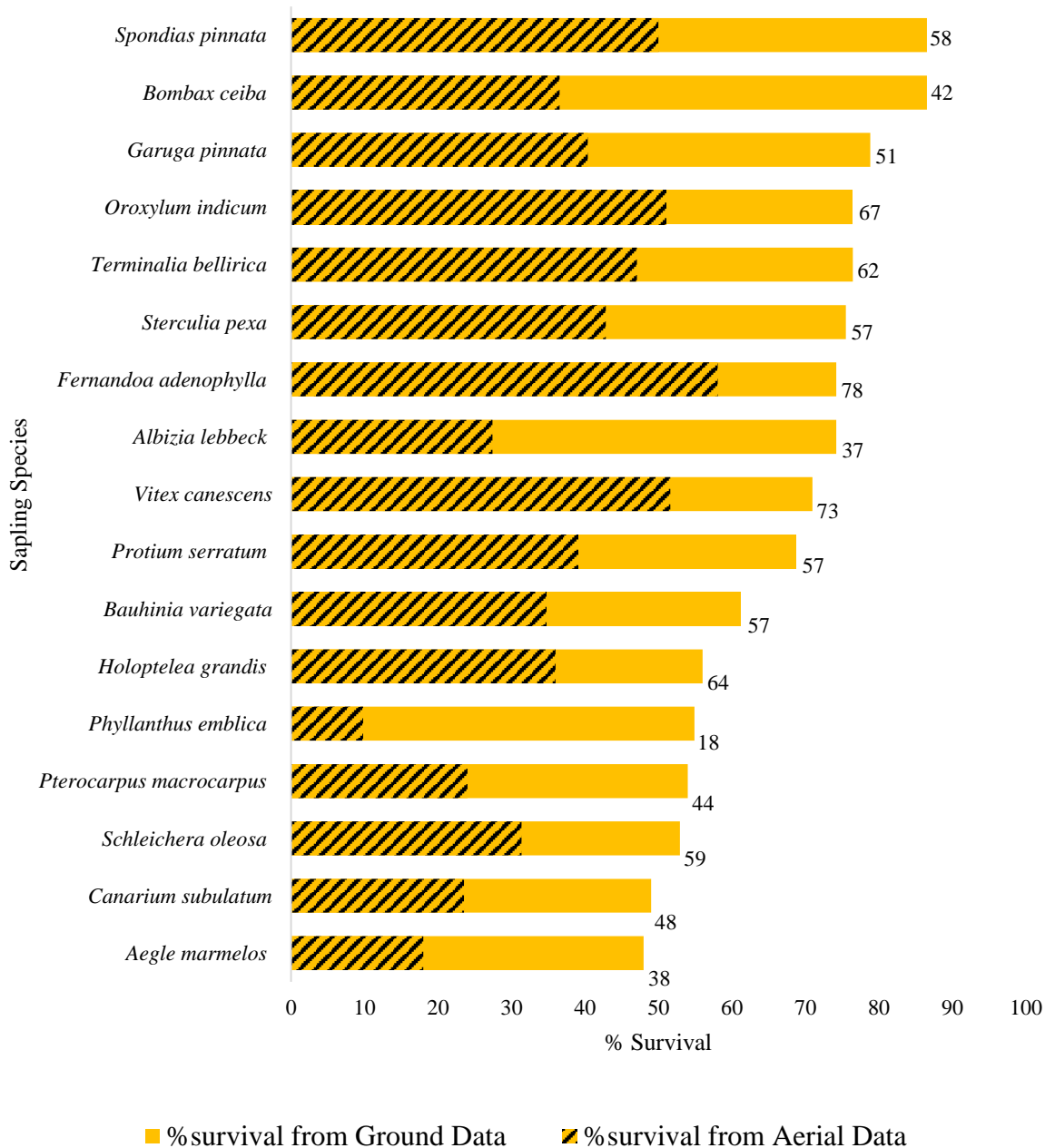


Figure 19 Percentage survival from ground and aerial surveys on the last data collection (16/9/2021). The number at the end of each bar is the per cent aerial detection rate of each species (drone-based survival as a percent of ground-based survival).

It was expected that higher detectability of trees as time progressed was due to increased tree size as they grew larger. However, at the species level, relationships between detectability and both mean sapling height and sapling crown area (by both CA-LW and direct-CA) were not significant among 17 species with 20 or more surviving individuals by September 2021 (Figure 20-21).

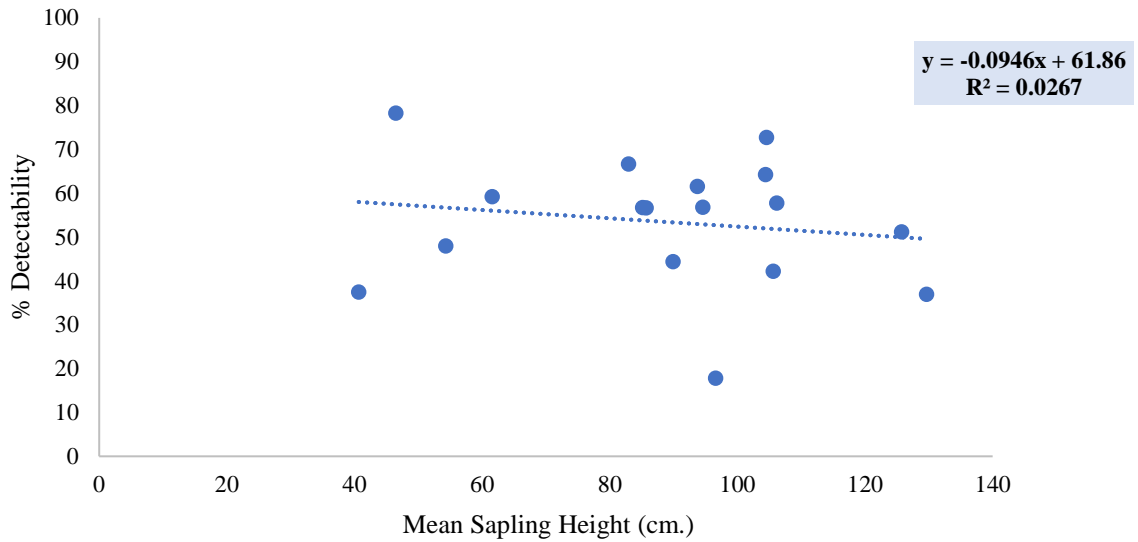


Figure 20 Scatter plot between species-level mean sapling height (cm) and percentage species-level detectability (17 species with $n > 20$) in September 2021

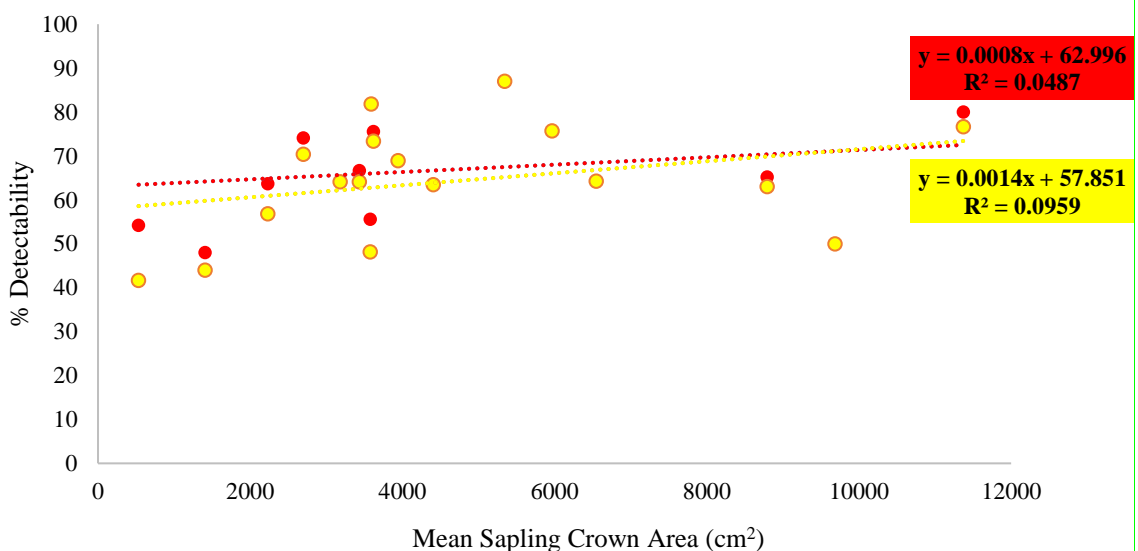


Figure 21 Scatter plot between species-level mean sapling crown area (cm²) and percentage species-level detectability from CA-LW (yellow dot, $R^2 = 0.0959$) and direct-CA (red dot, $R^2 = 0.0487$) method in September 2021

4.3.2 Aerial Measurements - Efficiency Over Time

Simple linear regressions were used to determine relationships between aerial and ground measurements of directly measured variables: height, crown area by both the length-and-width (CA-LW) and direct-crown-area (direct-CA) methods, and of the indirectly derived variable, root collar diameter (RCD) from predictive equation.

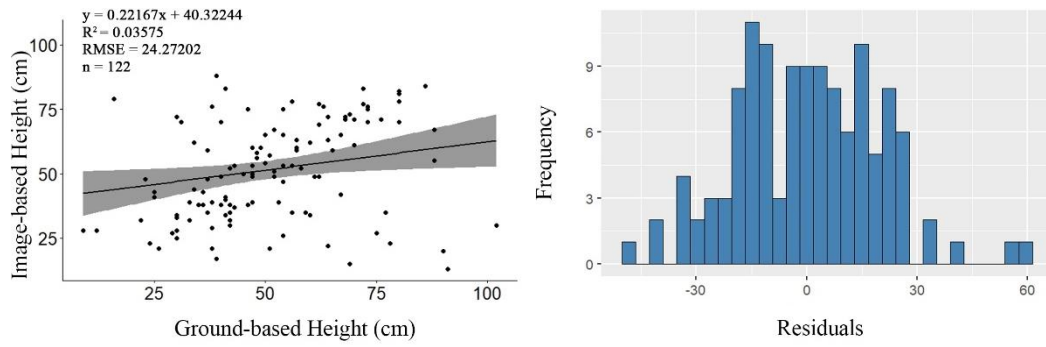
1) Directly Derived Variables from Aerial-based Measurement

Image-based measurements tended to underestimate sapling height (of ground data) during the dry season (by up -1 to -14%) and overestimate it during the rainy season (up to +19%), but the difference had declined to just 10% by the end of the study when the saplings were largest (Table 7). The strength of relationships between ground-based and image-based measurements increased with time and sample size, with no significant differences between mean height between the two methods over the whole study ($P > 0.05$). The residuals between the fitted line and the data before the dry period were normally distributed, whilst after the dry period, they were slightly right-skewed (Figure 22).

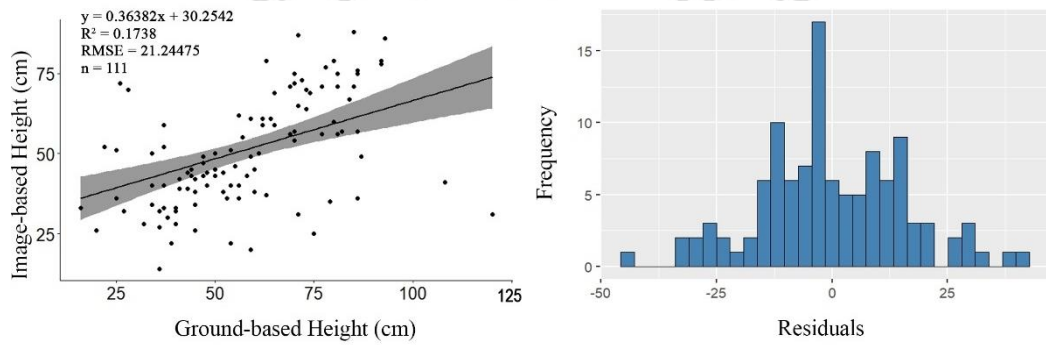
Table 7 Comparison of mean height from ground-based data, image-based data, and percentage of under/over-estimation.

Figure Session	Data Collection Date	Mean Height from Ground Data (cm)	Mean Height from Image Data (cm)	Mean Percentage Under/over-estimate	R ²
a	29/9/2020	50.90 ^a ± 22.69	52.78 ^a ± 23.68	18.97 ± 94.29	0.04
b	10/12/2020	55.76 ^a ± 30.60	53.14 ^a ± 23.12	-1.66 ± 49.67	0.17
c	11/3/2021	54.20 ^a ± 24.29	52.47 ^a ± 27.20	-14.08 ± 34.01	0.53
d	13/6/2021	69.27 ^a ± 32.84	70.52 ^a ± 32.26	3.28 ± 57.83	0.54
e	16/9/2021	88.80 ^a ± 51.24	92.42 ^a ± 44.66	10.14 ± 64.51	0.57

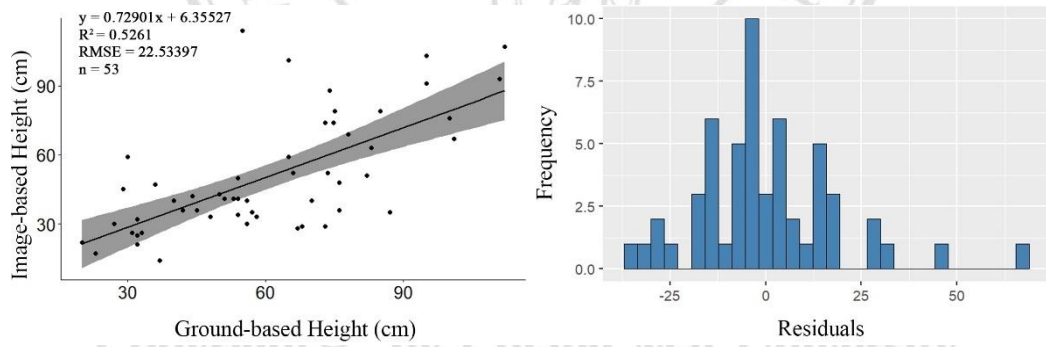
(a)



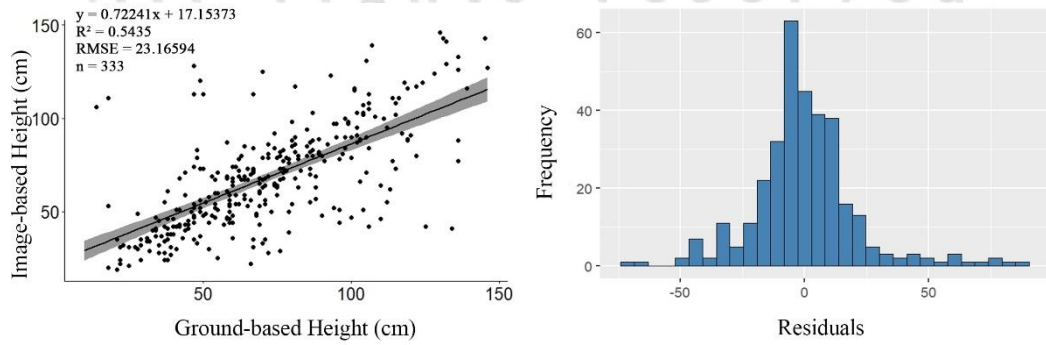
(b)



(c)



(d)



(e)

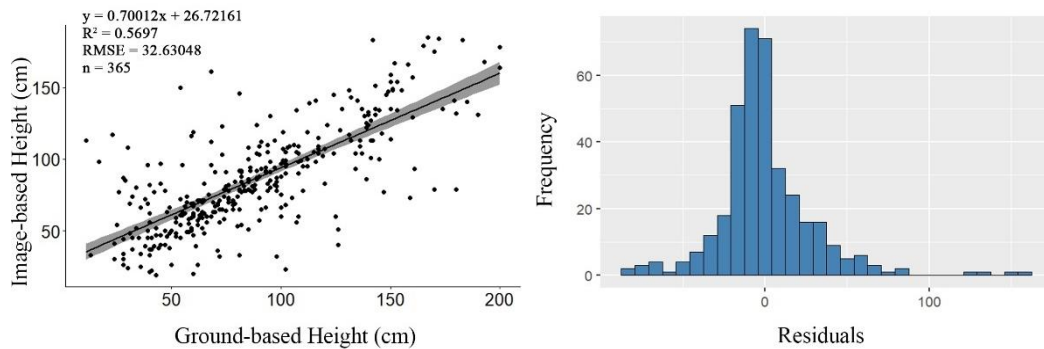


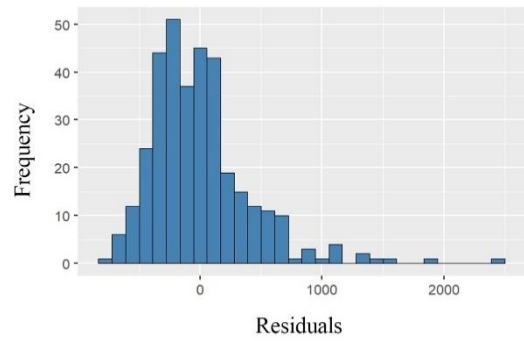
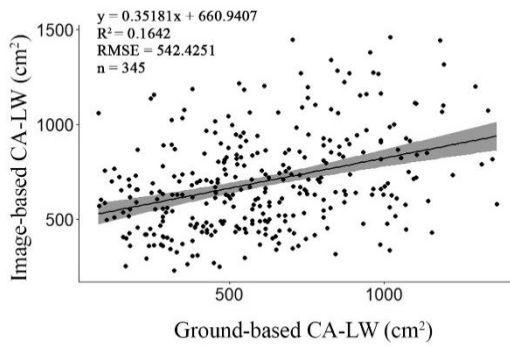
Figure 22 Regression analysis against height of ground-based and image-based data from each data collection; (a) 29/9/2020 10/12/2020 (b), 11/3/2021 (c), 13/6/2021 (d), and 16/9/2021 (e) (a-e; $P < 0.05$). Histogram of residuals indicates normality distribution between the fitted line and each data collection.

Using the CA-LW method, image-based measurements substantially overestimated crown area cf. ground data (by 65-299%), except at the end of the study, with no discernable trend in error with time or sapling size (Table 8). Relationships between ground-based and image-based measurements were generally weak from the beginning of the study until the dry period, but aerial data correlated better with ground data right after the dry period ($R^2 > 0.57$). Differences in the mean crown area among methods were insignificant ($P > 0.05$). All residuals between the fitted line and the data were not normally distributed around zero, which was slightly right skewed, except the data on 13/6/2021, which was slightly left-skewed (Figure 23).

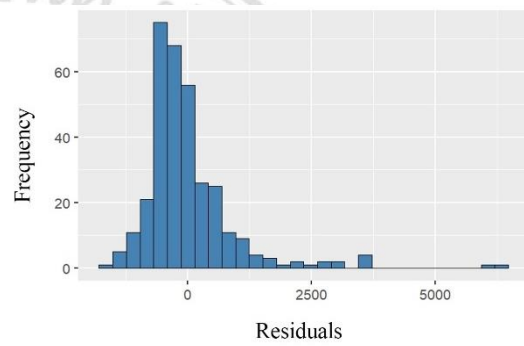
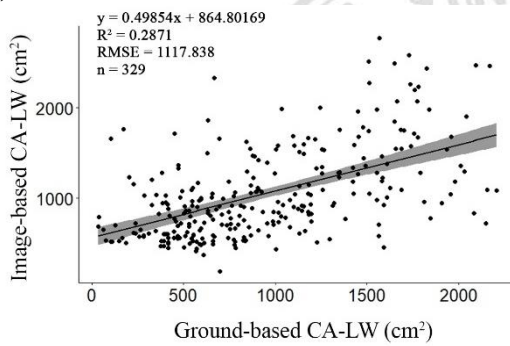
Table 8 Comparison of mean crown area (CA-LW) value from ground-based data, image-based data, and percentage of under/over-estimation.

Figure Session	Data Collection Date	Mean CA-LW from Ground Data (cm ²)	Mean CA-LW from Image Data (cm ²)	Mean Percentage Under/over-estimate	R ²
a	29/9/2020	468.26 ^a ± 405.62	762.31 ^b ± 362.86	76.37 ± 383.24	0.16
b	10/12/2020	802.31 ^a ± 836.12	1274.57 ^b ± 874.11	105.17 ± 600.63	0.29
c	11/3/2021	974.82 ^a ± 1326.01	1346.71 ^b ± 969.09	78.34 ± 328.36	0.43
d	13/6/2021	2584.07 ^a ± 2995.01	3079.86 ^b ± 2900.42	65.72 ± 215.27	0.57
e	16/9/2021	4563.12 ^a ± 7091.27	4306.60 ^a ± 5145.68	299.90 ± 2335.21	0.62

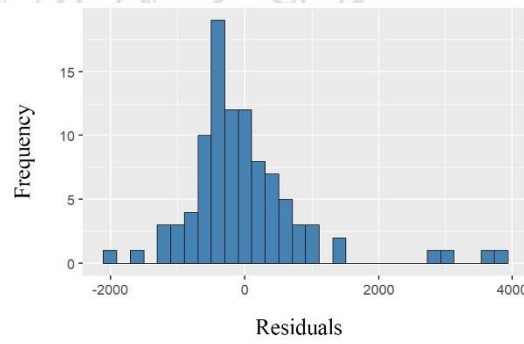
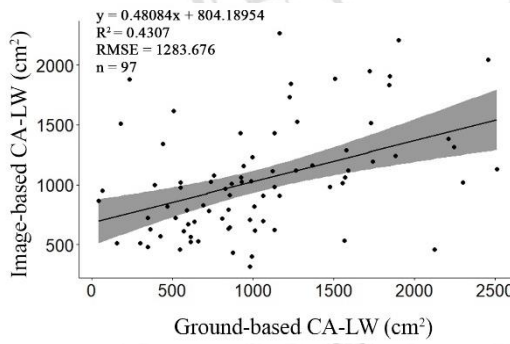
(a)



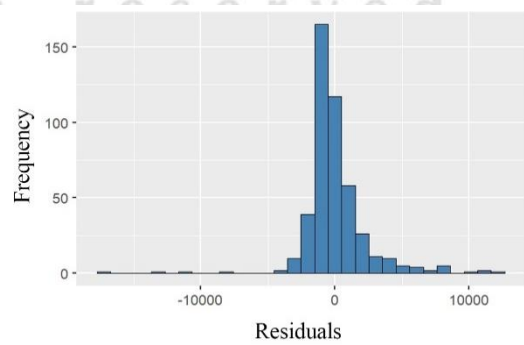
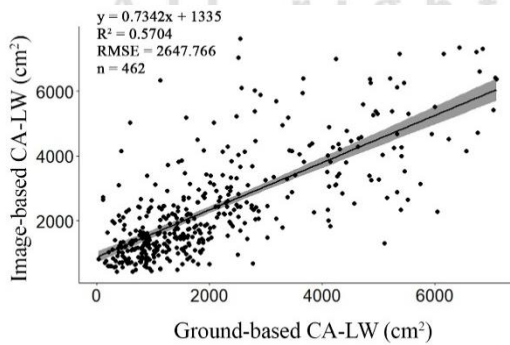
(b)



(c)



(d)



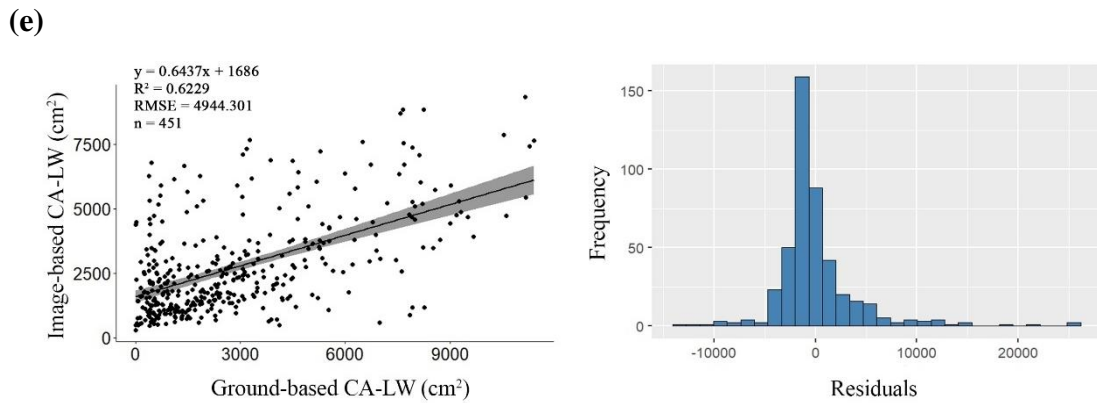


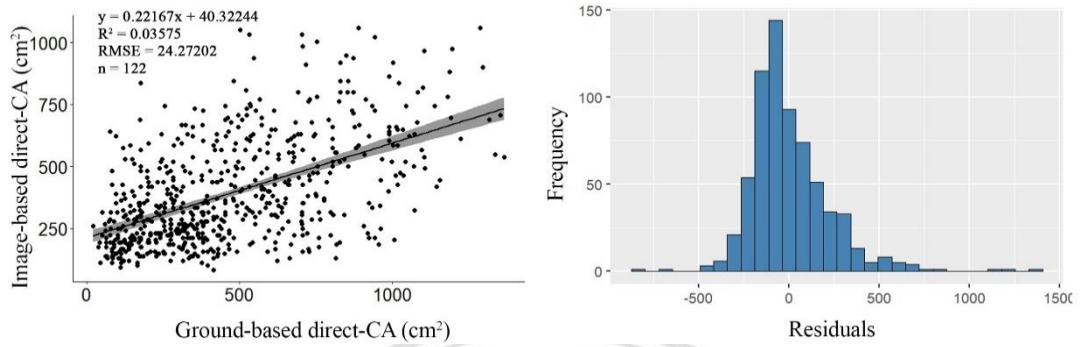
Figure 23 Regression analysis against CA-LW of ground-based and image-based data from each data collection; 29/9/2020 (a), 10/12/2020 (b), 11/3/2021 (c), 13/6/2021 (d), and 16/9/2021 (e) (a-e; $P < 0.05$). Histogram of residuals indicates normality distribution between the fitted line and each data collection.

The image-based direct-CA method overestimated crown area cf. ground data by 13-30%, except at the beginning and at the end of the study when the direct-CA method underestimated crown area. The error of measurement had no discernable trend with time or sapling size (Table 9). Relationships between ground-based and image-based measurements were moderate from the beginning of study until dry period but became more accurate after dry period ($R^2 > 0.60$, also higher than CA-LW method). Interestingly, mean crown area reveals no significant different among measurement during the dry season ($P > 0.05$). All residuals between the fitted line and the data were not normally distributed, which were slightly right skewed, except the data on 13/6/2021 was slightly left skewed (Figure 24).

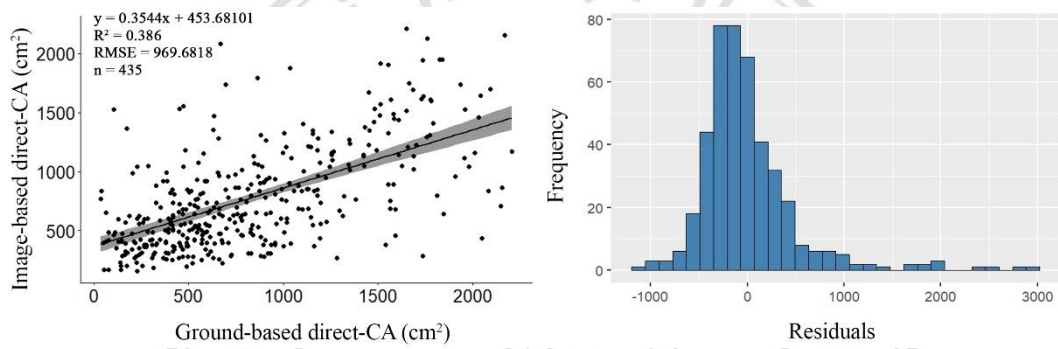
Table 9 Comparison of mean crown area (direct-CA) value from ground-based data, image-based data, and percentage of under/over-estimation.

Figure Session	Data Collection Date	Mean direct-CA from Ground Data (cm ²)	Mean direct-CA from Image Data (cm ²)	Mean Percentage Under/over-estimate	R ²
a	29/9/2020	468.26 ^a ± 405.62	424.87 ^b ± 287.12	-0.62 ± 166.40	0.27
b	10/12/2020	802.31 ^a ± 836.12	923.75 ^b ± 678.94	30.41 ± 320.75	0.39
c	11/3/2021	974.82 ^a ± 1326.01	1067.16 ^a ± 827.04	13.73 ± 191.07	0.44
d	13/6/2021	2584.07 ^a ± 2995.01	2648.71 ^a ± 2515.80	19.73 ± 156.75	0.60
e	16/9/2021	4563.12 ^a ± 7091.27	3817.69 ^b ± 4572.63	203.67 ± 1824.44	0.68

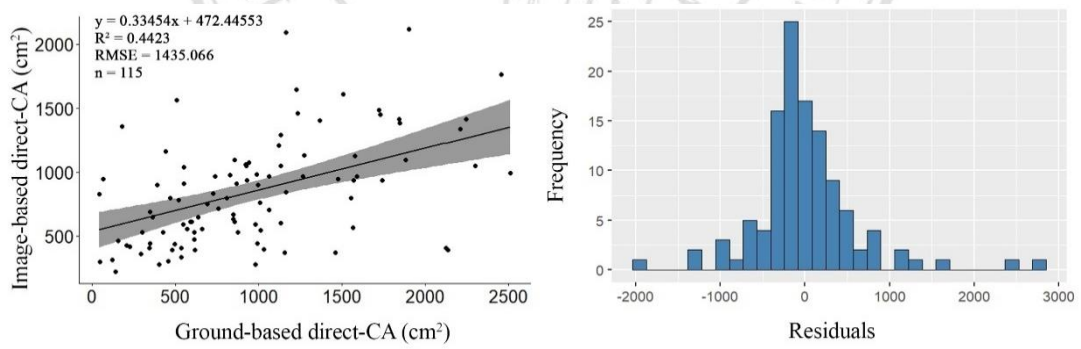
(a)



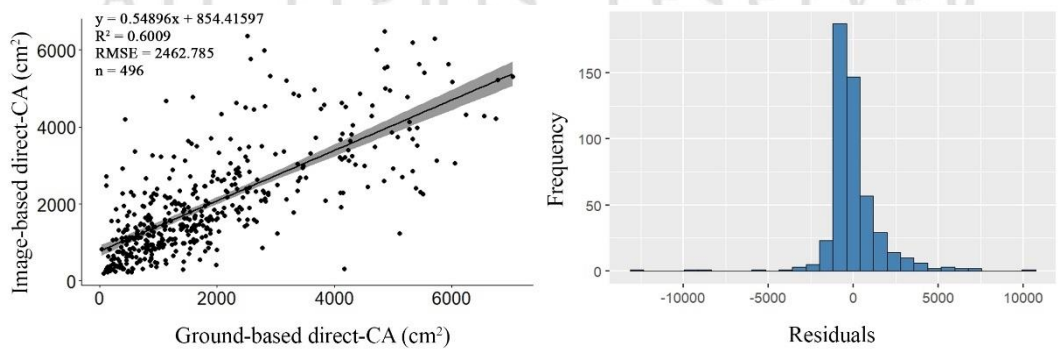
(b)



(c)



(d)



(e)

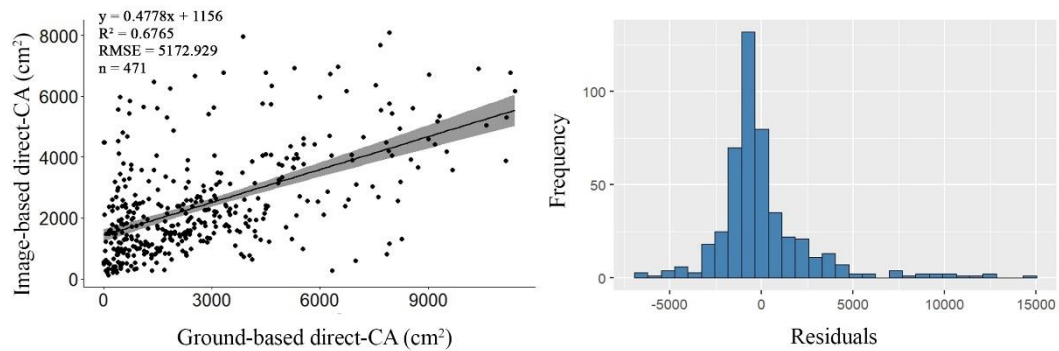


Figure 24 Regression analysis against direct-CA of ground-based and image-based data from each data collection; 29/9/2020 (a), 10/12/2020 (b), 11/3/2021 (c), 13/6/2021 (d), and 16/9/2021 (e) (a-e; $P < 0.05$). Histogram of residuals indicates normality distribution between the fitted line and each data collection.

2) Indirectly Derived Variable from Aerial-based Measurement

(Predicting RCD from other ground -measured variables)

Relationships between either height or CA with RCD (ground measurements) were weak ($R^2 < 0.5$) but grew stronger with increasing sapling age except for the relationship between CA with RCD by the end of the study (Table 10). The strongest relationship was attained from the last data collection date between height with RCD. Height was a slightly more reliable predictor of RCD than CA using ground data ($R^2 = 0.42$).

ลิขสิทธิ์มหาวิทยาลัยเชียงใหม่
Copyright© by Chiang Mai University
All rights reserved

Table 10 Correlation coefficient (r) and coefficient of determination (R²) from ground-survey data: height vs RCD, and CA vs root collar diameter.

Data Collection Date	RCD vs Height			RCD vs CA		
	r	R ²	P-value	r	R ²	P-value
29/9/2020	0.47	0.22	2 × 10 ⁻¹⁶	0.40	0.16	2 × 10 ⁻¹⁶
10/12/2020	0.39	0.15	2 × 10 ⁻¹⁶	0.49	0.24	2 × 10 ⁻¹⁶
11/3/2021	0.38	0.14	2 × 10 ⁻¹⁶	0.25	0.06	2 × 10 ⁻¹⁶
13/6/2021	0.62	0.38	2 × 10 ⁻¹⁶	0.63	0.40	2 × 10 ⁻¹⁶
16/9/2021	0.65	0.42	2 × 10 ⁻¹⁶	0.54	0.29	2 × 10 ⁻¹⁶
combined data	0.60	0.36	2 × 10 ⁻¹⁶	0.60	0.36	2 × 10 ⁻¹⁶

NOTE: All of correlation coefficient (r) and coefficient of determination (R²) are statistically significant (*p*-value < 0.001); **Bold value** indicates the highest value among its relationship.

The best equation to predict RCD from an aerially measurable variable was therefore:

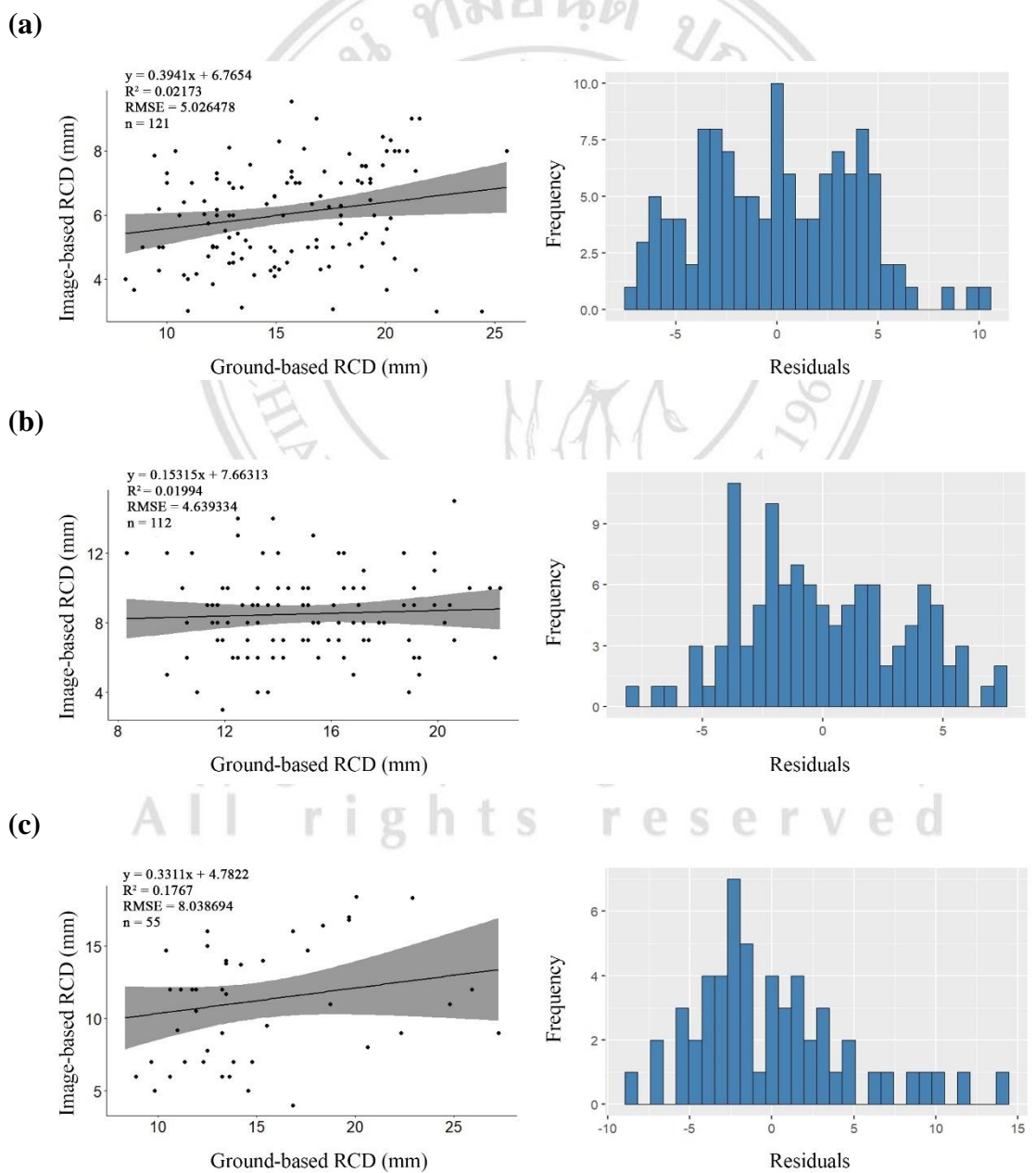
$$\text{Predicted RCD (mm)} = 0.1893(\text{Height (cm)}) + 5.6655 \quad (\text{Equation 6})$$

where *RCD* (mm) is the predicted root collar diameter and *Height* is the image-based height (cm) (RMSE = 0.2813; see also Appendix A, Table 16).

Initially, image-based measurements substantially over-estimated RCD cf. ground measurements; the difference ranged from +9 to + 59 % before dry period. The size of over-estimates decreased over time, as the saplings grew larger (Table 11). Differences in mean RCD between the two methods were insignificant during the dry season (*P* > 0.05). The strength of relationships between ground-measured and image-based RCD increased after the dry season but remained weak (highest R² = 0.36) (Figure 25). The residuals of RCD were mostly normally distributed except during the dry period (11/3/2021) when they were slightly right skewed (Figure 25).

Table 11 Comparison of mean RCD value from ground-based data, image-based data, and percentage of under/over-estimation.

Figure Session	Data Collection Date	Mean RCD from Ground Data (mm)	Mean RCD from Image Data (mm)	Mean Percentage Under/over-estimate	R ²
a	29/9/2020	5.67 ^a ± 2.33	9.05 ^b ± 3.79	59.97 ± 88.21	0.02
b	10/12/2020	5.57 ^a ± 3.70	9.12 ^b ± 3.60	9.20 ± 54.42	0.02
c	11/3/2021	9.39 ^a ± 5.36	9.23 ^a ± 5.16	-20.88 ± 53.22	0.18
d	13/6/2021	15.43 ^a ± 9.03	12.67 ^b ± 6.12	-17.42 ± 49.64	0.33
e	16/9/2021	22.57 ^a ± 13.45	16.78 ^b ± 8.45	-17.37 ± 80.27	0.36



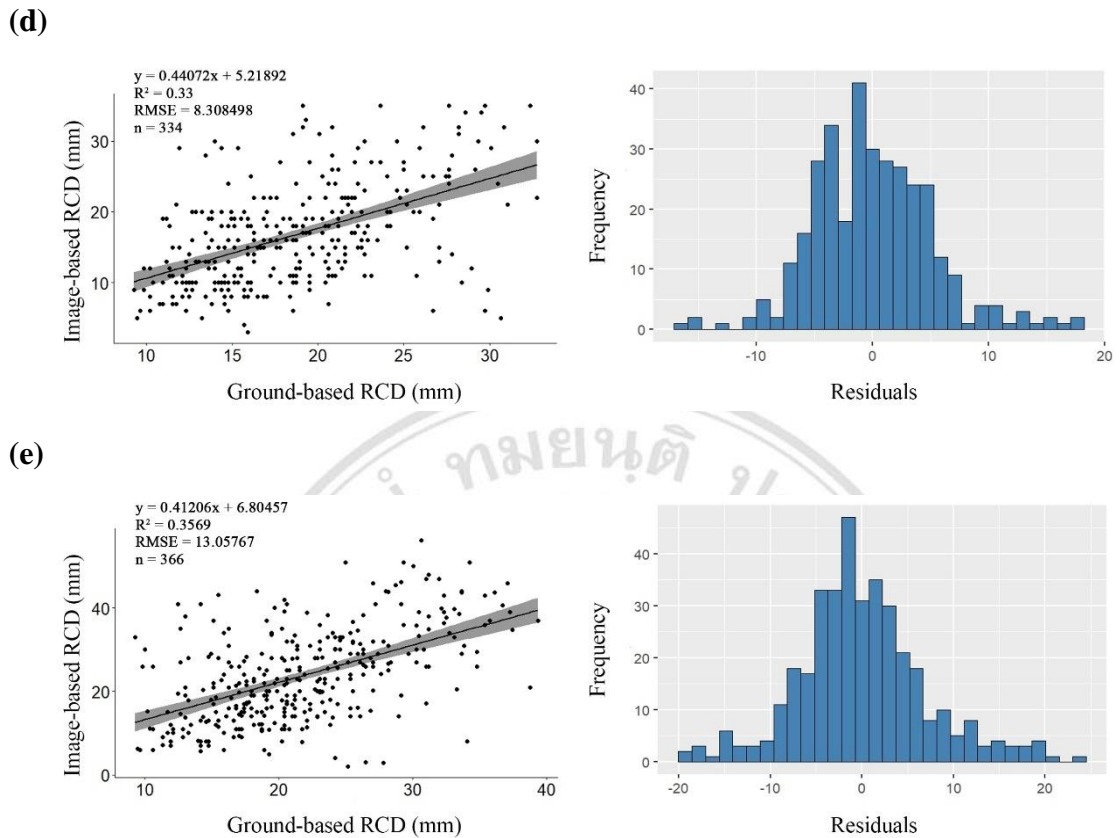


Figure 25 Regression analyses between RCD of ground-based and image-based data from each data collection; 29/9/2020 (a), 10/12/2020 (b), 11/3/2021 (c), 13/6/2021 (d), and 16/9/2021 (e) (a-c; $P > 0.05$, d-e; $P < 0.05$). Histogram of residuals indicates normality distribution between the fitted line and each data collection.

4.3.3 The Relative Growth (RGR-H) and Performance Index

Differences in height relative growth rates (RGR-H) between aerial and ground data varied among those 17 species with >20 individuals surviving from 29/9/2020 to 16/9/2021. Image-based RGR values greatly exceeded ground-based measurements for 12 species (Figure 26). The closest match in this group was for *Terminalia bellirica*, followed by *Schleichera oleosa*, *Bombax ceiba*, and *Garuga pinnata*. For those species for which image data underestimated RGR-H, *Albizia lebbek* had the closest match (Figure 26), followed by *Holoptelea grandis*, *Vitex canescens*, and *Pterocarpus macrocarpus*. In addition, detection of *Canarium subulatum* in images was too low to enable RGR-H to be calculated. Ground-based

RGR-H ranged from 3 to 120.7 % per year, whilst image-based values ranged from 0 to 172.69 % per year.

Schleichera oleosa, one and only species, performed image-based RPI almost equally to the ground-based RPI (Figure 27). The RPI of 9 out of 17 cohort species were overestimated in image-based data than ground-based data. *Sterculia pexa*, was the closest overestimated image-based RPI to the ground-based, followed by *Spondias pinnata*, and *Garuga pinnata* (these 3 species overestimated less than twice of ground-based RPI). Whilst *Terminalia bellirica*, was underestimated from image-based RGR but had closest estimates to the ground-based, followed by *Bombax ceiba*, *Holoptelea grandis*, and *Vitex canescens* (these 4 species underestimated not less than a half of ground-based RPI). The highest overestimated and the lowest underestimated of RPI among all species were *Aegle marmelos* and *Pterocarpus macrocarpus*, respectively. RPI was not calculated for *Canarium subulatum*.

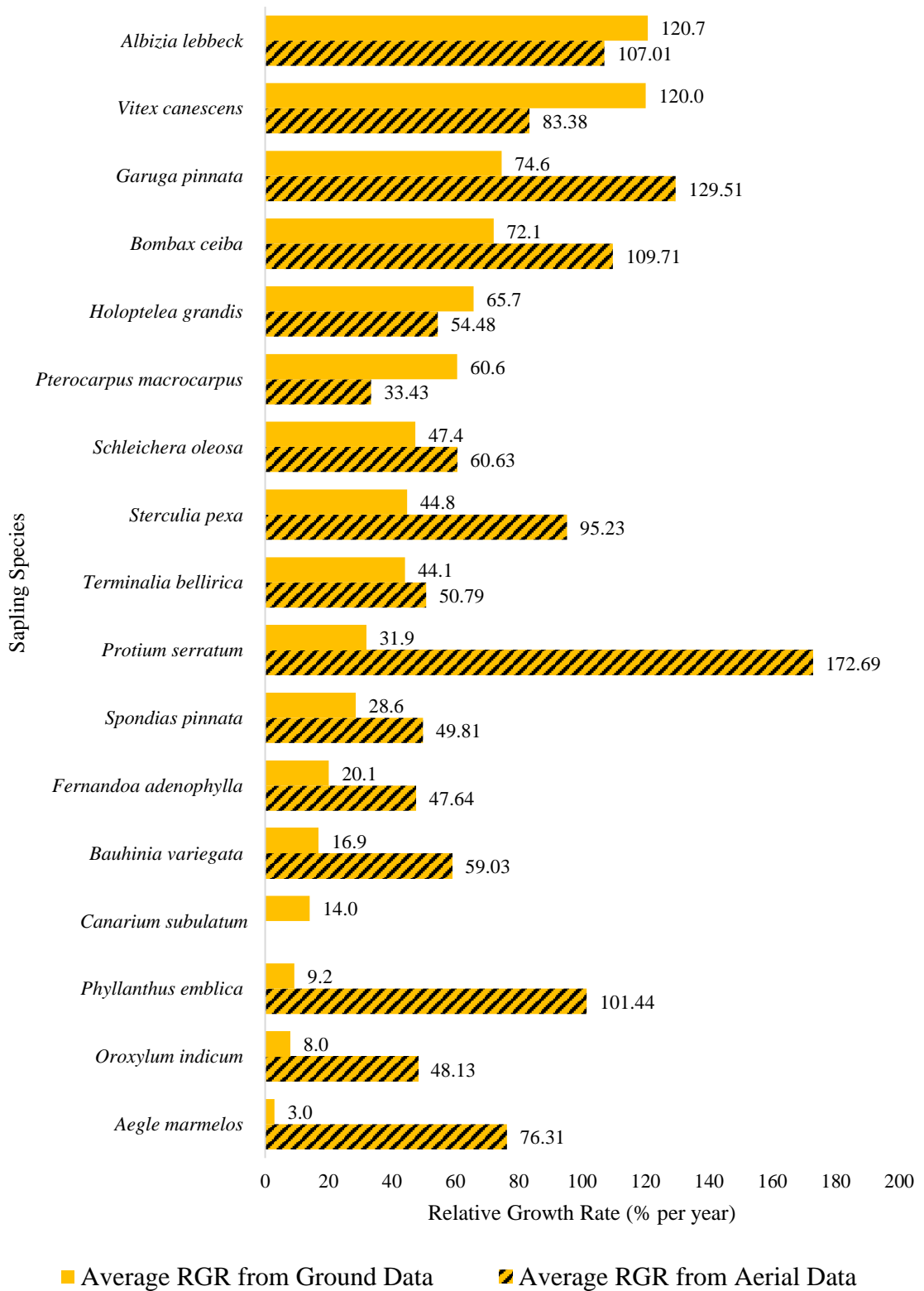


Figure 26 Relative growth rate calculated based on measured height of 17 cohort sapling species.

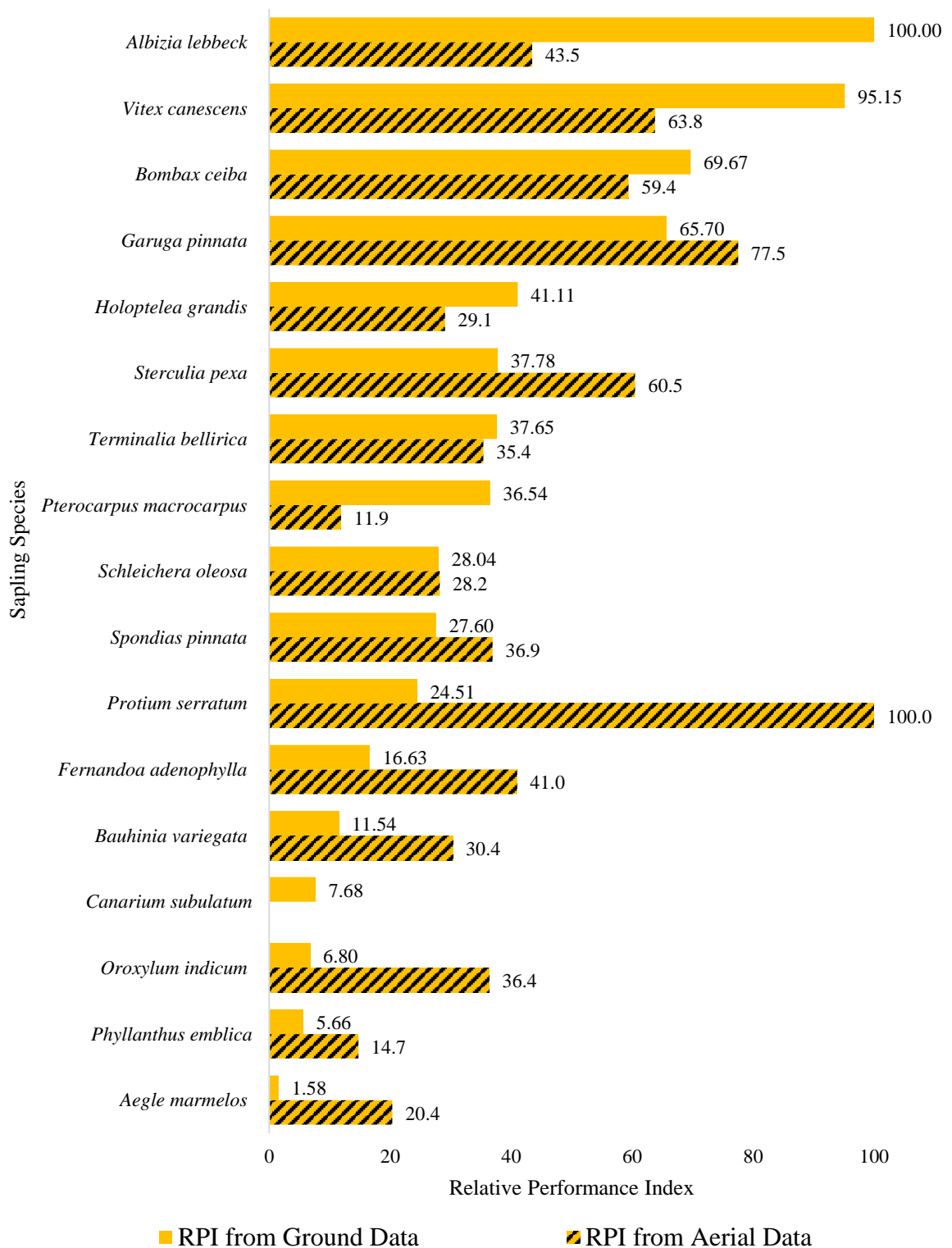


Figure 27 Relative Performance Index calculated from % survival and RGR of 17 cohort sapling species.

4.4 Discussion

4.4.1 Sapling Survivorship and Detection

The best in imaged based tree-detection method was the direct CA method, which registered approximately 85% of trees recorded during ground surveys. At the start of the study when the planted trees were very young (0-3 months old), the direct-CA method was also useful for measuring crown area, despite the trees' small size. Even during dry period (data collection on 11/3/2021), when detection rates for all methods was very low, the direct CA method performed better than the other techniques (17%), although its detection rate was not markedly higher than that of the CA-LW method subsequently.

The effectiveness of using orthomosaic images to detect and count saplings increased with sapling age and size. It reached >70% of ground counts by the time the trees were 9 months old. In contrast, using 3D point clouds achieved the highest detection of less than 60%, when trees were 1-year old. The height method of tree detection in 3D point clouds was less efficient when most of the trees were leafless in March (less than half of the saplings) because of the difficulty of discriminating bare tree stems from the mine substrate background. Gallardo-Salazar and Pompa-García (2020) also mentioned the challenge of distinguishing individual plants from surroundings due to lack of plant uniformity (i.e., different species, different arrangements). This challenge was also faced in our study which included 30 different species without fixed positions/arrangements. Furthermore, the lack of plant uniformity complicated manual sapling detection for every method in this study. Consequently, sapling detection by using 3D point clouds could not be used to report sapling survivorship report within the 1st year immediately following tree planting; only the orthomosaic images could be used to do so.

Smaller saplings were also more likely to be missed during ground surveys. The mean RCD of “alive-not-found” saplings was significant lower ($p < 0.05$) by 27 % on average, compared with those recorded alive (on 16/9/21). Both mean heights and RCD values were lower for alive-not-found saplings at other

times, but not significantly so (Table 12). The size of saplings (in terms of height and RCD) affected their detection during ground surveys, especially RCD when planted saplings were 1 year old.

Table 12 Comparison of mean root collar diameter and height from ground-based data between alive saplings and alive-not-found (ANF) saplings.

Data Collection Date	RCD (mm)		Height (cm)	
	Alive	ANF	Alive	ANF
10/12/2020	7.56 ± 3.70	-*	55.78 ± 30.60	-*
11/3/2021	9.47 ± 5.44	8.31 ± 3.86	54.36 ± 24.06	52.12 ± 26.87
13/6/2021	16.04 ± 14.45	15.55 ± 9.47	70.00 ± 33.64	66.97 ± 30.19
16/9/2021	23.11 ^a ± 13.52	16.64 ^b ± 16.64	89.88 ± 50.59	74.40 ± 56.71

Note: \bar{x} is calculated from values in the immediate subsequent survey.

* In ANF = no \bar{x} , only 1 datum. Differences between Alive and ANF not significant except for RCD on 16/9/2021 ($P > 0.05$).

In contrast, sapling detectability from image-based measurements did not appear to be related to RCD. Saplings with small crowns were not detected less than those with larger crowns. The R^2 results of correlation analyses between detectability and mean species sapling height (Figure 20) and between detectability using both image-based methods and mean species crown area (Figure 21), were very close to 0, suggesting that height and crown area had slight or no effect on detectability.

Apart from size, other species related to sapling crown characteristics might affect detectability. *Fernandoa adenophylla* and *Phyllanthus emblica* had the highest and the lowest detectability respectively in 3D point clouds and they possessed markedly different crown structures (Figure 28). *F. adenophylla*, has odd pinnate leaves with 2-5 pairs of leaflets with a long-stalked terminal leaflet, whilst *P. emblica* has insubstantial “feathery” pinnate leaves with tiny pinnae (Elliott et al., 2006). From the top-view, *F. adenophylla* crowns appear dense almost solid, whilst *P. emblica* presents insubstantial, thin and irregular crowns (Figure 27). Moura et al. (2021) also suggested that the characteristics of each tree species’ crown are related with ease of automatic detectability in UAV imagery. Auto recognition of sapling species in aerial images is not yet possible (Frame & Garzon-

Lopez, 2020). To fully automatic species detection and understand more about the sapling crown characteristics that affect sapling detectability further research to develop more advanced technologies is needed (Buters et al., 2019a),

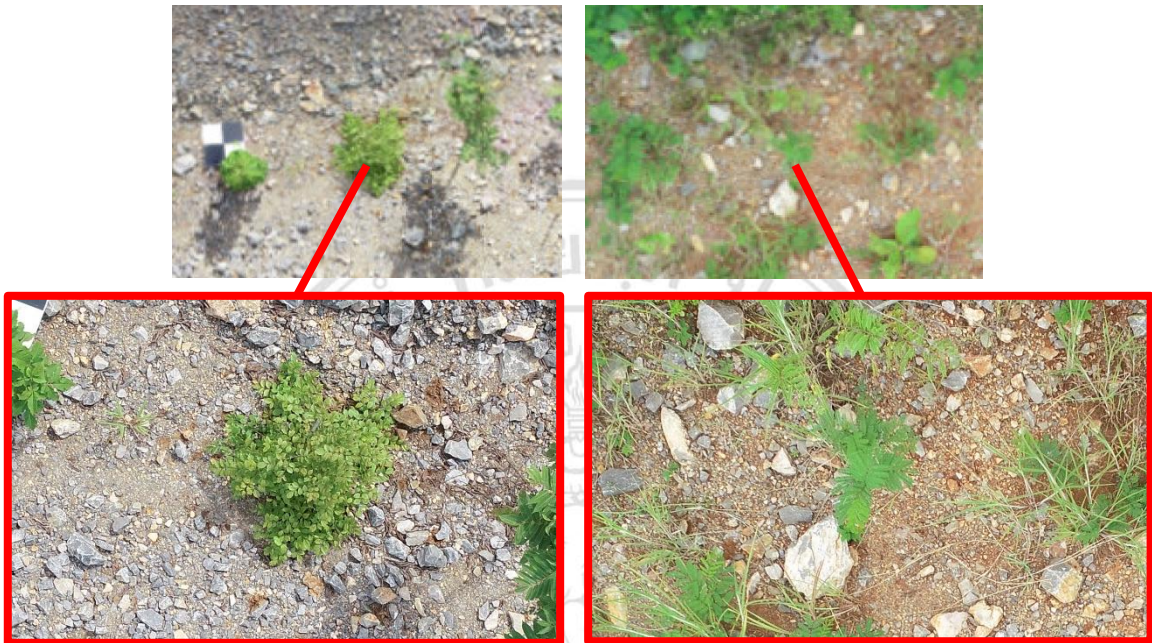


Figure 28 Comparison between *Fernandoa adenophylla* (left) and *Phyllanthus emblica* (right) leaf characteristic; upper row – orthomosaic image, lower row – raw RGB image.

4.4.2 The Correlation of Image-based Measurements

1) Height

Image-derived height data correlated significantly with ground survey data. The closeness of the correlation increased with time i.e., the taller the saplings, the stronger the correlation between ground and drone height measurements. Although height measurements were hindered by low tree detection in images during the dry season, the few trees that could be detected still yielded accurate height data. Therefore, the sapling age/height, at which height could be measured with strongest correlation (also highest detectability) in this study, was 1 year after planting at an average height of 0.8 m.

2) Crown Area from Length and Width (CA-LW)

Correlation of the image-based CA-LW gradually improved over time. CA-LW performed the best and with strongest correlation when the saplings flushed new leaves after dry season. Differences between mean CA-LW from ground-based data and image-based data were not significant at the end of the study (1-year old). This was also confirmed by the research at a plot planted 1 year earlier at the same site. Under the same conditions, Lee (2021), reported that differences in percent canopy cover between ground and UAV images were insignificant in a 1-year-old restoration plot adjacent to the one used in the study reported here. Therefore, the CA-LW method is recommended to monitor the saplings for crown area expansion after the first year of planting (at least after the first year dry period).

It was reasonable to expect that the correlation of CA-LW method would be stronger than that of the CA method, because ground-based CA was calculated in the same way as in the images (calculated from crown length and width, by assuming the crown shape was an ellipse). Nevertheless, CA-LW had slightly weaker correlation than direct-CA method over whole study. There are two possible explanations for this. Firstly, it is possible that the distance tool of DroneDeploy over-counted the ground surface pixel, when measured sapling crown length and width. As mentioned in section 2.3.2, DroneDeploy has limited zoom capability while using the tools, and therefore, image-based crown length and width could be overestimated. Another issue was that the longest crown dimension (crown length) may have been measured in different places in ground surveys compared with image analysis. Crowns tend to be viewed more from the side in ground surveys, so the perspective is different compared with the overhead view in images.

3) Direct Crown Area (direct-CA)

Correlation of image-based measurements of direct-CA also improved gradually over time. The correlation of the Direct-CA method was similar to that of the CA-LW method, but it was able to detect more saplings (Figure 18). However, differences in mean direct-CA from ground-based data compared with image-based data were insignificant only during dry season (11/63/22021) and when the saplings flushed new leaves (13/6/2021). Furthermore, there was no trend in mean percentage under/over-estimate for direct-CA method over the study period.

Differences between ground-based CA and image-based direct-CA might have arisen for the same reason as with the CA-LW method, as we used the same photogrammetric software (DroneDeploy), but a different tool. However, the last data collection (16/9/2021) was an exception in that mean direct-CA was lower than mean crown area from ground-based data. This indicated that area measuring tools in DroneDeploy not only over-counted ground pixels, but also may have miss-counted canopy pixels as well.

Although the direct-CA method was a fairly accurate way to monitor crown area during the dry season, further trials are needed to determine the trend beyond 1 year after planting.

4) Root Collar Diameter (RCD)

Height was a more reliable predictor of RCD than CA using ground data. The relationship between height and RCD became stronger as the saplings grew larger (but not the relationship between CA and RCD). The model, acquired from the height relationship using 1-year-old data (*equation 6*), had the highest fit (even better than the best CA relationship). Because when sapling's crown area was absent during the dry period (in March), the predicted RCD from every absent crown area sapling would be all the same ($CA = 0$).

Application of species-specific equations could result in a higher reliable predictor of RCD. For 14 of the 17 species correlation between height and RCD had higher fit than that of *equation 6* (see also Appendix A). Iida et al. (2011) suggested that prediction of RCD from models is species-specific, since species differ in their relative proportions (traits/habit). Khamyong et al. (2018) also stated that species-level characteristics should be considered when predicting tree variables, to reduce the error. Although, there was uncertainty with using only 1 equation, in terms of the rapid assessment/monitoring, it is not practical to apply species-specific equations to predict unmeasurable variables from image-based data. Therefore, further investigation should consider whether to apply species-specific equations appropriate to their study.

Table 13 Slope (m), intercept (c), and coefficient of determination (R^2) from relationship between height vs RCD for individuals of the 17 cohort species.

RCD vs Height			
Equation acquired from	Slope	intercept (c)	R^2
5th Data Collection (<i>equation 6</i>)	0.1851	5.96757	0.42
<i>Spondias pinnata</i>	0.18809	14.28255	0.73
<i>Phyllanthus emblica</i>	0.14866	4.20313	0.52
<i>Terminalia bellirica</i>	0.2093	2.82355	0.50
<i>Albizia lebbek</i>	0.1996	5.5309	0.72
<i>Protium serratum</i>	0.21579	1.90559	0.79
<i>Canarium subulatum</i>	0.22844	1.86584	0.60
<i>Pterocarpus macrocarpus</i>	0.12387	2.91336	0.71
<i>Garuga pinnata</i>	0.12712	17.92882	0.15
<i>Sterculia pexa</i>	0.20056	4.91627	0.58
<i>Holoptelea grandis</i>	0.20006	7.25224	0.55
<i>Schleichera oleosa</i>	0.28604	4.26029	0.64
<i>Oroxylum indicum</i>	0.22274	-1.45728	0.68
<i>Bauhinia variegata</i>	0.17353	3.84389	0.43
<i>Fernandoa adenophylla</i>	0.3247	19.6199	0.13
<i>Aegle marmelos</i>	0.09906	4.1613	0.28
<i>Bombax ceiba</i>	0.19657	3.59419	0.59
<i>Vitex canescens</i>	0.16763	10.98862	0.53

Note: R^2 represented in red means the fit of the regression result from that species is worse than the result of 5th Data Collection (*equation 6*).

RCD values, derived from image data, were not significantly correlated with ground-based direct RCD measurements (with exception of the dry period only); thus, correlation was weak. Although correlation stronger over time, it remained unacceptably low at the end of the study period. This may have been due to the application of non-species-specific predicting equations in this study. The youngest age of trees, at which RCD could be predicted with the strongest correlation from imagery was 1-year old. Therefore, use of non-specific equations to predict RCD is not recommended.

4.4.3 RGR and Relative Performance Index

1) RGR-H

Image-based measurements performed quite well for predicting RGR-H for faster-growing sapling species (where the height difference between first data collection and the end of the study was large). However, image-based measurements substantially overestimated RGR-H of slower-growing species (small difference in height) (e.g., *Aegle marmelos* (>1,000%) and *Phyllanthus emblica* (>2,000%), etc.). However, the lack of a relationship between species-level mean RGR-H (% per year) and percentage species-level detectability (Figure 29) meant that image-based measurement could not reliably predict RGR as accurately as ground-based measurements regardless of the size of height change.

Errors in predicting RGR-H from image-based measurements were compounded by weak correlation of height measurements, particularly at the start of the study, when sapling detectability was low and correlation between image and ground height measurements was very low ($R^2 < 0.05$). Therefore, use of image data to calculate RGR-H is not recommended before detectability and rates and height measurements become more reliable (i.e., at least 1 year after planting).

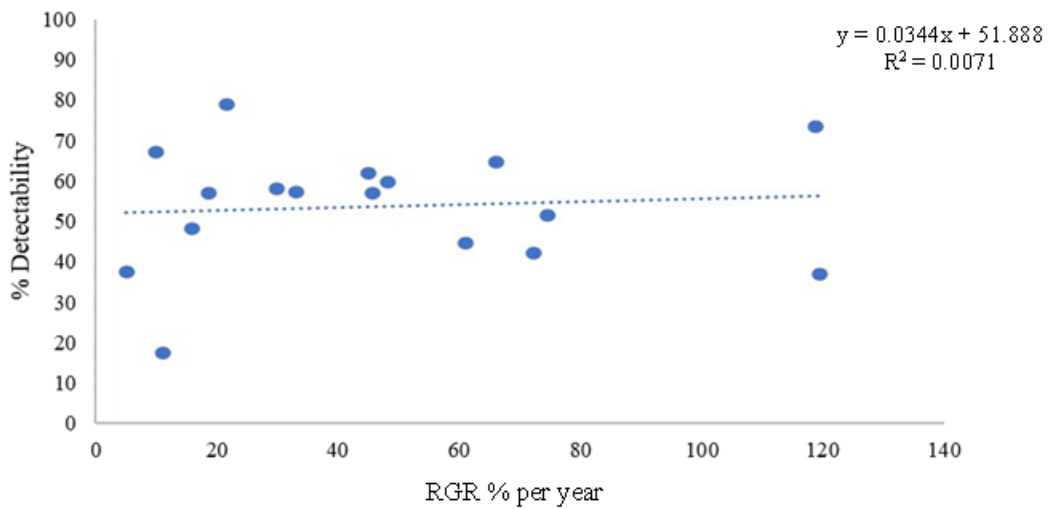


Figure 29 Scatter plot between species-level mean relative growth rate (% per year) and percentage species-level detectability (17 species with $n > 20$).

2) Relative Performance Index

Calculation of a standardized relative performance index has become an established method to rank species' suitability, when performing restoration trials with diverse species mixtures. The ultimate test of image-based technique is to determine if data from UAV imagery could be used to generate the same species-suitability ranking as from ground data (regardless of differences in *absolute* values).

Unfortunately, the species ranking produced from image-based technique was drastically different than that produced conventionally from ground-based data. The order of species ranking compared between ground-based and image-based measurements was not similar. For example, *Albizia lebbek* was the top-ranked species using ground-based data, whereas *Protium serratum* performed the best using image-based data. The error in percent detected saplings from height method and error of predicting RGR, were both became magnified by multiplication when calculating RPI. Finally, clearly large improvements in the collection and analysis of image-derived

data were needed, before image-based measurement techniques can adequately replace ground surveys.

4.4.4 Limitation of Image-based Techniques and Further Suggestion

1) Cost and speed of Image-based Technique

Our drone-based technique has the potential to minimize the involved labor input for the sapling monitoring. Flying the UAV autonomously, we required only 2 operators and were able to complete whole site data collection within 1 day. In contrast, ground-data collection required at least 6 people, to monitor all saplings over 2-3 working days. Consequently, staff hiring cost for data collection and transportation costs could be reduced by up to 2-3 times, using aerial methods. Ground measurements require only simple equipment, whereas drone methods require a considerable capital outlay at the start, although such equipment costs are spread more thinly as the number of projects increases.

After field work, 1 day is needed for ground data entry and analysis. Although image process of aerial data also requires 1 day, the process is autonomous (so no labor needed). Measuring variables within the images and models produce however is time consuming (at least 1 full day's work), but this step might be replaced in the near future with autonomous AI-based analyses. Therefore, it is likely that aerial based monitoring techniques will save both time and money as technologies advance. However, further work is needed to compare cost effectiveness between image-based and ground methods techniques.

2) Dried Period Effect and Tree habit

In Lampang Province, the dry season runs from November to April (SCG, 2015). Data collection in March, when most trees were leafless, was particularly difficult, as trees were less visible, both on the ground and in aerial images. Furthermore, many trees appeared dead, when in fact they were

dormant. Therefore, it is necessary to check whether the trees are actually dead or have poor health by scratching their stem to check for green tissue. If the saplings still have green tissue, they are assigned a low health score (health score ≤ 1), and the other variables are measured, except crown dimensions. At the same time, understanding trees' habit is also a key point to achieve aerial-based techniques to monitor young saplings planted for open-cast mine restoration on the first objective.

3) Non-target Trees

As planted saplings grew, non-target plants also grew up alongside them and became more abundant. Figure 30 shows a lot of green bushy plants within the study plot, many of which were potentially invasive non-natives. *Cajanus cajan* (Linn.) Millsp. (Common name: Pigeon Pea), had germinated along the bench from seeds scattered by SCG staff (sometimes covering planted saplings) on the assumption that it improves the soil nutrient status. However, the spread of the legume hindered sapling detection in both orthomosaic images and 3D point clouds. It was not a serious problem during ground-based surveys, since workers could easily distinguish trees from the legume close up. The study presented here was essentially a proof-of-concept trial, under conditions of maximum sapling visibility (against the plain background of the mining substrate). As most forest restoration sites are covered in herbaceous weeds, which can obscure small, planted trees, further research will be needed to ensure image-based monitoring methods can readily distinguish between tree crowns where there is a weedy background.

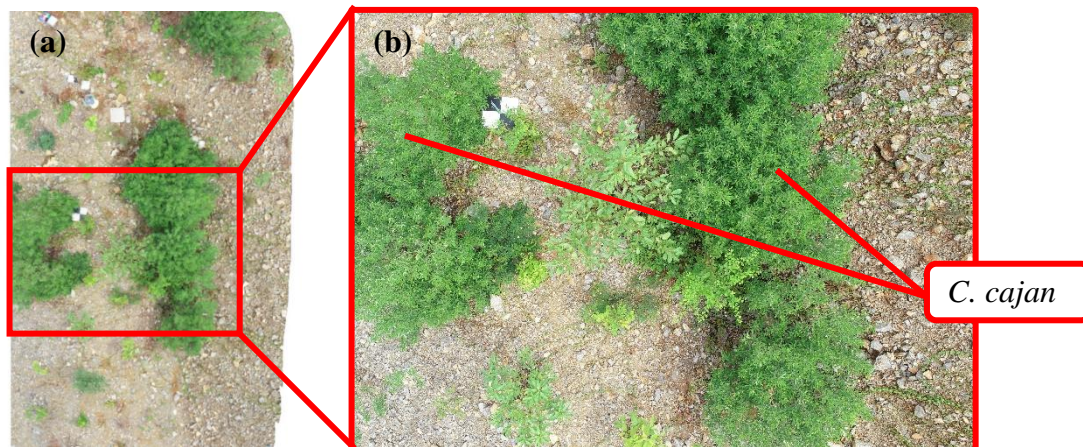


Figure 30 *Cajanus cajan* (Pigeon Pea) caused difficulty in tree distinction and variables measurement; A part of orthomosaic image on 16/9/2021 (1-year old tree) (a), one of the raw RGB images used in this processed image (b).

4) Software Setting and Performance

Image processing procedures in DroneDeploy are fixed as the default setting (no additional processing setting). For example, model quality, optimized alignment, key point and tie point limit, etc.) were all standard. All processed images were automatically generated from the input raw images. The quality of the input raw images plays an important role in image processing and therefore in tree detection. The type of input images is therefore an important consideration. For example, Buters et al. (2019a) used multispectral images to detect high numbers of saplings (even seeds were detected easily) correlation of $> 80\%$. In this study, since RGB images were used for image processing, potential tree detection may have been lower than it might have been with other image types. Figure 31 shows the difficulty of height measurement in 3D point clouds. The trees could hardly be distinguished from the ground surface in the original RGB-perspective, whilst edited color, showing altitude found no trees present. However, Buter's study was performed on a flat clear-cut area, eliminating many confounding external factors, while uncontrollable surrounding condition (such as dried period) of this study site in the mine restoration area.

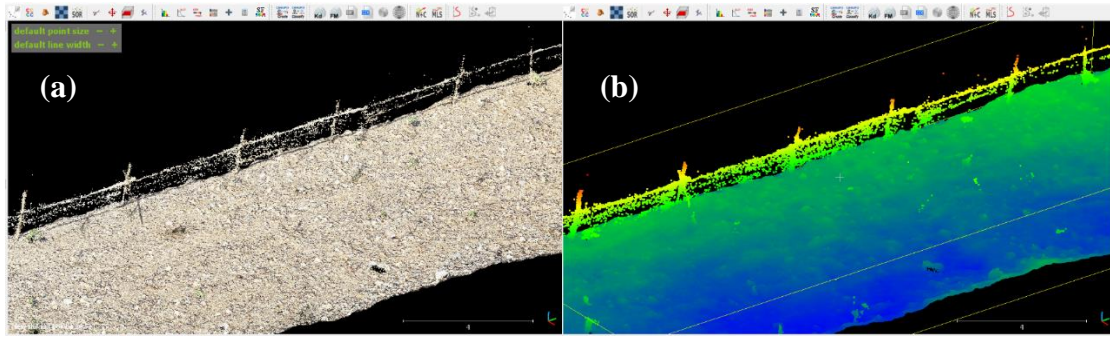


Figure 31 Difficulty of height measurement on the youngest age of planted sapling (0 month); original RGB-perspective (a), edited color related to attitude failed to detect sapling pixels (b).

5) Additional Equipment

In this study, acquisition of aerial images was only controlled by the flight planning application (LITCHI) and with the help of ground control points (black and white plastic boards, attached to PVC poles along benches) to indicate the boundary of the target bench for each flight mission. Several researchers have used advanced ground control points, linked to GPS systems, to improve correlation of aerial images. They tested use of ground control points, and more advanced methods, particularly using real-time-kinematic (RTK) and postprocessing-kinematic (PPK) technologies, to improve the correlation of coordinates and increase the feasibility of image-based measurements (Dempewolf et al., 2017).

Further advancement of UAV capabilities could revolutionize environmental recovery activities (Torresan et al., 2017, Yao et al., 2019), particularly monitoring of rehabilitated areas to provide accurate methods of tracking sapling communities and even high-value individuals, giving practitioners a reliable tool for predicting the trajectory of these communities by remotely measuring growth and development. Future research should also investigate the possibility of acquisition of required variables with combinations of sensors during single flights (e.g., thermal, multispectral, or hyperspectral sensors, etc.), which would cover the amount of data collected

in less time and lead the study closer to a one-pass solution for ecological monitoring (Gallardo-Salazar & Pompa-García, 2020). With more research and investment, UAV-based remote sensing could allow restoration practitioners to monitor plant performance earlier in the community recovery process, with greater correlation, precision, and cost-efficiency, and at much finer resolution over increasingly larger spatial scales, compared to other monitoring methods like ground survey/data collection (Buters et al., 2019c).

4.4.5 Pros and Cons of Manual Image-based Measurements (compared with AI analyses)

Pros	Cons
<ul style="list-style-type: none"> capital outlay is less (purchase of AI software not required) 	<ul style="list-style-type: none"> operators need to consider and solve every obstacle/unexpected situation by him/herself
<ul style="list-style-type: none"> speed in distinguish individual seedlings (to species level) depend on operator's skill 	<ul style="list-style-type: none"> requires more time when background is complex or non-target objects (weed) abundant
<ul style="list-style-type: none"> able to notice any mistakes of the target object (saplings), because operator need to run through step by step 	<ul style="list-style-type: none"> difficult to distinguish individual saplings when surrounding conditions change (e.g. dry period)
	<ul style="list-style-type: none"> scaling up to large areas is impractical

ลิขสิทธิ์มหาวิทยาลัยเชียงใหม่
 Copyright© by Chiang Mai University
 All rights reserved

CHAPTER 5

Conclusions

The main purpose of this study—to develop a rapid aerial-based technique to monitor young trees—was partially achieved for saplings 1 year or more after planting, with detectability rates up to 85% based on the direct-CA method (Figure 18) and 10% error in height measurements (Table 7).

Among the free versions of the three software tools tested, DroneDeploy is recommended for generating 3D point cloud models, and for acquiring sapling height data. This study can be used as a preliminary guideline for environmental researchers to choose suitable software for sapling measurement.

Sapling height and crown area variables can be quantified directly from low-altitude aerial imagery. For crown area measurement, either CA-LW or direct-CA method is recommended. RCD can be predicted from height, using equations acquired from ground-based correlations. Species-specific equations might not be practical for rapid sapling assessment/monitoring.

Highest tree-detection percentages using 1-year old orthomosaic images were 85% (direct-CA) and 81% (CA-LW), and in 3D point clouds it was 64 %. Orthomosaic images have a much higher resolution than 3D models, so trees are far more easily distinguished in them. Saplings were mostly undetectable (missed) when leafless during the dry season. Individual characteristics of sapling species, like leaf size and crown architecture may influence detectability more than overall tree size since smaller trees were not less detectable than larger ones in both orthomosaic images and 3D point cloud.

When saplings were young and small most image-based measurements were exaggerated compared with ground measurements. As the size and age of saplings increased, the extent of overestimations of image-based measurements varied inconsistently among variables.

Image-based height measurements correlated moderately with ground-based measurements, with a moderate correlation ($R^2 = 0.57$, $P < 0.001$) after the trees had been growing 1 year). CA from image-based measurement moderately correlated when compared ground-based measurements, ($R^2 = 0.62$ and 0.68 , $P < 0.001$ in CA-LW and in direct-CA method, respectively) after the trees had been growing 1 year. Predicted image-based RCD correlated weakly with ground-based RCD with weak correlation ($R^2 = 0.36$, $P < 0.001$) after the trees had been growing 1 year. Species-specific equations perform better and would help to increase correlation of RCD estimates from image-based height measurements.

Tree detection and measurement correlation became more reliable during the second rainy season after planting (after the trees had been growing 1 year), when most of the trees were taller than 0.8 meters. Therefore, aerial monitoring is recommended from the second rainy day after planting, onwards when the trees are 9 months old.

Errors in measurements of survival and growth became compounded and magnified when calculating RPI. Consequently, image-based RPI values drastically altered the ranking of species by overall field performance, compared with RPI values derived directly from ground data. Clearly, further research will be needed to improve technologies and processing at all stages of drone-based monitoring, before image data could contribute meaningfully towards species-selection decision making, based on young field trials.

Although this study has yielded promising results in terms of sapling detectability and height measurements in a simplified environment, more work is needed before developing the technique to monitor sites of greater complexity. The study has shown that seasonality (particularly deciduousness), species traits (e.g., crown density and leaf size/arrangement) and above all, appropriate age and size of the target trees all need to be considered when developing appropriate aerial techniques to monitor the progress of forest ecosystem restoration on more complex sites.

REFERENCES

- Aerts, R., & Honnay, O. (2011). Forest restoration, biodiversity and ecosystem functioning. *BMC Ecology*, *11*(1), 29. <https://doi.org/10.1186/1472-6785-11-29>
- Aerts, R., Hundera, K., Berecha, G., Gijbels, P., Baeten, M., Van Mechelen, M., Hermy, M., Muys, B., & Honnay, O. (2011). Semi-forest coffee cultivation and the conservation of Ethiopian Afromontane rainforest fragments. *Forest Ecology and Management*, *261*(6), 1034–1041. <https://doi.org/10.1016/j.foreco.2010.12.025>
- Anderson, K., & Gaston, K. J. (2013). Lightweight unmanned aerial vehicles will revolutionize spatial ecology. *Frontiers in Ecology and the Environment*, *11*(3), 138–146. <https://doi.org/10.1890/120150>
- Berni, J. A. J., Zarco-Tejada, P. J., Suárez, L., & Fereres, E. (2009). Thermal and narrowband multispectral remote sensing for vegetation monitoring from an unmanned aerial vehicle. *IEEE Transactions on Geoscience and Remote Sensing*, *47*(3), 722–738. <https://doi.org/10.1109/TGRS.2008.2010457>
- Brudvig, L. A. (2011). The restoration of biodiversity: Where has research been and where does it need to go? *American Journal of Botany*, *98*(3), 549–558. <https://doi.org/10.3732/ajb.1000285>
- Buters, T., Belton, D., & Cross, A. (2019). Seed and seedling detection using unmanned aerial vehicles and automated image classification in the monitoring of ecological recovery. *Drones*, *3*(3), 1–16. <https://doi.org/10.3390/drones3030053>
- Buters, T. M., Bateman, P. W., Robinson, T., Belton, D., Dixon, K. W., & Cross, A. T. (2019). Methodological ambiguity and inconsistency constrain unmanned aerial vehicles as a silver bullet for monitoring ecological restoration. *Remote Sensing*, *11*(10). <https://doi.org/10.3390/rs11101180>
- Buters, T. M., Belton, D., & Cross, A. T. (2019). Multi-sensor uav tracking of individual seedlings and seedling communities at millimetre correlation. *Drones*, *3*(4), 1–20. <https://doi.org/10.3390/drones3040081>

- Chen, W., Li, X., He, H., & Wang, L. (2018). A review of fine-scale land use and land cover classification in open-pit mining areas by remote sensing techniques. *Remote Sensing*, 10(1). <https://doi.org/10.3390/rs10010015>
- Chisholm, R. A., and T. Swinfield. 2020. Automated Vegetation Monitoring for Forest Restoration. In S. Elliott, G. Gale, and M. Robertson (editors), *Automated Forest Restoration: Could Robots Revive Rain Forests?* FORRU-CMU
- Dash, J. P., Watt, M. S., Pearse, G. D., Heaphy, M., & Dungey, H. S. (2017). Assessing very high resolution UAV imagery for monitoring forest health during a simulated disease outbreak. *ISPRS Journal of Photogrammetry and Remote Sensing*, 131, 1–14. <https://doi.org/10.1016/j.isprsjprs.2017.07.007>
- Dempewolf, J., Nagol, J., Hein, S., Thiel, C., & Zimmermann, R. (2017). Measurement of within-season tree height growth in a mixed forest stand using UAV imagery. *Forests*, 8(7), 1–15. <https://doi.org/10.3390/f8070231>
- DroneDeploy. Available online: <https://www.dronedeploy.com/> (accessed on 28 February 2022).
- Elliott, S., Baker, P. J., & Borchert, R. (2006). Leaf flushing during the dry season: the paradox of Asian monsoon forests. *Global Ecology and Biogeography*, 15(3), 248–257. <https://doi.org/10.1111/j.1466-822x.2006.00213.x>
- Elliott, S., G. Gale and M. Robertson (Eds.). (2020). *Automated Forest Restoration: Could Robots Revive Rain Forests?* Forest Restoration Research Unit, Chiang Mai University, Thailand. 254 pp.
- Elliott, S., Navakitbumrung, P., Zangkum, S., Kuarak, C., Kerby, J., Blakesley, D., & Anusarnsunthorn, V. (2000). Performance of Six Native Tree Species, Planted To Restore Degraded Forestland in Northern Thailand and Their Response To Fertiliser. *Forest Restoration for Wildlife Conservation*, January 2000, 244–255.
- Erskine, P. D., & Fletcher, A. T. (2013). Novel ecosystems created by coal mines in central Queensland's Bowen Basin. *Ecological Processes*, 2(1), 1–12. <https://doi.org/10.1186/2192-1709-2-33>

- FAO. (2020). Global Forest Resources Assessment 2020 – Key findings. Rome.
<https://doi.org/10.4060/ca8753en>
- FAO and UNEP. (2020). The State of the World's Forests 2020. Forests, biodiversity
- Frame, D. & C. Garzon-Lopez. (2020). Applications of remote sensing for tropical forest restoration: challenges and opportunities. Chapter 3, pp46-53, in Elliott S., G, Gale & M. Robertson (Eds), Automated Forest Restoration: Could Robots Revive Rain Forests? Proceedings of a brain-storming workshop, Chiang Mai University, Thailand. 254 pp.
- Forest Restoration Research Unit, 2005. How to Plant a Forest: The Principles and Practice of Restoring Tropical Forests. Compiled by Elliott, S., D. Blakesley, J.F. Maxwell, S., Doust & S. Suwannaratana. Biology Department, Science Faculty, Chiang Mai University, Thailand, 200 pp.
- Forest Restoration Research Unit, 2008. Research for Restoring Tropical Forest Ecosystems: A Practical Guide. Chiang Mai University, Forest Restoration Research Unit, Thailand. 144 pp
- Fromm, M., Schubert, M., Castilla, G., Linke, J., & McDermid, G. (2019). Automated detection of conifer seedlings in drone imagery using convolutional neural networks. *Remote Sensing*, 11(21). <https://doi.org/10.3390/rs11212585>
- Fujimoto, A., Haga, C., Matsui, T., Machimura, T., Hayashi, K., Sugita, S., & Takagi, H. (2019). An end to end process development for UAV-SfM based forest monitoring: Individual tree detection, species classification and carbon dynamics simulation. *Forests*, 10(8), 1–27. <https://doi.org/10.3390/f10080680>
- Gallardo-Salazar, J. L., & Pompa-García, M. (2020). Detecting individual tree attributes and multispectral indices using unmanned aerial vehicles: Applications in a pine clonal orchard. *Remote Sensing*, 12(24), 1–22. <https://doi.org/10.3390/rs12244144>

- Gann, G. D., McDonald, T., Walder, B., Aronson, J., Nelson, C. R., Jonson, J., Hallett, J. G., Eisenberg, C., Guariguata, M. R., Liu, J., Hua, F., Echeverría, C., Gonzales, E., Shaw, N., Decler, K., & Dixon, K. W. (2019). International principles and standards for the practice of ecological restoration. Second edition. *Restoration Ecology*, 27(S1), S1–S46. <https://doi.org/10.1111/rec.13035>
- Gatziolis, D., Lienard, J. F., Vogs, A., & Strigul, N. S. (2015). 3D tree dimensionality assessment using photogrammetry and small unmanned aerial vehicles. *PLoS ONE*, 10(9), 1–21. <https://doi.org/10.1371/journal.pone.0137765>
- Grenzdörffer, G. J., Engel, A., & Teichert, B. (2008). The Photogrammetric Potential of Low-Cost UAVs in Forestry and Agriculture. *The International Archives of the Photogrammetry, Remote Sensing and Spatial Information Sciences*, Vol. XXXVII, 31(B3), 1207–2014.
- Heliguy, (2022). Drone partner. Available online: <https://www.heliguy.com/blogs/posts/traditional-surveying-vs-drone-surveying> (accessed on 28 February 2022).
- Iida, Y., Kohyama, T. S., Kubo, T., Kassim, A. R., Poorter, L., Sterck, F., & Potts, M. D. (2011). Tree architecture and life-history strategies across 200 co-occurring tropical tree species. *Functional Ecology*, 25(6), 1260–1268. <https://doi.org/10.1111/j.1365-2435.2011.01884.x>
- Itkin, M., Kim, M., & Park, Y. (2016). Development of cloud-based UAV monitoring and management system. *Sensors (Switzerland)*, 16(11), 1–19. <https://doi.org/10.3390/s16111913>
- IUCN International Union for Conservation of Nature, Bonn Challenge (2020). Available online: <https://www.bonnchallenge.org> (accessed on 27 September 2022).
- Johansen, K., Erskine, P. D., & McCabe, M. F. (2019). Using Unmanned Aerial Vehicles to assess the restoration performance of open cut coal mines. *Journal of Cleaner Production*, 209, 819–833. <https://doi.org/10.1016/j.jclepro.2018.10.287>

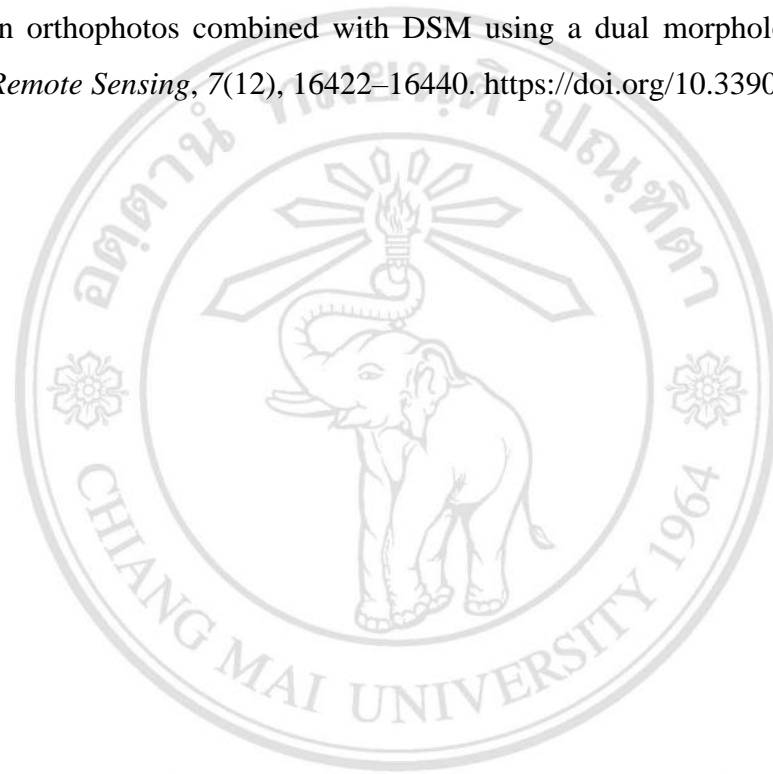
- Khamyong, N., Wangpakapattanawong, P., Chairuangri, S., Inta, A., & Tiansawat, P. (2018). Tree species composition and height-diameter allometry of three forest types in Northern Thailand. *Chiang Mai University Journal of Natural Sciences*, 17(4), 289–306. <https://doi.org/10.12982/CMUJNS.2018.0021>
- Klein Hentz, Â. M., & Strager, M. P. (2018). Cicada (<i>Magicicada</i>) Tree Damage Detection Based on UAV Spectral and 3D Data. *Natural Science*, 10(01), 31–44. <https://doi.org/10.4236/ns.2018.101003>
- Kyere-Boateng, R., & Marek, M. V. (2021). Analysis of the social-ecological causes of deforestation and forest degradation in Ghana: Application of the dpsir framework. *Forests*, 12(4), 1–29. <https://doi.org/10.3390/f12040409>
- Lee (2021). Developing a Forest-Degradation Index for Forest Ecosystem Restoration Using UAV-based RGB Photography [Unpublished master's thesis]. Chiang Mai University, Chiang Mai, Thailand.
- Lindberg, E., & Holmgren, J. (2017). Individual Tree Crown Methods for 3D Data from Remote Sensing. *Current Forestry Reports*, 3(1), 19–31. <https://doi.org/10.1007/s40725-017-0051-6>
- Mahlein, A. K., Rumpf, T., Welke, P., Dehne, H. W., Plümer, L., Steiner, U., & Oerke, E. C. (2013). Development of spectral indices for detecting and identifying plant diseases. *Remote Sensing of Environment*, 128, 21–30. <https://doi.org/10.1016/j.rse.2012.09.019>
- Maxwell, J. F. & S. Elliott, 2001. Vegetation and Vascular Flora of Doi Sutep–Pui National Park, Chiang Mai Province, Thailand. Thai Studies in Biodiversity 5. Biodiversity Research & Training Programme, Bangkok. 205 pp.
- McKenna, P. B., Lechner, A. M., Phinn, S., & Erskine, P. D. (2020). Remote sensing of mine site restoration for ecological outcomes: A global systematic review. *Remote Sensing*, 12(21), 1–32. <https://doi.org/10.3390/rs12213535>

- Miranda, A., G. Catalán, A. Altamirano & M. Cavieres. (2020). Automating site assessments using data from UAVs. Pp 64-73 in Elliott S., G. Gale & M. Robertson (Eds), *Automated Forest Restoration: Could Robots Revive Rain Forests? Proceedings of a brain-storming workshop*, Chiang Mai University, Thailand. 254 pp
- Moreno-de las Heras, M., Nicolau, J. M., & Espigares, T. (2008). Vegetation succession in reclaimed coal-mining slopes in a Mediterranean-dry environment. *Ecological Engineering*, 34(2), 168–178. <https://doi.org/10.1016/j.ecoleng.2008.07.017>
- Moura, M. M., de Oliveira, L. E. S., Sanquetta, C. R., Bastos, A., Mohan, M., & Corte, A. P. D. (2021). Towards amazon forest restoration: Automatic detection of species from uav imagery. *Remote Sensing*, 13(13). <https://doi.org/10.3390/rs13132627>
- Nebiker, S., Annen, A., Scherrer, M., & Oesch, D. (2008). A Light-weight Multispectral Sensor for Micro UAV – Opportunities for Very High Resolution Airborne Remote Sensing. *International Archives of the Photogrammetry, Remote Sensing and Spatial Information Sciences*, Vol. XXXVI(2008), 1193–1200. http://www.isprs.org/proceedings/XXXVII/congress/1_pdf/204.pdf
- Ogden, L. E. (2013). Drone Ecology. *BioScience*, 63(9), 776. <https://doi.org/10.1525/bio.2013.63.9.18>
- Omeja, P. A., Lawes, M. J., Corriveau, A., Valenta, K., Sarkar, D., Paim, F. P., & Chapman, C. A. (2016). Recovery of tree and mammal communities during large-scale forest regeneration in Kibale National Park, Uganda. *Biotropica*, 48(6), 770–779. <https://doi.org/10.1111/btp.12360>
- Özyeşil, O., Voroninski, V., Basri, R., & Singer, A. (2017). A survey of structure from motion. *Acta Numerica*, 26(May), 305–364. <https://doi.org/10.1017/S096249291700006X>
- Pádua, L., Vanko, J., Hruška, J., Adão, T., Sousa, J. J., Peres, E., & Morais, R. (2017). UAS, sensors, and data processing in agroforestry: a review towards practical applications. *International Journal of Remote Sensing*, 38(8–10), 2349–2391. <https://doi.org/10.1080/01431161.2017.1297548>

- Park, S., & Choi, Y. (2020). Applications of unmanned aerial vehicles in mining from exploration to reclamation: A review. *Minerals*, 10(8), 1–32. <https://doi.org/10.3390/min10080663>
- Picchio, R., Mederski, P. S., & Tavankar, F. (2020). How and How Much, Do Harvesting Activities Affect Forest Soil, Regeneration and Stands? *Current Forestry Reports*, 6(2), 115–128. <https://doi.org/10.1007/s40725-020-00113-8>
- Piermattei, L., Karel, W., Wang, D., Wieser, M., Mokroš, M., Surový, P., Koreň, M., Tomašík, J., Pfeifer, N., & Hollaus, M. (2019). Terrestrial structure from motion photogrammetry for deriving forest inventory data. *Remote Sensing*, 11(8). <https://doi.org/10.3390/rs11080933>
- Reis, B. P., Martins, S. V., Fernandes Filho, E. I., Sarcinelli, T. S., Gleriani, J. M., Leite, H. G., & Halassy, M. (2019). Forest restoration monitoring through digital processing of high resolution images. *Ecological Engineering*, 127(November 2018), 178–186. <https://doi.org/10.1016/j.ecoleng.2018.11.022>
- Rokhmana, C. A. (2015). The Potential of UAV-based Remote Sensing for Supporting Precision Agriculture in Indonesia. *Procedia Environmental Sciences*, 24(November), 245–253. <https://doi.org/10.1016/j.proenv.2015.03.032>
- Sasaki, N., Asner, G. P., Knorr, W., Durst, P. B., Priyadi, H. R., & Putz, F. E. (2011). Approaches to classifying and restoring degraded tropical forests for the anticipated REDD+ climate change mitigation mechanism. *IForest*, 4(JANUARY), 1–6. <https://doi.org/10.3832/ifor0556-004>
- Schober, P., & Schwarte, L. A. (2018). Correlation coefficients: Appropriate use and interpretation. *Anesthesia and Analgesia*, 126(5), 1763–1768. <https://doi.org/10.1213/ANE.0000000000002864>
- Shimizu, K., Ota, T., Kajisa, T., Mizoue, N., Yoshida, S., Takao, G., Hirata, Y., Furuya, N., Sano, T., Heng, S., & Vuthy, M. (2014). Estimation of aboveground biomass using manual stereo viewing of digital aerial photographs in tropical seasonal forest. *Land*, 3(4), 1270–1283. <https://doi.org/10.3390/land3041270>

- Tahar, K. N. (2015). Efficiency and cost comparison of UAV/Field survey. *International Conference on Space Science and Communication, IconSpace, 2015-Septe*, 428–433. <https://doi.org/10.1109/IconSpace.2015.7283774>
- Talib, N., Saad, M. S. M., Anshah, S. A., Saad, N. M., Ghazali, M. D., Abdullah, M. A., & Wan Mohd Jailani, W. J. H. (2021). A comparative flight altitude using multi-rotor uav for oil palm tree counting. *IOP Conference Series: Earth and Environmental Science*, 620(1). <https://doi.org/10.1088/1755-1315/620/1/012006>
- Torresan, C., Berton, A., Carotenuto, F., Di Gennaro, S. F., Gioli, B., Matese, A., Miglietta, F., Vagnoli, C., Zaldei, A., & Wallace, L. (2017). Forestry applications of UAVs in Europe: a review. *International Journal of Remote Sensing*, 38(8–10), 2427–2447. <https://doi.org/10.1080/01431161.2016.1252477>
- Vetter, T. R., & Schober, P. (2018). Regression: The Apple Does Not Fall Far From the Tree. *Anesthesia and Analgesia*, 127(1), 277–283. <https://doi.org/10.1213/ANE.00000000000003424>
- Wangpakapattanawong, P., & Elliott, S. (2008). Testing the Framework Species Method for Forest Restoration in Chiang Mai, Northern Thailand. *Walailak J Sci & Tech*, 5(1), 1–15.
- Westoby, M. J., Brasington, J., Glasser, N. F., Hambrey, M. J., & Reynolds, J. M. (2012). “Structure-from-Motion” photogrammetry: A low-cost, effective tool for geoscience applications. *Geomorphology*, 179, 300–314. <https://doi.org/10.1016/j.geomorph.2012.08.021>
- Yaduv, V. K., Srivastava, A. K., & Khare, P. K. (2018). Tropical Forest and Ecosystem Services in Indian Context. *Current World Environment*, 13(1), 151–158. <https://doi.org/10.12944/cwe.13.1.14>
- Yang, G., Liu, J., Zhao, C., Li, Z., Huang, Y., Yu, H., Xu, B., Yang, X., Zhu, D., Zhang, X., Zhang, R., Feng, H., Zhao, X., Li, Z., Li, H., & Yang, H. (2017). Unmanned aerial vehicle remote sensing for field-based crop phenotyping: Current status and perspectives. In *Frontiers in Plant Science*. <https://doi.org/10.3389/fpls.2017.01111>

- Yao, H., Qin, R., & Chen, X. (2019). Unmanned aerial vehicle for remote sensing applications - A review. *Remote Sensing*, 11(12). <https://doi.org/10.3390/rs11121443>
- Yue, L., Hongli, Z., & Jinghui, F. (2015). Application of Remote Sensing Technology in Mine Environment Monitoring. *MATEC Web of Conferences*, 22, 1–6.
- Zhang, Q., Qin, R., Huang, X., Fang, Y., & Liu, L. (2015). Classification of ultra-high resolution orthophotos combined with DSM using a dual morphological top hat profile. *Remote Sensing*, 7(12), 16422–16440. <https://doi.org/10.3390/rs71215840>



ลิขสิทธิ์มหาวิทยาลัยเชียงใหม่
Copyright© by Chiang Mai University
All rights reserved



APPENDICES

ลิขสิทธิ์มหาวิทยาลัยเชียงใหม่

Copyright© by Chiang Mai University

All rights reserved

APPENDIX A

(Additional) Ground-based Data

Table 14 Number of live saplings detected in ground surveys by time and species.

Code	Specie	Starting Cohort	1 st Data	2 nd Data	3 rd Data	4 th Data	5 th Data
S01	<i>Gmelina arborea</i> Roxb.	43	38	23	17	14	8
S04	<i>Spondias pinnata</i> (L.f.) Kurz	41	39	37	35	35	33
S06	<i>Phyllanthus emblica</i> L.	44	39	29	25	23	21
S07	<i>Azelia xylocarpa</i> (Kurz) Craib	39	37	37	31	27	21
S08	<i>Terminalia bellirica</i> (Gaertn.) Roxb.	37	35	33	28	28	28
S09	<i>Tectona grandis</i> L.f.	27	25	22	17	15	14
S11	<i>Bauhinia purpurea</i> L.	46	45	43	36	32	30
S26	<i>Albizia lebbek</i> (L.) Benth.	44	42	41	36	34	29
S30	<i>Protium serratum</i> (Wall. ex Colebr.) Engl.	45	43	41	39	30	29
S34	<i>Canarium subulatum</i> Guillaumin	44	40	38	32	22	21
S36	<i>Pterocarpus macrocarpus</i> Kurz	32	32	31	26	22	19
S39	<i>Xylia xylocarpa</i> (Roxb.) Taub.	39	33	25	15	10	7
S40	<i>Careya arborea</i> Roxb.	9	9	7	4	3	3
S43	<i>Garuga pinnata</i> Roxb.	41	37	37	34	31	29
S45	<i>Acrocarpus fraxinifolius</i> Arn.	40	37	27	20	18	17
S46	<i>Erythrina stricta</i> Roxb.	8	8	3	3	3	2
S49	<i>Sterculia pexa</i> Pierre.	44	39	36	35	31	29
S50	<i>Pentacme siamensis</i> (Miq.) Kurz	25	20	4	1	0	0
S60	<i>Holoptelea grandis</i> (Hutch.) Mildbr.	38	26	25	23	20	19
S65	<i>Schleichera oleosa</i> (Lour.) Merr.	37	35	31	24	20	19
S66	<i>Oroxylum indicum</i> (L.) Kurz	41	40	37	34	32	31
S67	<i>Dipterocarpus obtusifolius</i> Teijsm. ex Miq.	38	36	15	2	0	0
S69	<i>Bauhinia variegata</i> L.	43	43	38	36	32	27
S70	<i>Fernandoa adenophylla</i> (Wall. ex G.Don) Steenis	27	24	24	23	21	20
S71	<i>Artocarpus lacucha</i> Buch.-Ham.	36	33	27	13	8	8
S72	<i>Aegle marmelos</i> (L.) Corrêa	39	40	37	28	22	17
S79	<i>Mitragyna rotundifolia</i> (Roxb.) Kuntze	8	8	8	6	6	6
S80	<i>Bombax ceiba</i> L.	42	40	35	34	33	32
S81	<i>Vitex canescens</i> Kurz	26	23	22	20	19	18
S82	<i>Breonia chinensis</i> (Lam.) Capuron	25	21	19	14	12	10
Total		1048	967	832	691	603	547

NOTE: The date of each data collection 1st data (29/9/2020), 2nd data (10/12/2020), 3rd data (11/3/2021), 4th (13/6/2021), and 5th (16/9/2020)

Table 15 Numbers of sample saplings for which ground-based data acquired during each time of data collection by bench and time

Bench Order	Comparable samples	Data Collection Date				
		29/9/2020	10/12/2020	11/3/2021	13/6/2021	16/9/2020
1 st	290	274	221	162	178	179
2 nd	204	185	156	122	104	103
3 rd	166	152	119	86	59	64
4 th	144	139	112	84	82	74
5 th	129	119	100	96	84	79
6 th	115	95	85	3	78	71
Total	1048	964	793	553	585	570

Table 16 Simple regression coefficient predicting root collar diameter (N=428).

Dependent Variable	Independent Variables	Variable Estimation	Standard Error	t-value	Significance	RMSE
Root Collar Diameter	Constant	5.6655	0.2105	-4.52	6.41×10^{-6}	0.2813
	Ground-based Height	0.1893	0.0029	67.68	$< 2 \times 10^{-16}$	

Table 17 Simple regression coefficient predicting root collar diameter of individual sapling cohort species (N>20).

S	Dependent Variable	Independent Variables	Variable Estimation	Standard Error	t-value	Significance	RMSE
04	Root Collar Diameter	Constant	14.28255	2.22775	6.411	4.44×10^{-7}	1.164982
		Ground-based Height	0.18809	0.02066	9.104	3.89E-10	
S 06	Root Collar Diameter	Constant	4.20313	3.1899	1.318	0.204151	0.5951467
		Ground-based Height	0.14866	0.03186	4.667	0.000192	
S 08	Root Collar Diameter	Constant	2.82355	3.78348	0.746	0.462	0.9992698
		Ground-based Height	0.2093	0.03945	5.306	1.50×10^{-5}	
S 26	Root Collar Diameter	Constant	5.5309	3.1286	1.768	0.0898	0.0139025
		Ground-based Height	0.1996	0.0245	8.147	2.28×10^{-8}	
S 30	Dependent Variable	Independent Variables	Variable Estimation	Standard Error	t-value	Significance	RMSE

	Root Collar Diameter	Constant	1.90559	2.0848	0.914	0.369	0.415993
		Ground-based Height	0.21579	0.02047	10.544	2.95E-11	
S	Dependent Variable	Independent Variables	Variable Estimation	Standard Error	t-value	Significance	RMSE
34	Root Collar Diameter	Constant	1.86584	2.29596	0.813	0.426	1.121462
		Ground-based Height	0.22844	0.04106	5.563	2.30× 10 ⁻⁵	
S	Dependent Variable	Independent Variables	Variable Estimation	Standard Error	t-value	Significance	RMSE
36	Root Collar Diameter	Constant	2.91336	1.65876	1.756	0.097	0.6382105
		Ground-based Height	0.12387	0.01846	6.71	3.66 × 10 ⁻⁶	
S	Dependent Variable	Independent Variables	Variable Estimation	Standard Error	t-value	Significance	RMSE
43	Root Collar Diameter	Constant	17.92882	6.35316	2.822	0.00943	0.6704281
		Ground-based Height	0.12712	0.05481	2.319	0.0292	
S	Dependent Variable	Independent Variables	Variable Estimation	Standard Error	t-value	Significance	RMSE
49	Root Collar Diameter	Constant	4.91627	2.77841	1.769	0.0881	1.378986
		Ground-based Height	0.20056	0.03154	6.36	8.25× 10 ⁻⁷	
S	Dependent Variable	Independent Variables	Variable Estimation	Standard Error	t-value	Significance	RMSE
60	Root Collar Diameter	Constant	7.25224	4.73873	1.53	0.144308	2.857235
		Ground-based Height	0.20006	0.04161	4.808	0.000164	
S	Dependent Variable	Independent Variables	Variable Estimation	Standard Error	t-value	Significance	RMSE
65	Root Collar Diameter	Constant	4.26029	3.0485	1.398	0.18	1.554621
		Ground-based Height	0.28604	0.05012	5.707	2.57E-05	
S	Dependent Variable	Independent Variables	Variable Estimation	Standard Error	t-value	Significance	RMSE
66	Root Collar Diameter	Constant	-1.45728	2.51909	-0.578	0.567	1.788513
		Ground-based Height	0.22274	0.02726	8.171	4.03E-09	
S	Dependent Variable	Independent Variables	Variable Estimation	Standard Error	t-value	Significance	RMSE
69	Root Collar Diameter	Constant	3.84389	3.64582	1.054	0.301815	0.8568805
		Ground-based Height	0.17353	0.03831	4.53	0.000126	
S	Dependent Variable	Independent Variables	Variable Estimation	Standard Error	t-value	Significance	RMSE
70							

	Root Collar Diameter	Constant	19.6199	8.1222	2.416	0.028	2.297233
		Ground-based Height	0.3247	0.1711	1.898	0.0759	
S	Dependent Variable	Independent Variables	Variable Estimation	Standard Error	t-value	Significance	RMSE
72	Root Collar Diameter	Constant	4.1613	1.544	2.695	0.0159	0.2963402
		Ground-based Height	0.09906	0.03619	2.737	0.0146	
S	Dependent Variable	Independent Variables	Variable Estimation	Standard Error	t-value	Significance	RMSE
80	Root Collar Diameter	Constant	3.59419	3.11521	1.154	0.257	0.1218554
		Ground-based Height	0.19657	0.02803	7.012	5.08E-08	
S	Dependent Variable	Independent Variables	Variable Estimation	Standard Error	t-value	Significance	RMSE
81	Root Collar Diameter	Constant	10.98862	3.92377	2.801	0.01229	0.3960762
		Ground-based Height	0.16763	0.03652	4.591	2.60E-04	

Note: Code numbers were species code were listed as the following:

S04	<i>Spondias pinnata</i>	S60	<i>Holoptelea grandis</i>
S06	<i>Phyllanthus emblica</i>	S65	<i>Schleichera oleosa</i>
S08	<i>Terminalia bellirica</i>	S66	<i>Oroxylum indicum</i>
S26	<i>Albizia lebbbeck</i>	S69	<i>Bauhinia variegata</i>
S30	<i>Protium serratum</i>	S70	<i>Fernandoa adenophylla</i>
S34	<i>Canarium subulatum</i>	S72	<i>Aegle marmelos</i>
S36	<i>Pterocarpus macrocarpus</i>	S80	<i>Bombax ceiba</i>
S43	<i>Garuga pinnata</i>	S81	<i>Vitex canescens</i>
S49	<i>Sterculia pexa</i>		

ลิขสิทธิ์มหาวิทยาลัยเชียงใหม่
Copyright© by Chiang Mai University
All rights reserved

APPENDIX B

(Additional) Image-based Data

Table 18 Information reported from photogrammetric outputs of 1st Bench; in the order of the first data collection to last data collection

Data Collection Date	Orthomosaic Resolution (in/px)	Average GPS Trust (m)	Area Coverage (m ²)	RMSE (m)	Point Cloud Density (points/m ²)
29/9/2020	0.35	10.00	4061.40	0.54	2207.03
10/12/2020	0.35	10.00	4064.15	0.59	7406.54
11/3/2021	0.35	10.00	3944.76	1.12	2090.03
13/6/2021	0.35	10.00	4547.39	0.49	2274.41
16/9/2021	0.35	10.00	4240.54	0.48	6166.75

Table 19 Information reported from photogrammetric outputs of 2nd Bench; in the order of the first data collection to last data collection

Data Collection Date	Orthomosaic Resolution (in/px)	Average GPS Trust (m)	Area Coverage (m ²)	RMSE (m)	Point Cloud Density (points/m ²)
29/9/2020	0.35	10.00	2710.21	0.63	2610.68
10/12/2020	0.35	10.00	3132.24	0.74	609.99
11/3/2021	0.35	10.00	3406.35	1.00	2734.46
13/6/2021	0.35	10.00	4404.05	0.50	1512.11
16/9/2021	0.35	10.00	4358.34	0.37	5681.62

Table 20 Information reported from photogrammetric outputs of 3rd Bench; in the order of the first data collection to last data collection

Data Collection Date	Orthomosaic Resolution (in/px)	Average GPS Trust (m)	Area Coverage (m ²)	RMSE (m)	Point Cloud Density (points/m ²)
29/9/2020	0.35	10.00	2985.63	0.55	591.48
10/12/2020	0.35	10.00	2971.16	0.78	592.34
11/3/2021	0.35	10.00	3928.15	0.70	4071.88
13/6/2021	0.35	10.00	4137.75	0.57	6820.23
16/9/2021	0.35	10.00	3315.95	0.46	6207.12

Table 21 Information reported from photogrammetric outputs of 4th Bench; in the order of the first data collection to last data collection

Data Collection Date	Orthomosaic Resolution (in/px)	Average GPS Trust (m)	Area Coverage (m ²)	RMSE (m)	Point Cloud Density (points/m ²)
29/9/2020	0.35	10.00	1427.21	0.49	464.03
10/12/2020	0.35	10.00	1409.96	0.59	638.84
11/3/2021	0.35	10.00	1624.18	0.96	826.45
13/6/2021	0.35	10.00	1709.35	0.52	8152.69
16/9/2021	0.35	10.00	1833.49	0.55	6540.47

Table 22 Information reported from photogrammetric outputs of 5th Bench; in the order of the first data collection to last data collection

Data Collection Date	Orthomosaic Resolution (in/px)	Average GPS Trust (m)	Area Coverage (m ²)	RMSE (m)	Point Cloud Density (points/m ²)
29/9/2020	0.35	10.00	1147.46	0.53	2628.22
10/12/2020	0.35	10.00	1136.75	0.92	2666.11
11/3/2021	0.35	10.00	1258.25	1.19	2726.93
13/6/2021	0.35	10.00	1442.47	0.80	2029.43
16/9/2021	0.35	10.00	1748.72	0.55	6399.58

Table 23 Information reported from photogrammetric outputs of 6th Bench; in the order of the first data collection to last data collection

Data Collection Date	Orthomosaic Resolution (in/px)	Average GPS Trust (m)	Area Coverage (m ²)	RMSE (m)	Point Cloud Density (points/m ²)
29/9/2020	0.35	10.00	660.74	0.34	1051.10
10/12/2020	0.35	10.00	1071.41	0.40	341.32
11/3/2021	0.35	10.00	1566.52	0.45	780.60
13/6/2021	0.35	10.00	915.92	0.39	4938.81
16/9/2021	0.35	10.00	1082.98	0.29	10.12

Copyright© by Chiang Mai University
All rights reserved



Figure 32 The orthomosaic images of 1st Bench. In the order of the first data collection to last data collection (left to right); **a-e**, respectively. The letter “N” to represent North

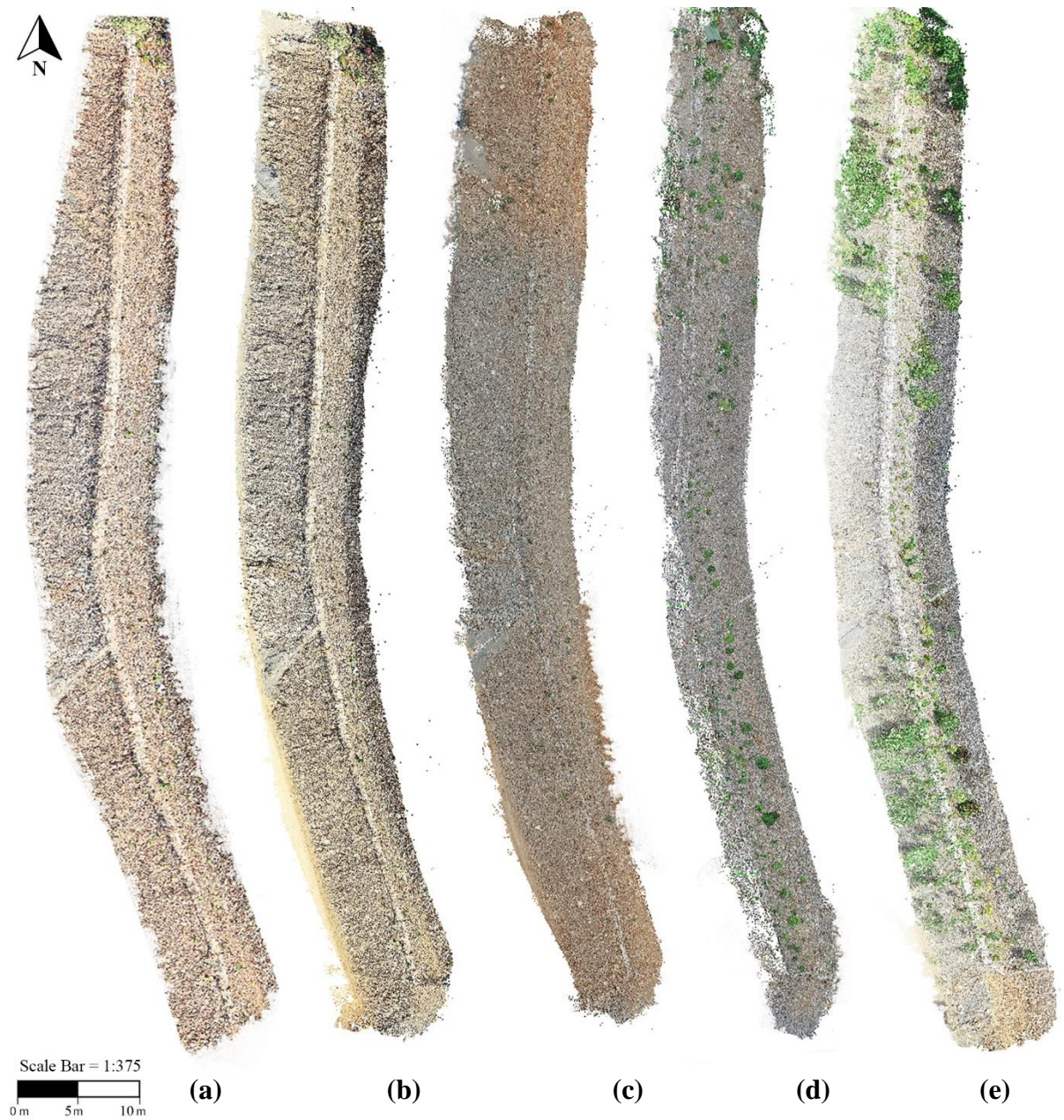


Figure 33 The 3D point clouds images of 1st Bench. In the order of the first data collection to last data collection (left to right); **a-e**, respectively. The letter “N” to represent North.



Figure 34 The orthomosaic images of 2nd Bench. In the order of the first data collection to last data collection (left to right); **a-e**, respectively. The letter “N” to represent North



Figure 35 The 3D point clouds of 2nd Bench. In the order of the first data collection to last data collection (left to right); **a-e**, respectively. The letter “N” to represent North

สงวนลิขสิทธิ์โดยมหาวิทยาลัยเทคโนโลยีพระจอมเกล้าธนบุรี
 All rights reserved



Figure 36 The orthomosaic images of 3rd Bench. In the order of the first data collection to last data collection (left to right); **a-e**, respectively. The letter “N” to represent North



Figure 37 The 3D point clouds of 3rd Bench. In the order of the first data collection to last data collection (left to right); **a-e**, respectively. The letter “N” to represent North



Figure 38 The orthomosaic images of 4th Bench. In the order of the first data collection to last data collection (left to right); **a-e**, respectively. The letter “N” to represent North



Figure 39 The 3D point clouds of 4th Bench. In the order of the first data collection to last data collection (left to right); **a-e**, respectively. The letter “N” to represent North



Figure 40 The orthomosaic images of 5th Bench. In the order of the first data collection to last data collection (left to right); **a-e**, respectively. The letter “N” to represent North



Figure 41 The 3D point clouds of 5th Bench. In the order of the first data collection to last data collection (left to right); **a-e**, respectively. The letter “N” to represent North



Figure 42 The orthomosaic images of 6th Bench. In the order of the first data collection to last data collection (left to right); **a-e**, respectively. The letter “N” to represent North

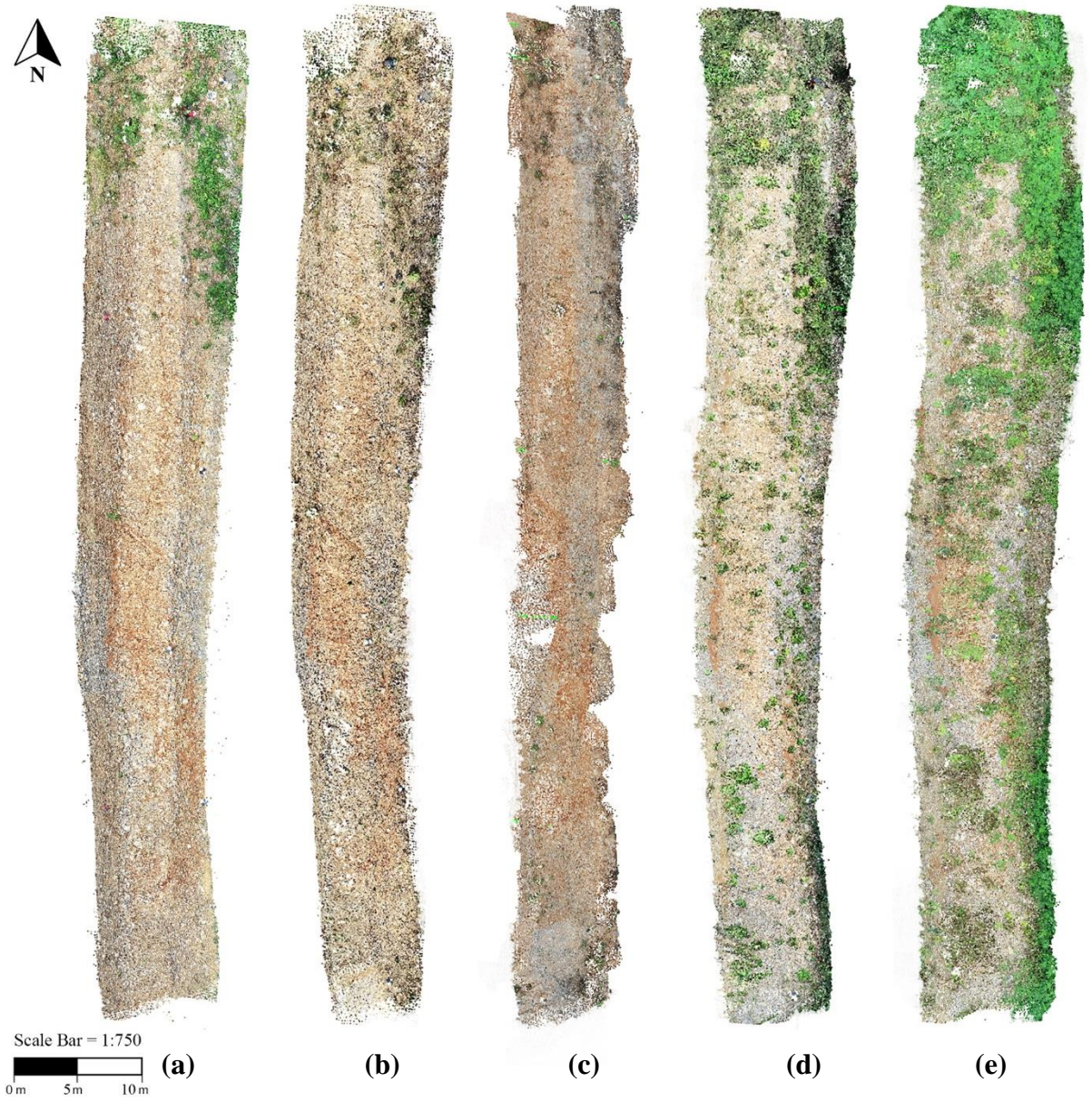


Figure 43 The 3D point clouds of 6th Bench. In the order of the first data collection to last data collection (left to right); **a-e**, respectively. The letter “N” to represent North

ลิขสิทธิ์มหาวิทยาลัยเชียงใหม่
Copyright © by Chiang Mai University
All rights reserved

CURRICULUM VITAE

Author's Name	Mr. Punnat Changsalak
Place of Birth	Chanthaburi Province, Thailand
Education	2019 Bachelor of Science, Major in Biology (Ecology), Chiang Mai University, Thailand
Scholarship	2018 – present Development and Promotion of Science and Technology scholarship (DPST scholarship)



ลิขสิทธิ์มหาวิทยาลัยเชียงใหม่
Copyright© by Chiang Mai University
All rights reserved